UNITED STATES DEPARTMENT OF COMMERCE
JESSE H. JONES, Secretary
NATIONAL BUREAU OF STANDARDS
Lyman J. Briggs, Director

✦

Journal of Research

of the

National Bureau of Standards

✦

Volume 29, Number 2

August 1942

[Published with approval of the Director of the Budget]

UNITED STATES
GOVERNMENT PRINTING OFFICE
WASHINGTON : 1942

For sale by the Superintendent of Documents, Washington, D. C. - - - - - - Price 30 cents
$3.50 per year on subscription

The prices of the separate Research Papers appearing in this JOURNAL are given on the front cover page. If 100 or more copies of any separate are ordered, a discount of 25 percent is allowed. Those who desire copies of separate Research Papers should send their orders and remittances without delay to the Superintendent of Documents, U. S. Government Printing Office, Washington, D. C. This will aid him to determine the number of copies to be printed for sale. Research Papers are not printed from electrotypes, and usually no more reprints can be had when the first and only printing is exhausted.

MATHEMATICAL TABLES

A list of the mathematical tables now obtainable from the National Bureau of Standards is printed on pages 3 and 4 of the JOURNAL cover. New tables will be announced from time to time as they become available.

U. S. DEPARTMENT OF COMMERCE NATIONAL BUREAU OF STANDARDS

RESEARCH PAPER RP1489

Part of Journal of Research of the National Bureau of Standards, Volume 29, August 1942

METALLOGRAPHIC STUDY OF THE FORMATION OF AUSTENITE FROM AGGREGATES OF FERRITE AND CEMENTITE IN AN IRON-CARBON ALLOY OF 0.5 PERCENT CARBON

By Thomas G. Digges and Samuel J. Rosenberg

ABSTRACT

The formation of austenite on heating aggregates of ferrite and cementite in a high-purity alloy of iron and carbon (0.50 percent carbon) is described. In fine pearlite, austenite was preferentially nucleated at the interfaces of ferrite and carbide at the boundaries of pearlite colonies and proeutectoid ferrite or at the boundaries between pearlite colonies, although it occasionally formed within the colonies. In spheroidized structures, nucleation occurred at ferrite-carbide interfaces at the cementite network or at isolated cementite particles. Austenite formed at numerous interfaces, so that in the initial stages it was always *fine-grained*. However, if the rate of heating is slow, rapid grain growth takes place in the Ac_1-Ac_3 temperature range. The predominant factor in establishing the austenite grain size in this alloy was the rate of growth and not the rate of nucleation.

CONTENTS

	Page
I. Introduction	113
II. Previous investigations	114
III. Experimental procedure	115
IV. Discussion	115
1. Formation of austenite from fine pearlite	116
2. Formation of austenite from an aggregate of spheroidized cementite and ferrite	118
3. Effect of rate of heating on nucleation of austenite	119
V. Summary	120
VI. References	121

I. INTRODUCTION

The mechanism of the formation of austenite from pearlite has been studied by various investigators, and it is now generally recognized that austenite forms from pearlite by nucleation and growth. These studies, however, have been made principally on plain carbon steels. It should be of interest to study the formation of austenite in iron-carbon alloys, in which any possible effects due to the presence of extraneous elements would be kept to a minimum. Since iron-carbon alloys of high purity are known to be relatively coarse-grained, it might be expected that transformations in such alloys could be more easily followed than in steels.

In previous studies [1][1] of the influence of certain factors on austenite grain size [1, 2] and its accompanying effect on hardenability [3],

[1] Figures in brackets indicate the literature references at the end of this paper.

some observations were made on the mechanism of the formation of austenite in high-purity alloys of iron and carbon. The present report describes this mechanism in an alloy containing 0.50 percent of carbon with initial structures of either fine pearlite (sorbite) or spheroidized cementite.

II. PREVIOUS INVESTIGATIONS

Grossmann [4, 5] studied the formation of austenite grains and the manner in which they coarsen in low-carbon steels. He briefly summarized the mechanism as follows: "When, upon heating, the steel reaches the temperature at which it begins to transform to austenite, the first very minute austenite crystals form within a pearlite island or in the boundaries between ferrite grains. These small austenite grains then grow across the pearlite islands and across the ferrite grains, until they meet other austenite grains which have grown from other nuclei. When all the austenite grains have thus met, so that the whole piece consists of austenite, it is clear that a certain set of grain-sizes will have been established." He pointed out that these initial austenite grains, usually in the range of American Society for Testing Materials numbers 5 to 8, do not grow even if the steel is heated for considerable periods of time just above the transformation temperature or to somewhat higher temperatures.

The strucutral changes occurring in steel on heating have been described by Carpenter and Robertson [6]. In each area of pearlite in hypoeutectoid steel, austenite begins to form at several points on the boundaries between pearlite and ferrite. The austenite spreads as the change proceeds, but the way in which this takes place is not related to the structure of the pearlite. At all times during the change the austenite areas have an irregular shape, and their outlines contain reentrant curves. In all steels, whatever their previous treatment, the austenite grains existing just above the critical range are small.

From a study made with carbon steels ranging in carbon from 0.45 to 1 percent, Baeyertz [7] reported that the austenite grains formed in entirely different ways in the same steel, depending on whether the prior structure was pearlite or martensite. In pearlite, nucleation of austenite grains occurred at the boundaries of the ferrite-cementite lamellas within pearlite colonies and not in the ferrite grain boundaries. The austenite grains grew along the pearlite lamellas, so that in the absence of coarsening, the structure contained elongated and irregularly shaped grains which took their conformation from the pearlite lamellas in which they formed. Austenite grains did not readily grow across the ferrite grain boundaries which separated the pearlite colonies; in the absence of coarsening, therefore, the austenite grain size at the end of the transformation was equal to or less than that of the prior pearlite colony. In spheroidized structures, the formation of austenite began in the grain boundary of the prior austenite. The nuclei for austenite formed at the ferrite-cementite phase boundaries around those cementite particles which were in the ferrite grain boundaries. With martensite, spheroidization occurred very readily below the Ac_1. The austenite produced just above the Ac_1 was formed not from martensite proper but from a spheroidized structure.

Mehl [8] reported that the rate of austenitizing was the greater the finer the spacing of the pearlite and that fine-grained steel (aluminum-killed) austenitized more slowly than coarse-grained steel. No detectible difference was found in the rates of nucleation for austenitizing of any of the specimens employed. At that time, Mehl was inclined to believe that the rate of growth was the important variable in austenitizing, and not the rate of nucleation.

The formation of austenite in plain carbon steels was also investigated by Hultgren [9] and by Shapiro [10]. Hultgren discussed the factors that caused the Ac_1 to occur over a range of temperatures, and he pointed out the need of similar experiments with high-purity iron-carbon alloys. Shapiro presented photomicrographs showing the mechanism of the alpha to gamma transformation in steels with different structures consisting of either pearlite, troostite, or spheroidized cementite.

III. EXPERIMENTAL PROCEDURE

Specimens of a high-purity alloy of iron and carbon (less than 0.031 percent of identifiable impurities) containing 0.50 percent of carbon were heated in such a manner that a portion passed through the Ac_1 transformation, whereas the remainder was below this temperature. The austenite thus formed was then decomposed into martensite or nodular troostite (fine pearlite) by rapid quenching. The specimens (approximately 1/16 by 1/10 by 1/4 inch) had initial structures of either fine pearlite (sorbite) and ferrite, or spheroidized cementite. Each specimen was heated within a Nichrome coil in vacuum at a selected rate to the desired temperature, held for a predetermined period and then quenched directly in gas (helium) in a manner similar to that previously described [3]. The quenched specimens were prepared by the usual means for metallographic study. The structural features of the changes are shown in the accompanying photomicrographs.

IV. DISCUSSION

In a study of the structural changes accompanying the heating of a hypoeutectoid iron-carbon alloy, it appears pertinent to examine the initial transformation of austenite from different aggregates of ferrite and carbide and to follow progressively the nucleation and growth of these austenite grains with time and with temperature.

Attention should be directed to the fact that the carbon content of pearlite in a hypoeutectoid steel may be less than that of the eutectoid. In order that the composition of pearlite in such a steel may correspond to that of the eutectoid, relatively slow cooling from above the critical range is necessary. If cooling is hastened, less free ferrite is precipitated, and hence the carbon content of the pearlite is less than that of the eutectoid. The more rapid the cooling, the more pronounced is this effect until the structure consists entirely of pearlite, which will then have a carbon content corresponding to that of the steel. The fine pearlite in the iron-carbon alloy used in the present study was produced by relatively rapid cooling. The amount of proeutectoid ferrite in this initial structure was small, and it was estimated from the microstructure that the carbon content of the pearlite possibly was as low as 0.55 percent, and certainly not more than 0.6 percent.

1. FORMATION OF AUSTENITE FROM FINE PEARLITE

The beginning of the formation of austenite from fine, carbon-poor pearlite is illustrated in figure 1. This specimen was heated sufficiently rapidly to the Ac_1 temperature to retain some of the cementite plates in the pearlite. At the Ac_1 temperature, austenite began to form at the interfaces of ferrite and cementite, as shown by the presence of troostite (a decomposition product of austenite) obtained by quenching. Evidently the small area of troostite shown at the lower left of the photomicrograph (fig. 1, *A*) was originally austenite that was nucleated at the point of contact of lamellar carbide with proeutectoid or free ferrite, whereas the minute area of troostite shown near the center of the photomicrograph was austenite that was formed in the region of a boundary common to two colonies of pearlite. Although austenite appeared to be preferentially nucleated in these regions, it occasionally originated within a pearlite colony (fig. 1, *B*).

With increase in time at the Ac_1 temperature, the areas of austenite increased in size and additional nuclei became active in different regions of pearlite, as illustrated in figue 2, *A*. As the specimen was maintained at this temperature, new austenite grains continued to form and grow (fig. 2, *B*) and the already existing grains increased in size, usually preferentially along the cementite lamellas (fig. 3, *A*), until all the pearlite was consumed and only two phases remained, ferrite and austenite (transformed to martensite and troostite) containing eutectoid carbon (fig. 3, *B*). With increase of temperature above that of the Ac_1 transformation, the percentage of austenite increased, and its carbon content decreased as ferrite was absorbed. At a temperature somewhat below the Ac_3 transformation there remained only a small percentage of ferrite (fig. 4, *A*); at the Ac_3 temperature the absorption of the ferrite was completed and only one phase remained—austenite (transformed to martensite on quenching) with an average carbon content of 0.50 percent (fig. 4, *B*). Although the austenite grains can grow with increase in temperature above Ac_3, no further structural changes take place until melting begins.

Austenite is nucleated at a cementite-ferrite interface. In pearlite (plus ferrite) such interfaces may be located (1) at the boundary between a pearlite area and proeutectoid ferrite, (2) at the common boundary of two or more pearlite colonies, and (3) within a pearlite colony.

The formation of austenite from lamellar pearlite is illustrated by figure 5. This sketch shows the nucleation of austenite at ferrite-cementite interfaces within a pearlite colony, but the initial formation of austenite and its growth in fine pearlite is believed to be similar, regardless of where nucleation occurs.

Figure 5, *A*, illustrates an individual colony of pearlite having alternate lamellas of cementite (Fe_3C) and ferrite (α-iron). For comparison with the iron-carbon alloy, it is assumed that the carbon content of this entire colony is considerably less than that of the eutectoid, i. e., this pearlite is also carbon-poor. If this *entire* area of pearlite should transform to austenite at the Ac_1 temperature, then one of two possibilities must exist. Either the austenite must have a carbon content corresponding to that of the pearlite (less than eutectoid) or, if the carbon content of the austenite approximates that of the eutectoid, then free ferrite must exist in conjunction with the austenite. Microscopic evidence supports the latter possibility.

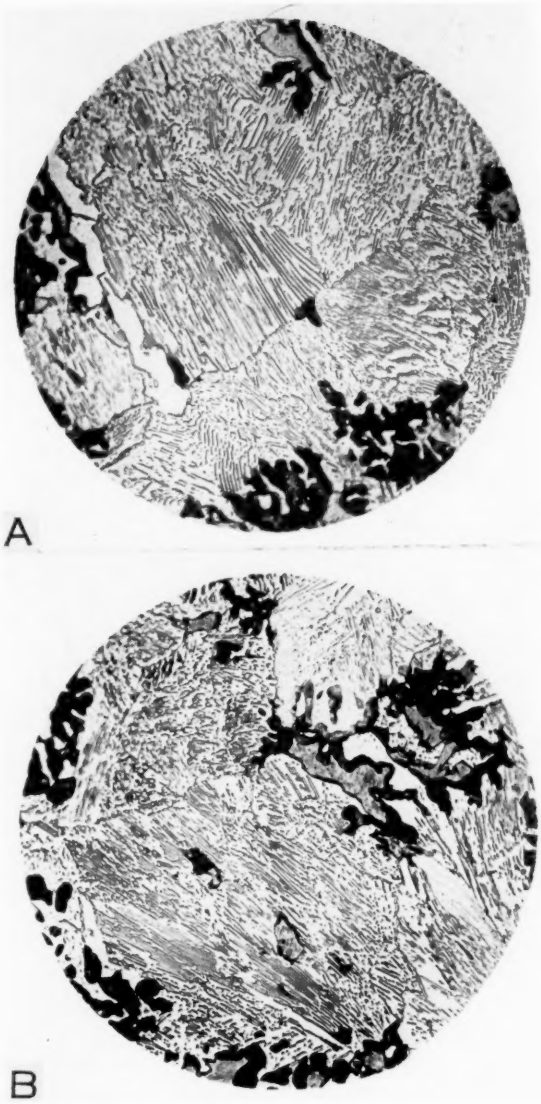

FIGURE 1.—*Nucleation of austenite from fine pearlite at the Ac_1 temperature.*

A, The small area of troostite (dark) (7 o'clock position) was originally austenite nucleated at the point of contact of lamellar cementite with proeutectoid ferrite (white). The small area of troostite near the center was originally austenite nucleated at the boundary common to two colonies of pearlite.

B, The several small areas (martensite (gray) and troostite) in the lower central portion of the photomicrograph were originally austenite nucleated within a pearlite colony. Note tendency of the austenite to grow in the direction of the pearlite lamellas.

Etched with 1 percent nital. ×500.

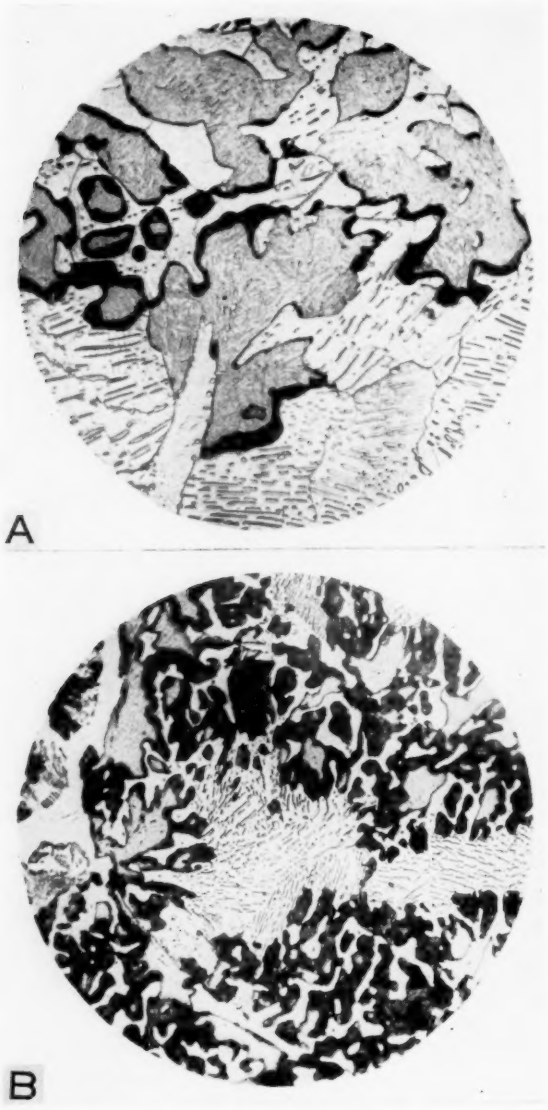

FIGURE 2.—*Nucleation and growth of austenite from fine pearlite at the Ac_1 temperature.*

A, A more advanced stage in the formation of austenite than that shown in figure 1. Note depletion of cementite lamellas near many of the original austenite areas (now martensite and troostite). ×1000.

B, A further stage in the formation and growth of austenite. Note finger-like growth of austenite areas (now martensite and troostite) and envelopment of small areas of ferrite. ×500.

Etched with 1 percent nital.

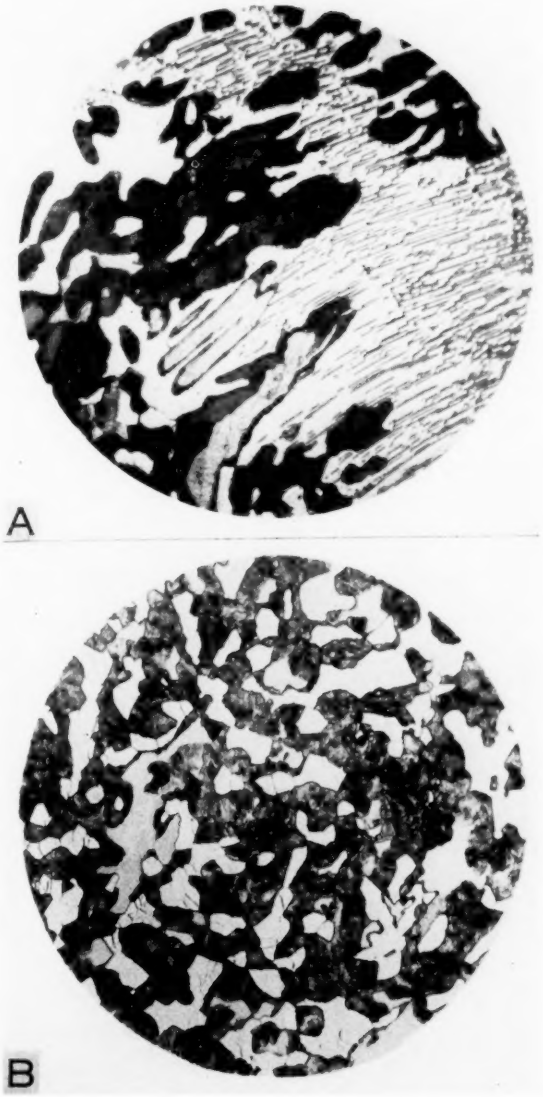

FIGURE 3.—*Nucleation and growth of austenite from fine pearlite at the Ac_1 temperature.*

A, The austenite, now martensite (light gray) and troostite (dark), has grown in a finger-like fashion in the direction of the lamellas. Note disappearance of cementite near many of the prior austenite areas, leaving ferrite (white). ×1000.

B, Structure after all the pearlite has transformed to austenite. Areas which were austenite at the time of quenching are now martensite and troostite. White areas are ferrite. ×500.

Etched with 1 percent nital.

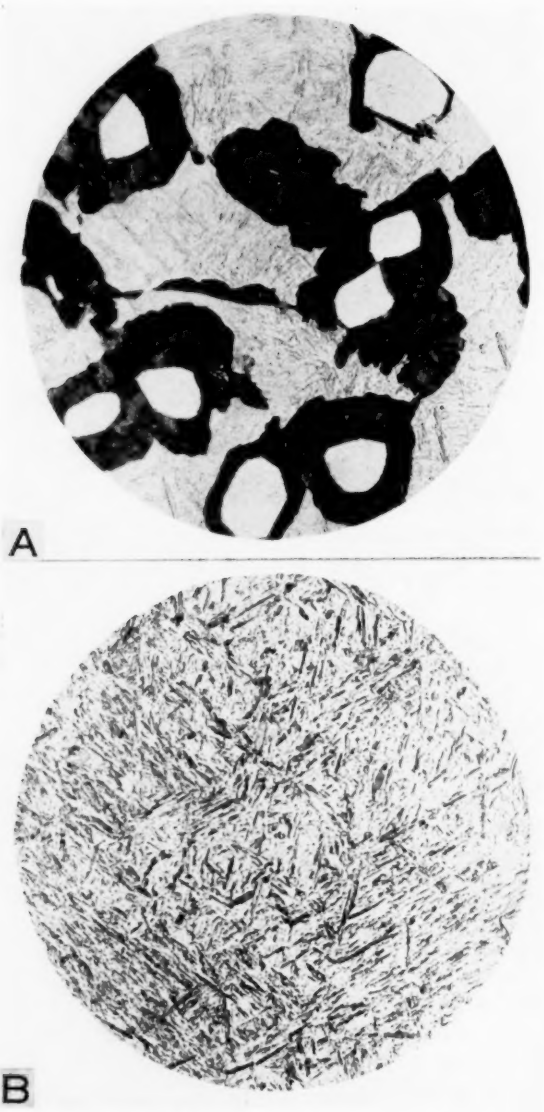

FIGURE 4.—*Absorption of ferrite by austenite formed from fine pearlite.*

A, Structure somewhat below Ac_3. Some of the ferrite (white) has not yet been absorbed by the austenite. On quenching, the austenite was transformed into martensite (light gray) and troostite (dark).

B, Structure just above Ac_3. All of the ferrite has been absorbed by the austenite (transformed to martensite on quenching).

Etched with 1 percent nital. ×500.

Figure 5, *B*, illustrates the formation of a minute area of austenite at the interface of a cementite and a ferrite lamella. It is postulated that cementite reacts with sufficient ferrite to form austenite of approximately eutectoid composition, which then grows (fig. 5, *C*) by absorbing cementite and part of the surrounding ferrite, thus leaving some excess ferrite. As this area of austenite spreads, a ferrite lamella is bridged (fig. 5, *D*), the cementite plate is completely absorbed, some of the carbon diffuses from an adjacent cementite plate into the austenite, and some of the ferrite is absorbed, leaving the remainder as free ferrite. Simultaneously, another grain of austenite begins at some other ferrite-carbide interface, and this grain grows in the same manner as the first grain. The austenite thus formed is of eutectoid carbon, although a carbon concentration gradient of sub-

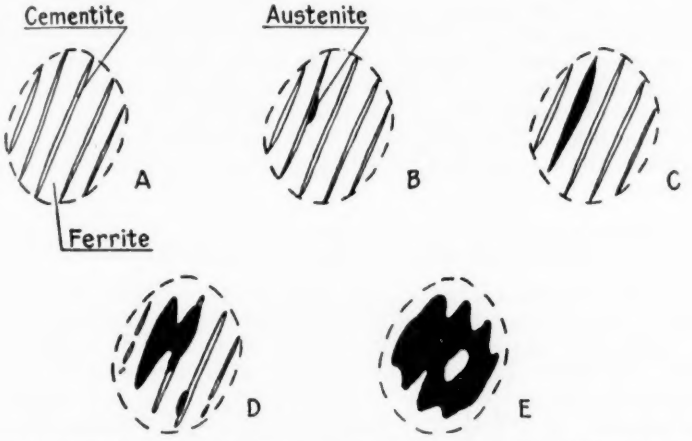

FIGURE 5.—*Sketch to illustrate nucleation and growth of austenite within a carbon-poor pearlite colony.*

Pearlite of eutectoid carbon (0.83% C) contains approximately 87.5 percent of ferrite and 12.5 per cent of cementite, or about 7 parts of ferrite for each part of cementite by weight. Pearlite of 0.50 percent *C*, therefore, contains about 11.6 parts of ferrite for each part of cementite.

microscopic dimensions must surely exist, since the austenite in contact with the cementite must be relatively high in carbon, whereas the austenite in contact with the ferrite must be relatively low in carbon. At a more advanced stage all of the cementite is consumed by the austenite, around which may be found more or less irregular areas of free ferrite (fig. 5, *E*). This growth occurs both in the direction of and across the lamellas. However, because the pearlite is carbon-poor, the austenite tends to grow in a fingerlike fashion along the cementite lamellas, which are carbon-rich, thus leaving free ferrite between. As the formation of austenite proceeds, some of these areas of ferrite are enclosed by the advancing austenite. At this stage the grains are invariably quite small. As growth continues, two or more grains will meet; whether they will merge depends upon such factors as time, temperature, relative size, orientation, etc. With sufficient time at this temperature (the Ac_1), all of the pearlite will transform to austenite (of eutectoid carbon content) thus leaving some free

ferrite. As the temperature is raised these ferrite areas, as well as the areas of proeutectoid ferrite, are gradually absorbed by the austenite until, at the Ac_3 temperature, all of the ferrite has been absorbed by the austenite, the carbon content of which is now 0.50 percent.

Comment has already been made on the fact that, since this pearlite is carbon-poor, if the austenite originally formed is of eutectoid composition, free ferrite must exist in conjunction with the austenite. Many of the structures examined suggested the possibility that, at the Ac_1, carbon diffused from the cementite of untransformed areas of pearlite to the adjoining austenite grains. This phenomenon was particularly evident in specimens which had been heated slowly and held for only 5 minutes in the vicinity of the Ac_1. Attention is directed to the several areas of martensite and troostite (originally austenite) shown in the lower right center of figure 6, *A*. All of these areas apparently are located within an individual colony of pearlite, yet the complete absence of cementite between them is evidence of the fact that migration of carbon toward the austenite grains has occurred. This is also shown in figure 6, *B*, particularly by the area in the lower right quadrant. The diffusion of carbon through alpha iron must be essentially the same as that which occurs on spheroidization of lamellar pearlite.

2. FORMATION OF AUSTENITE FROM AN AGGREGATE OF SPHEROIDIZED CEMENTITE AND FERRITE

When fine pearlite is heated, spheroids are formed from the cementite plates as the temperature approaches the Ac_1; the final degree of its spheroidization depends on the time it is held in this temperature range. In figure 7, *A* is shown the beginning of the formation of austenite in fine pearlite that was heated rapidly up to a temperature of about 700° C and then slowly to the Ac_1 temperature. The total time this specimen was held within the temperature range of about 700° C to the Ac_1 was about 22 minutes. Partial spheroidization occurred and the active nuclei for austenite formation were usually located in the vicinity of the ferrite boundaries.

Nucleation of austenite in an alloy with a structure containing cementite both as lamellas and as spheroids may occur at any cementite-ferrite interface. The formation of austenite from lamellar pearlite has already been described; its formation from an aggregate of spheroidized cementite and ferrite can best be studied by using specimens that have been intentionally spheroidized.

Specimens of the iron-carbon alloy with a structure of fine pearlite, therefore, were heated in vacuum in the temperature range of 680° to 720° C (below Ac_1) for about 9 hours. Although this treatment produced nearly complete spheroidization, the carbides tended to collect in the form of a network (fig. 7, *B*). Apparently this network bears no definite relation to the preexisting austenite grains from which the fine pearlite had been formed or to the colonies of pearlite in the initial structure. Had the period of the spheroidizing treatment been prolonged sufficiently, it seems possible that nearly all the carbides would have collected in the network. This is evidenced by the results of a microscopic examination, which showed either no indication of carbides or only small and finely divided particles in a few of the areas enclosed by the network.

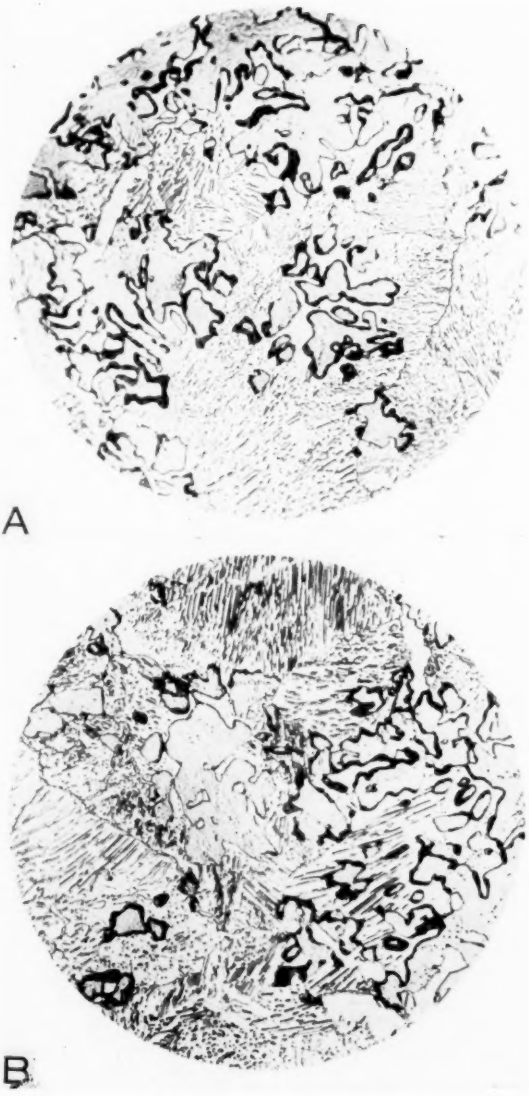

FIGURE 6.—*Formation of austenite from fine pearlite at the Ac_1 temperature.*

A, Note depletion of cementite between austenite grains (now martensite and troostite) in colony of pearlite shown in lower right center of photomicrograph.

B, Note depletion of cementite in areas adjacent to austenite (now martensite and troostite), particularly in lower right quadrant of photomicrograph.

Etched with 1 percent nital. ×500.

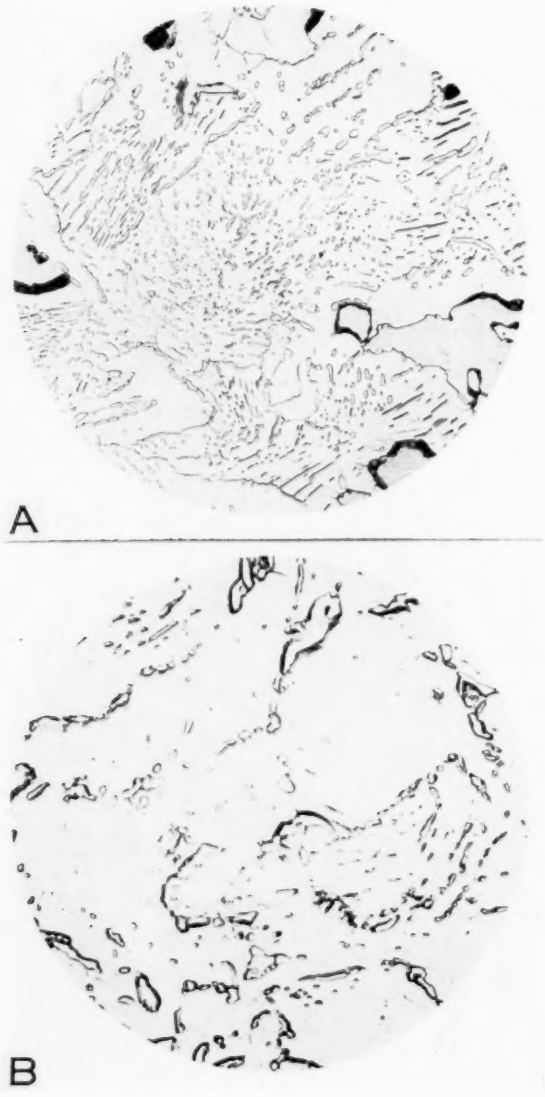

FIGURE 7.

A, Nucleation of austenite from fine pearlite at the Ac_1 temperature. Specimen was heated slowly. Note partial spheroidization. Etched with 1 percent nital. ×500.

B, Structure of iron-carbon alloy after spheroidization. Note tendency of carbides to collect in the form of a network. Etched with 1 percent nital. ×500.

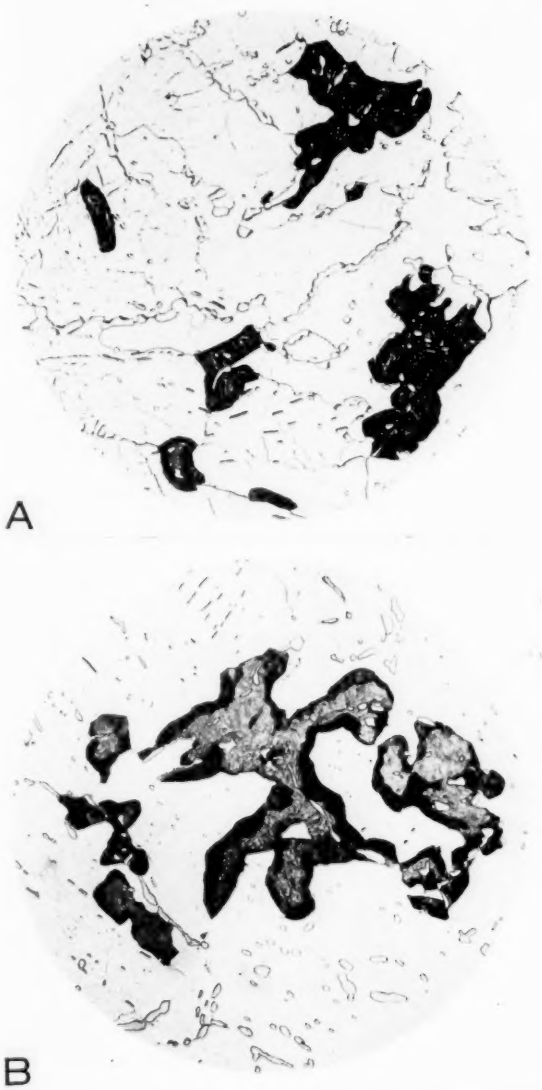

FIGURE 8.—*Nucleation and growth of austenite from aggregates of spheroidized cementite and ferrite at the Ac_1 temperature.*

A, The austenite grains (now martensite and troostite) were nucleated at the interfaces of ferrite and the carbide network and, in some cases, at interfaces within the interior of the network.

B, The austenite grains (now martensite and troostite) have grown preferentially along the cementite network. Note almost complete disappearance of carbides from the ferrite enclosed by the originally austenite grains.

Etched with 1 percent nital. ×500

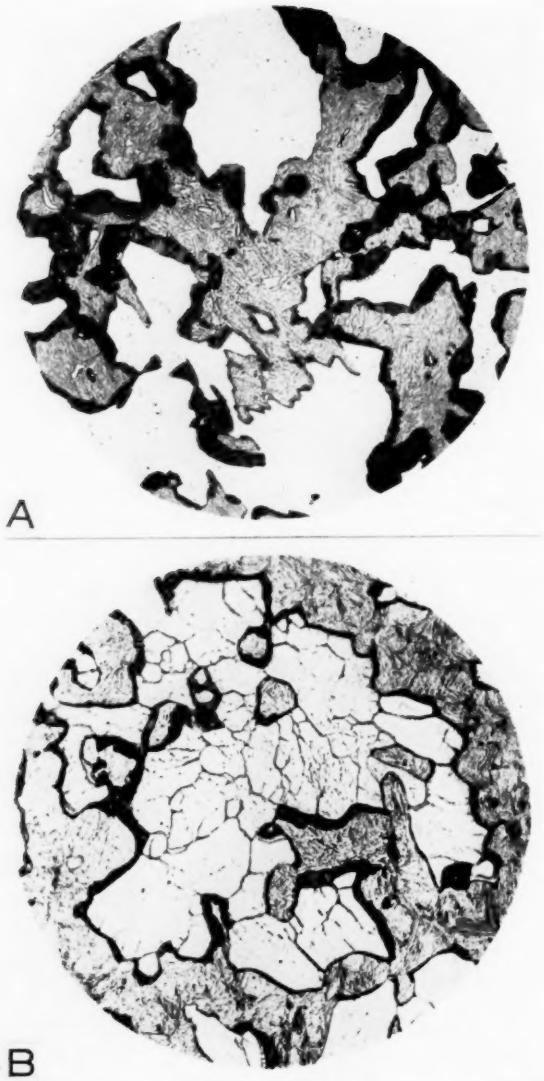

FIGURE 9.—*Nucleation and growth of austenite from an aggregate of spheroidized cementite and ferrite at the Ac_1 temperature.*

A, The formation of austenite (now martensite and troostite) of eutectoid carbon is nearly complete. Note almost complete absence of carbides in the ferrite. Austenite still contained occasional undissolved carbides at the time of quenching.

B, The formation of austenite of eutectoid carbon is complete. Only two phases exist—ferrite (white) and austenite (transformed into martensite and troostite).

Etched with 1 percent nital. ×500.

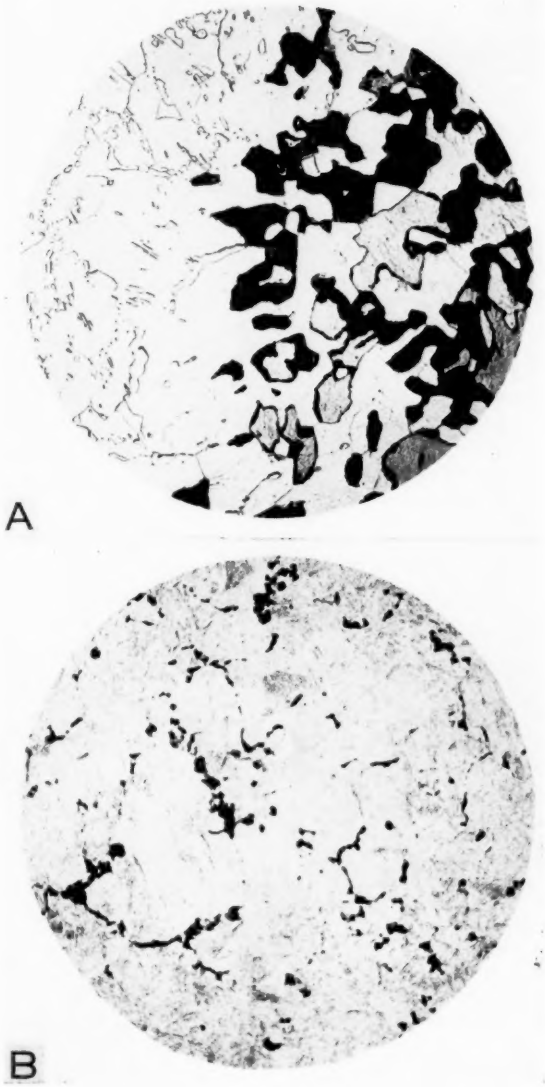

FIGURE 10.—*Effect of time and temperature on the size of austenite grains.*

A. The grains of austenite (now martensite and troostite) formed at the Ac_1 temperature are quite small. The structure was originally fine pearlite, which spheroidized during the slow heating. ×500.

B. Same specimen as *A*. The grains of austenite, transformed into martensite with troostite at the boundaries, are quite large at the Ac_3 temperature. ×100.

Etched with 1 percent nital.

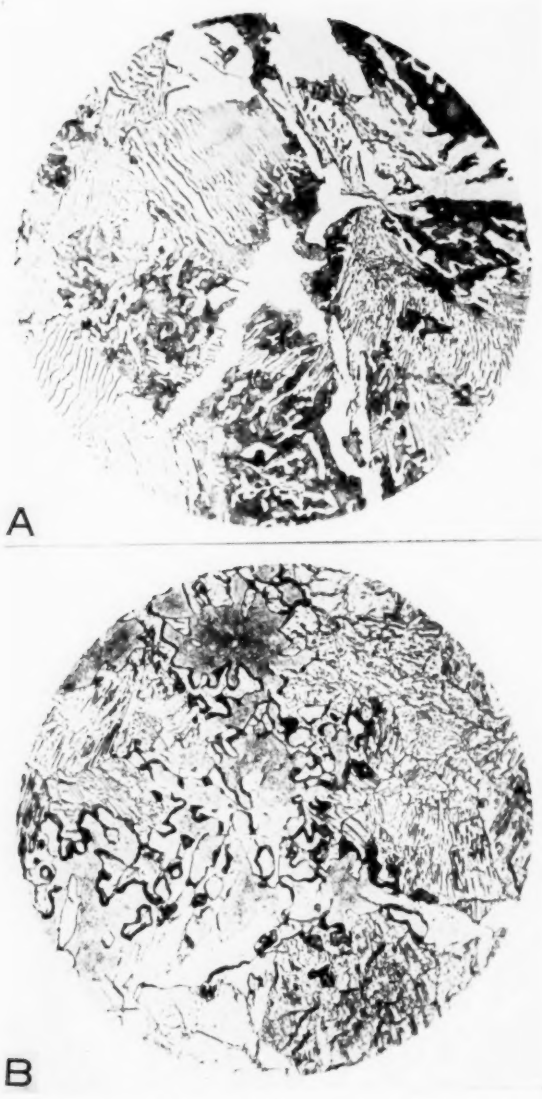

FIGURE 11.—*Effect of rate of heating on nucleation of austenite from fine pearlite at the Ac_1 temperature.*

A, Heated very rapidly. Note considerable number of active nuclei as evidenced by the numerous small areas of troostite.

B, Heated rather slowly. Note smaller number of active nuclei, as evidenced by the fewer and larger areas of martensite and troostite.

Etched with 1 percent nital. ×500.

When a specimen with such a spheroidized structure was heated to the Ac_1 temperature, austenite grains were nucleated at the interface of ferrite and the carbide network, and, in some cases, at the interface of ferrite and carbide within the network, as shown by the decomposition products of austenite in figure 8, *A*. With increase in either time or temperature, the newly formed austenite grains grew and new grains were formed, usually along the network, as illustrated in figure 8, *B*. Simultaneously with this initial formation of austenite, the carbides located within the network, which were not active as centers for nucleation, decreased in number and size by the diffusion of carbon to the network or to the existing grains of austenite (fig. 8, *B*). This phenomenon might be viewed simply as a further step in the spheroidization of the cementite.

Nucleation, growth, and diffusion continued, and a stage was reached where the austenite grains merged in the neighborhood of the original cementite network, thus leaving only a few finely divided carbides embedded in the ferrite, as illustrated in figure 9, *A*. It is noteworthy that at this stage of the transformation the austenite contained some undissolved carbide particles that were considerably larger than the remaining carbides embedded in the ferrite or untransformed portion of the specimen. Since this transformation had been occurring at the Ac_1 temperature, it is apparent that the austenite was of approximately eutectoid composition. However, carbon gradients must have existed in the austenite which was in contact with cementite in the interior of the grains and with ferrite at the grain boundaries. With increase either in time at this temperature or in temperature, the carbon from the cementite continued to diffuse through the austenite to the austenite-ferrite boundary, where additional austenite was formed. Simultaneously, the carbides located in the ferrite continued to be absorbed until the alloy reached equilibrium, and consisted of two phases, austenite (transformed to martensite and troostite) and ferrite, as is shown in figure 9, *B*. Upon heating to the Ac_3 temperature or above, the absorption of ferrite was completed and the austenite attained a uniform composition (0.50 percent of carbon).

3. EFFECT OF RATE OF HEATING ON NUCLEATION OF AUSTENITE

Variation in the rate of heating through the Ac_1-Ac_3 transformation range is known to have a marked influence on the austenite grain size of this alloy at temperatures either just above or considerably higher than the Ac_3 [1, 3]. Relatively fine grains are produced by rapid heating and coarse grains by slow heating. However, even on slow heating through the Ac_1 transformation, sufficient nuclei become active to render the austenite fine-grained in the initial stage of its formation. This is shown by the microstructure in the zone of transformation (fig. 10, *A*) of a specimen that was differentially heated, so that a portion was heated slowly through the Ac_1 and held for 15 minutes before quenching. The austenite was fine-grained when first formed, but it was coarse-grained, figure 10, *B* (estimated ASTM grain No. 2 to No. 4), at the Ac_3 temperature.

Although with relatively slow rates of heating sufficient nuclei act to produce fine-grained austenite, this condition does not necessarily imply that the rate of heating does not influence the rate of nucleation of this alloy. It is believed that the rate of heating does affect

the rate of nucleation. With this high-purity alloy, which is relatively free from grain-growth inhibitors, more nuclei are effective in the formation of austenite from fine pearlite when heating is relatively rapid than when heating is slow.

The more rapidly fine pearlite is heated through the Ac_1 temperature, the more numerous are the active nuclei. The initial formation of austenite in the low-carbon pearlite of a specimen which was heated very rapidly to the Ac_1 (50 seconds from room temperature to the Ac_1) and then immediately quenched is shown by its decomposition products in figure 11, *A*, and the initial transformation in another specimen of the same material when heated rather slowly to the Ac_1, held for 5 minutes and then quenched, is shown in figure 11, *B*. The austenite grains initially formed in each specimen were very small indeed, but it is apparent that more nuclei were active in forming austenite in the rapidly heated specimen (fig. 11, *A*) than in the one heated rather slowly (fig. 11, *B*) or in the one heated very slowly (fig. 10, *A*). It is further apparent that the austenite grains were larger and less numerous in the slowly heated specimens than in the rapidly heated specimen.

It is evident that when such an alloy is heated to the Ac_1 temperature certain nuclei become active in formation of grains of austenite. If the rate of heating is slow, relatively few nuclei are effective and ample time exists for growth of these grains. If the rate of heating is very rapid the alloy is, in effect, superheated; a considerable number of nuclei then become active because of the higher temperature at which the Ac_1 transformation occurs. Determinations of the Ac_1 showed that, when the alloy was heated slowly, this transformation began at about 725° C, whereas, with very rapid heating, it occurred at about 740° C. Had the rapidly heated specimen been held just above the Ac_1 temperature, it is believed that considerable growth would have taken place in the austenite grains.

Since the final austenite grain size depends upon the rate of nucleation and rate of growth, it is evident that, for this alloy, the latter is the dominant factor in establishing this grain size. With this high-purity alloy, and with other alloys of similar purity but having higher percentages of carbon, rapid growth occurred within the transformation temperature range when heating was slow. That is, these alloys are very susceptible to coarsening within the temperature range of the Ac_1-Ac_3 transformation. Whether coarsening occurred within this range depended upon the rate of heating (time within this temperature range). At temperatures as high as 980 ° C, however, these alloys were coarse-grained, regardless of the rate of heating.

V. SUMMARY

1. A study was made of the nucleation and growth of austenite on heating a high-purity alloy of iron and carbon containing 0.50 percent of carbon. The changes that occurred in both fine pearlite and an aggregate of spheroidized cementite and ferrite were followed by differentially heating small specimens in vacuum at various rates to temperatures within and slightly above the Ac_1-Ac_3 transformation range and quenching directly in helium. The different stages in the formation of austenite from the aggregates of ferrite and carbide are shown in photomicrographs and illustrated schematically.

2. On heating fine pearlite (plus ferrite), austenite was nucleated at the interfaces of ferrite and carbide, preferentially at the boundaries of pearlite and proeutectoid ferrite and at the boundaries of the pearlite colonies. It was also nucleated occasionally within the pearlite colonies. Fingerlike growths (irregular shapes) occurred, usually in the directions of the lamellas, but growth also extended across the lamellas.

3. During spheroidization of this alloy the carbides tended to collect in the form of a network. On heating a specimen with such a structure, austenite started to form at ferrite-carbide interfaces, usually at the cementite network and to some extent within the network. In the initial stages of transformation these grains grew preferentially along the cementite network.

4. During the formation of austenite from fine, carbon-poor pearlite or an aggregate of spheroidized cementite and ferrite, the carbon diffused through ferrite to the austenite grains and also through the austenite during the absorption of the ferrite.

5. Regardless of the rate at which this alloy was heated through the Ac_1 transformation, austenite was nucleated at numerous interfaces of ferrite and carbide, so that in the initial stage of its formation the austenite was *always* fine-grained. However, rapid grain growth may occur in the Ac_1-Ac_3 transformation range by the absorption or coalescence of the grains initially formed. If the rate of heating through the Ac_1-Ac_3 transformation range was extremely rapid, this grain growth was largely inhibited, and the resulting austenite was relatively fine-grained at temperatures considerably above the Ac_3. If heating was less rapid, grain growth was not inhibited, and the resulting austenite was very coarse-grained. The predominant factor in establishing the final austenite grain size of this alloy, therefore, was the rate of growth and not the rate of nucleation.

VI. REFERENCES

[1] S. J. Rosenberg and T. G. Digges, *Effect of rate of heating through the transformation range on austenitic grain size*, J. Research NBS **25,** 215 (1940) RP1332. Trans. Am. Soc. Metals **29,** 33 638 (1941).

[2] T. G. Digges and S. J. Rosenberg, *Influence of initial structure and rate of heating on the austenitic grain size of 0.5-percent carbon steels and iron-carbon alloy*, J. Research NBS **29,** (1942) RP1481.

[3] T. G. Digges, *Influence of austenitic grain size on the critical cooling rate of high-purity iron-carbon alloys*, J. Research NBS **24,** 723 (1940) RP1308; Trans. Am. Soc. Metals **29,** 285 (1941).

[4] M. A. Grossmann, *On grain size and grain growth*, Trans. Am. Soc. Metals **21,** 1079 (1933).

[5] M. A. Grossmann, *Grain size in metals, with special reference to grain growth in austenite*, Trans. Am. Soc. Metals **22,** 861 (1934).

[6] H. C. H. Carpenter and J. M. Robertson, *Structural changes in hypoeutectoid steels on heating*, J. Iron & Steel Inst. **127,** No. 1, 259 (1933); Metals, Oxford University Press **2,** 914 (1939).

[7] M. Baeyertz, *Effects of Initial Structure on Austenite Grain Formation and Coarsening*, Paper presented at the Twenty-third Annual convention Trans. Am. Soc. Metals, **30,** 458 (1942). Preprint No. 20.

[8] R. F. Mehl, *The structure and rate of formation of pearlite*, Trans. Am. Soc. Metals **29,** 813 (1941).

[9] Axel Hultgren, *The Ac_1 range of carbon steel and related phenomena*, Trans. Am. Soc. Steel Treating **16,** 227 (1929).

[10] C. L. Shapiro, *The effect of heat treatment, aging, and working upon the condition of carbon in steel*, Iron & Steel Institute, Carnegie Scholarship Memoirs **25,** 141 (1936).

WASHINGTON, MAY 8, 1942.

U. S. Department of Commerce National Bureau of Standards

RESEARCH PAPER RP1490

Part of Journal of Research of the National Bureau of Standards, Volume 29,

August 1942

FRACTIONATION OF CELLULOSE ACETATE

By Arnold M. Sookne,[1] Henry A. Rutherford,[1] H. Mark,[2] and Milton Harris [1]

ABSTRACT

By means of a series of three successive fractional precipitations, a solution containing 2 kg of commercial cellulose acetate was separated into 15 fractions varying in degree of polymerization from 30 to 380. The procedure involved the fractional precipitation of the acetate from a solution in acetone, using ethyl alcohol as the precipitant.

From the viscometrically estimated chain-lengths of the fractions, the distribution of chain-lengths in the starting material (excepting the first fraction) was obtained. The first fraction was not completely soluble in acetone or Methyl Cellosolve, and therefore no estimate of its degree of polymerization was obtained. It was shown that a large proportion of the ash and haze-producing materials are contained in this first fraction. All of the other fractions have very low ash contents, and with the exception of the fractions of very low degrees of polymerization, the acetyl contents are constant. A phase diagram showing some of the solubility relationships of the starting material and several of the fractions is given.

CONTENTS

	Page
I. Introduction	123
II. Experimental procedure	124
1. Materials	124
2. Methods	124
(a) Estimation of relative chain-length	124
(b) Estimation of acetyl content	144
(c) Fractionation procedure	124
III. Results and discussion	125
IV. References	130

I. INTRODUCTION

It is generally recognized that cellulose and its derivatives are composed of long, unbranched, chainlike molecules of varying lengths. The recognition of this fact has led to a number of investigations, reviewed elsewhere [1, 2],[3] concerning the relation of chain-length to certain mechanical properties. In most of these studies, a quantity of cellulosic material was fractionated with respect to chain-length, and the mechanical properties of the fractions were then investigated. It appears, however, that much of this earlier work has been handicapped by the lack of a sufficient quantity of the fractionated materials to allow them to be satisfactorily characterized. In addition, with

[1] Research Associates at the National Bureau of Standards representing the Textile Foundation.
[2] Professor of organic chemistry at the Brooklyn Polytechnic Institute.
[3] Figures in brackets indicate literature references at the end of this paper.

few exceptions, the fractionations have consisted in a division of the materials into a very few portions, without adequate repeated separations. In order to overcome such shortcomings, the fractionation of a large quantity of cellulose acetate was undertaken, and the mechanical properties of the various fractions and their blends were studied. The present report is limited to a description of the separation and a few of the characteristics of the fractions.

II. EXPERIMENTAL PROCEDURE

1. MATERIALS

The starting material was 150 liters of a filtered solution of commercial cellulose acetate of the type used in rayon manufacture.[4] It contained 2.5 percent of cellulose acetate, 95.5 percent of acetone, and 2.0 percent of water by weight. The acetate had an Eastman viscosity of 93 seconds in 4:1 acetone solution [3], a precipitation value of 68.8 percent [3], a melting point of 250° C, and a char point of 301° C. The acetyl and ash contents were 38.6 and 0.06 percent, respectively.

2. METHODS

(a) ESTIMATION OF RELATIVE CHAIN-LENGTH

The relative degrees of polymerization[5] (henceforth referred to as *DP*) of the starting material and the various fractions were estimated viscometrically by the use of Staudinger's relationship $DP=\eta_{sp}/K_mC$ [6], where η_{sp} is the specific viscosity, K_m is Staudinger's constant of proportionality, C is the concentration in grams of solute per liter of solution, and DP is the degree of polymerization.

The specific viscosities were measured of solutions containing 2.64 g of cellulose acetate per liter of solution at temperatures of 25.1° C and 60.6° C, with Methyl Cellosolve (ethylene glycol monomethyl ether) as the solvent. Staudinger constants of 9.7×10^{-4} and 7.0×10^{-4} were used for calculating the results at 25.1° C and 60.6° C, respectively. These constants were obtained from Staudinger's value for the constant at 20° C [6], using the assumption that the molecular weight of a given sample is the same at all three temperatures. The *DP* values reported in tables 1 and 2 are the means of the values obtained by measurements at 25.1° and 60.6° C.

(b) ESTIMATION OF ACETYL CONTENT

The acetyl contents of the samples were estimated by the method of Eberstadt, according to the recommendations of Genung and Mallatt [7]. The samples were first ground in a Wiley mill, to promote intimate contact between the sample and the solution.

FRACTIONATION PROCEDURE

The fractional precipitation technique was used in preference to other fractionation procedures, since the method appears to be as

[4] We are indebted to the Tennessee Eastman Corporation for furnishing us with this material.

[5] By "degree of polymerization" is meant the average number of glucose residues per chain. The calculated molecular sizes have been expressed as *DP* values in this paper as a matter of convenience; *DP* values are directly converted to molecular weights by multiplying by the equivalent weight, in this case, 260. Because of the limitations of the method of determining them [4, 5], the *DP* values should be considered as relative values.

effective as others and much more convenient. On the basis of the results of preliminary experiments, 95 percent ethyl alcohol was chosen as the precipitant. The general procedure was to add a quantity of ethyl alcohol insufficient to cause a permanent precipitate to a solution of cellulose acetate at room temperature (20° to 25° C) contained in a 5- or 10-gallon bottle. The concentration of acetate after the addition of alcohol was 1.2 percent or less throughout the first fractionation. The precipitate initially formed by high local concentrations of alcohol was dissolved by stirring until a homogeneous solution was obtained. The vessel was then slowly cooled to a temperature of 10° C. A gelatinous precipitate slowly formed in the bottom of the vessel, the quality of the precipitate being such that the supernatant solution could be easily removed by decantation. The attainment of equilibrium was hastened by occasional stirring and by scratching the bottles. That the process is a reversible one was shown by the fact that the precipitate could readily be redissolved and a homogeneous solution obtained by warming the system to room temperature. The supernatant solution was separated from the precipitate by decantation, and an additional quantity of alcohol was added to the solution. The process described above was then repeated until the desired number of fractions was obtained. The quantity of alcohol to be added was determined in each case by a preliminary test-tube experiment, after which the test sample was returned to the solution.

With the possible exception of the precipitate obtained by the first addition of alcohol, for which no estimate of the *DP* could be obtained (see section III), materials of high molecular weight were precipitated first by this procedure, and successive additions of alcohol precipitated materials of lower molecular weight in a progressive manner.

The acetate solution was divided into 3 portions of about 50 liters each, and each of these was then treated so as to obtain 7 fractions of roughly equal weights. In each case the first fraction was not completely soluble in acetone. These first fractions, which will be described later, were combined and set aside. Fractions of approximately equal *DP*'s among the remaining fractions were combined to give 7 mixtures, which were then refractionated to yield a total of 29 fractions. The concentration of acetate after the addition of alcohol was 5 percent or less in this and the subsequent fractionation. Fractions of similar *DP* were again combined to 7 mixtures, which were again split into a total of 28 fractions. The fractions of approximately equal *DP* were finally combined into 14 fractions, which will be described later.

III. RESULTS AND DISCUSSION

The results of the complete fractionations, with the exception of the first fractions, are shown in table 1. The third column for each fractionation gives the value of the integral distribution function, $I(P)$,[8] corresponding to each *DP* value given in the first columns. The values of $I(P)$ were obtained as follows: To one-half of the weight percentage of each fraction was added the sum of the weight percentages of all of the fractions appearing above it in the table. The values of $I(P)$ so obtained represent the total percentage of the entire material with *DP* values between unity and the *DP* under consideration.[6]

[6] This procedure for obtaining $I(P)$ involves the assumption that the chain-lengths in any fraction are symmetrically distributed about the average chain-length of the fraction [8].

TABLE 1.—*Results of three successive fractionations of a cellulose acetate sample*

First fractionation			Second fractionation			Third fractionation		
DP	Weight	*I*(*P*)	*DP*	Weight	*I*(*P*)	*DP*	Weight	*I*(*P*)
	Percent			*Percent*			*Percent*	
81	9.9	5.0	52	5.6	2.8	24	1.8	0.9
88	7.5	13.7	56	6.2	8.7	37	0.9	2.3
95	4.5	19.7	94	6.1	14.9	67	6.6	6.0
110	8.8	26.3	95	2.4	19.1	78	8.4	13.5
137	7.0	34.2	105	1.8	21.2	80	2.1	18.8
143	3.2	39.3	107	7.0	25.6	111	8.5	24.1
145	10.7	46.3	136	6.4	32.3	131	4.3	30.3
146	6.9	55.1	136			140	2.7	34.0
149	2.9	60.0	139	4.4	37.7	149	3.5	37.1
184	3.3	63.1	140	5.7	42.8	151	4.7	41.2
228	6.0	67.7	157	2.6	46.9	162	3.9	45.5
229	5.2	73.3	158	2.4	49.4	166	5.5	50.2
• 245	7.7	79.8	172	1.2	51.2	185	1.7	53.8
245			175	2.4	53.0	189	1.2	55.2
277	7.0	87.1	187	4.5	56.5	193	4.9	58.3
284	6.6	93.9	192	5.7	61.6	213	4.3	62.8
290	3.0	98.7	203	2.2	65.5	214	3.3	66.7
			211	2.2	67.7	238	2.4	69.5
			215	3.6	70.6	241	2.9	72.2
			216	0.6	72.7	263	3.4	75.3
			223	3.9	75.0	273	1.4	77.7
			234	2.7	78.3	291	4.9	80.9
			248	2.2	80.7	292	1.8	84.2
			253	4.1	83.9	298	4.4	87.3
			253			351	3.3	91.2
			270	3.9	87.9	361	2.9	94.3
			290	1.8	90.7	370	2.3	96.9
			332	4.9	94.1	397	1.9	99.0
			337	3.9	98.5			

• In a number of cases, 2 fractions of identical *DP* were obtained. The values for these fractions are combined in columns 2 and 3.

In figure 1, the values of $I(P)$ are plotted as ordinates against the corresponding *DP* values as abscissas, for each of the three fractionations. The integral weight-distribution curves shown in this figure appear to show a slight displacement toward the higher *DP* values in the second and third fractionations as compared with the first. This is particularly noticeable at the upper ends of the curves. It therefore appears that a precise estimation of the distribution of chain-lengths in the starting material can be obtained only by the use of a relatively thorough fractionation procedure. The improvement of the homogeneity of the individual fractions as the fractionation was continued was indicated by the fact that separation became increasingly difficult, because the size of the precipitate was increasingly more sensitive to the quantity of alcohol added.

It must be pointed out that after the procedure described above, the fractions are not homogeneous; their homogeneity has, however, been greatly improved. Since relatively little further improvement is to be expected on continued fractionation beyond this point [8], the present experiments were limited to three fractionations.

The differential distribution curve shown in figure 2 was obtained from the smooth integral weight-distribution curve for the second and third fractionations (solid line, fig. 1). The tangents to this smooth curve (estimated graphically) are plotted as the ordinates in figure 2, against the corresponding *DP* values as the abscissas. Since the material in the first fraction is not included for reasons discussed later, the distribution of chain-lengths in the starting material is not precisely represented. The inclusion of this fraction would raise the curve slightly in the region of higher *DP*'s.

In marked contrast with the other fractions, the first fraction precipitated in a fibrillar form, which after centrifuging or long standing acquired gel-like properties. The precipitate was not completely soluble in acetone or Methyl Cellosolve, and for this reason, an esti-

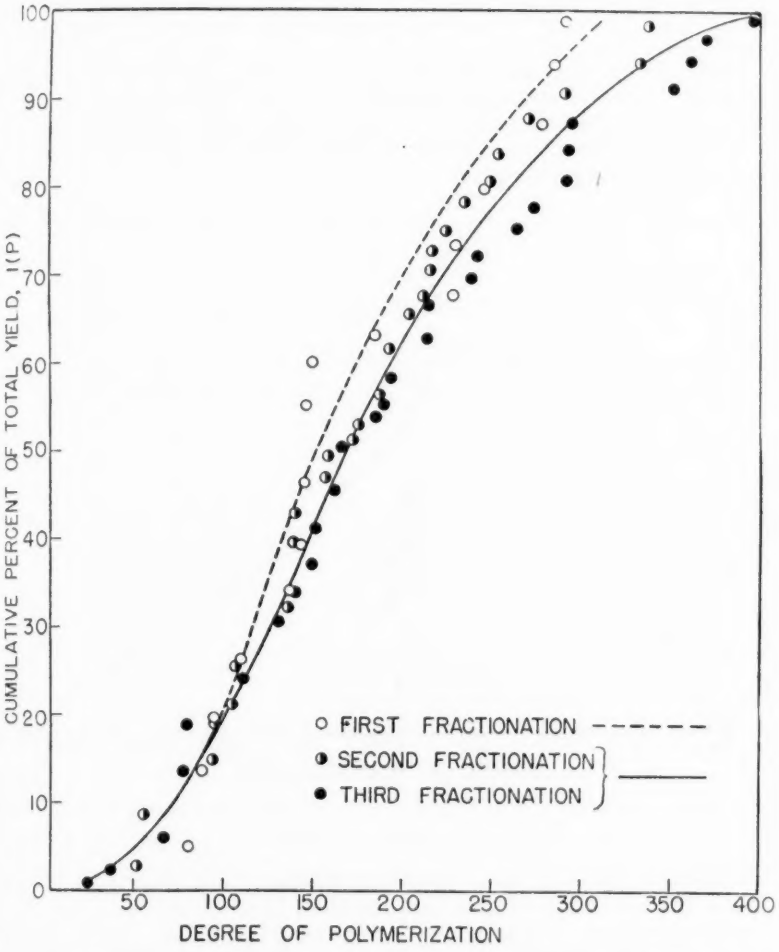

FIGURE 1.—*Integral weight-distribution diagrams, representing the results of the three fractionations of a cellulose acetate.*

The first fractions are omitted. The ordinates represent the cumulative percentages of the total yield included at a given *DP*. For complete explanation, see the text.

mate of its *DP* was not obtained. This fraction contained a large proportion of the ash (see table 1) and the haze-producing materials of the entire starting material, which is in agreement with the results of other investigators [1, 9, 10]. Films and solutions prepared from

this fraction were characterized by their very bad haziness in contrast with those prepared from the other fractions. These results suggest that an improvement in the clarity of films might be effected by a rough fractionation to remove a small percentage of the starting material. Spectroscopic analysis indicated that the ash consisted principally of calcium and to a lesser extent of magnesium, iron, aluminum, and zinc. In addition, the first fraction contained 0.11 percent of SO_4.

Further examination of this material indicated that it could be separated into an acetone-soluble fraction, a chloroform-soluble fraction, and a fraction which was insoluble in both solvents. It is of interest to note that the last of these fractions contained a large proportion of the total ash.

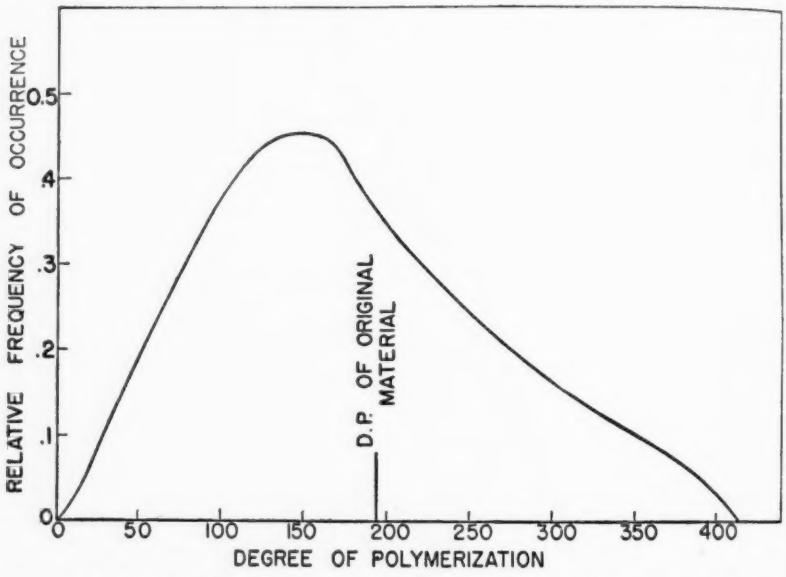

FIGURE 2.—*Differential distribution curve for the cellulose acetate used in this work.*
The first fractions are omitted.

The properties of the remaining fractions are shown in table 2. With the exception of the first fraction, the ash contents are in all cases very low. Similarly, with the exception of the three fractions of lowest *DP*, the acetyl contents are also identical with that of the starting material within the experimental error. The somewhat high acetyl contents of these three fractions may be explained by the presence of an extra esterifiable hydroxyl group on the glucose residue on one end of each chain. The influence of this extra functional group is not noticeable except in the fractions of very low *DP*, when it becomes an appreciable proportion of the total number of hydroxyl groups. The results therefore indicate that with the exception of the first fraction, the separation has apparently been primarily with respect to chain-length.

TABLE 2.—*Properties of the starting material and the fractions of cellulose acetate*

Fraction	Specific viscosity at—		*DP*	Acetyl content	Ash content	Melting point *
	25.1° C	60.6° C				
				Percent	*Percent*	° *C*
Starting material	0.498	0.362	194	38.6	0.06	250
1				38.6	.33	
2	1.019	.687	380	38.5	.06	255
3	0.921	.626	345	38.5	.03	253
4	.770	.531	291	38.5	.07	255
5	.699	.473	262	38.5	.07	255
6	.630	.428	236	38.3	.04	257
7	.550	.390	211	38.4	.03	254
8	.520	.347	194	38.5	.03	253
9	.429	.313	167	38.6	.03	248
10	.382	.271	146	38.5	.02	255
11	.335	.239	129	38.7	.02	247
12	.303	.223	118	38.6	.05	248
13	.197	.156	81	38.9	.02	246
14	.171	.128	68	39.0	.00	242
15	.074	.058	30	39.3	.04	237

* We are indebted to F. D. Pilgrim and W. O. Kearse, of the Tennessee Eastman Corporation, for making the melting-point measurements reported in this table.

As further means of characterizing the fractions, a number of solubility measurements were made, the results being shown in figure 3.

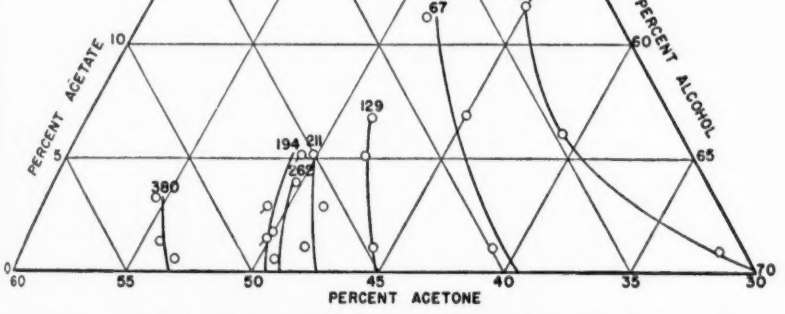

FIGURE 3.—*Phase diagram, showing some of the solubility relationships of the cellulose acetate and several of its fractions.*

Fractions, ○; starting material, ○. For complete description, see text. The number above each curve represents the *DP* of the material.

The procedure involved the titration with absolute ethyl alcohol of solutions of different concentrations of the acetate samples in acetone at 21° C. The weight composition of the solution when the first permanent cloud appeared is represented by a point on the diagram. The results indicate that a better separation can be obtained in dilute solutions, since the curves are more widely separated in the region of low concentrations. In addition, the wider relative separation of the curves for materials of lower *DP*'s indicates that more thorough fractionation would be expected for the materials of lower molecular weight. These results are consistent with the conclusions reached by Schulz on theoretical grounds [8, 11]. The curve for the starting material is, of course, displaced from the position that would be

occupied by a fraction of corresponding average *DP*, since it contains a large proportion of materials of high molecular weight. It is interesting to note, however, that this displacement is considerably less than might have been expected. Thus, the curve for the starting material might perhaps have been expected to fall near that for the fraction of *DP* 380, since some of this fraction is in the starting material. The fact that it does not, indicates that the presence of smaller chains apparently increases the solubility of the long-chain material.

The authors are indebted to Albert Bartovics for having made the viscosity measurements reported in this paper.

IV. REFERENCES

[1] H. M. Spurlin, Ind. Eng. Chem **30,** 538 (1938).
[2] H. Mark, Paper Trade J. **113,** 34 (1941).
[3] Eastman Cellulose Acetate and Cellulose Triacetate, (Tennessee Eastman Corporation, Nov. 1939).
[4] E. O. Kraemer, Ind. Eng. Chem. **30,** 1200 (1938).
[5] E. O. Kraemer, J. Franklin Inst. **231,** 1 (1941).
[6] H. Staudinger, Die Hochmolekularen Organischen Verbindungen, (J. Springer, Berlin, 1932).
[7] L. B. Genung and R. C. Mallatt, Ind. Eng. Chem., Anal. Ed. **13,** 369 (1941).
[8] G. V. Schulz, Z. physik. Chem. [B] **47,** 155 (1940).
[9] F. Ohl, Kunstseide **12,** 468 (1930).
[10] H. Rocha, Kolloid Beihefte **30,** 230 (1930).
[11] G. V. Schulz, Z. physik. Chem [A] **179,** 321 (1937).

WASHINGTON, June 26, 1942.

U. S. Department of Commerce — National Bureau of Standards

RESEARCH PAPER RP1491

Part of Journal of Research of the National Bureau of Standards, Volume 29, August 1942

OXIDATION OF CELLULOSE: THE REACTION OF CELLULOSE WITH PERIODIC ACID

By Henry A. Rutherford, Francis W. Minor, Albert R. Martin, and Milton Harris[1]

ABSTRACT

An investigation has been made of the mode of attack of cellulose by periodic acid during the early stages of the oxidation (that is, oxidation of approximately 1 percent of the glucose residues). Under these conditions, it is shown that the reaction is confined to oxidation of the secondary hydroxyl groups to aldehyde groups, and results in a rupture in the carbon chain between carbon atoms 2 and 3 of the glucose unit. In accordance with this mechanism it is shown that two moles of aldehyde groups are produced for each mole of oxidant consumed. The aldehyde groups of the periodic acid-oxycellulose can readily be converted to carboxyl groups, titration of which provides an independent check on the content of the former.

Periodic acid-oxycellulose is characterized by its susceptibility to further attack by alkaline solutions. The alkali-sensitivity of these materials, as measured by solubility in hot dilute sodium hydroxide and by cuprammonium fluidity, appears to be proportional to the content of aldehyde groups. However, upon conversion of all of the aldehyde groups to carboxyl groups, the alkali-lability practically disappears. The results suggest that the sensitivity of periodic acid-oxycellulose to alkali does not depend solely on the rupture of the glucose ring between carbon atoms 2 and 3, but is related to the specific instability towards alkali of the dialdehyde formed during the oxidation.

CONTENTS

	Page
I. Introduction	131
II. Experimental procedure	133
1. Preparation of materials	133
2. Methods	133
III. Results and discussion	135
1. Estimation of oxidant consumed by cellulose	135
2. Course of oxidation of cellulose by periodic acid	136
3. Relation between aldehyde content and alkali-sensitivity	137
IV. References	140

I. INTRODUCTION

Cellulose can undergo many modifications in oxidizing media, and accordingly the properties of oxidized celluloses, generally referred to as oxycelluloses, vary widely. It appears that the attack on cellulose by oxidizing agents is principally confined to three points: (1) the aldehyde end-groups, of which there are few, if any, in native cellulose [1] [2] and which can be oxidized to carboxyl groups, (2) the primary alcohol groups which can be oxidized to the aldehyde or carboxyl stage, and (3) the glycol group (the 2,3-dihydroxy group) which can be oxidized to the ketone, aldehyde, or carboxyl stage. Until recently,

[1] Research Associates, at the National Bureau of Standards, representing the Textile Foundation.
[2] Figures in brackets indicate the literature references at the end of this paper.

it has generally been assumed that the oxidative attack occurred principally at the primary alcohol groups, a hypothesis which gave rise to considerable confusion. This hypothesis did not adequately explain the different behaviors of oxycelluloses prepared with various oxidizing agents. Thus, whereas Clibbens and Ridge [2] were able to show that treatment of cotton with any acid resulted in the same corresponding increase in cuprammonium fluidity and decrease in tensile strength, a similar general relationship did not exist for all types of oxycellulose. The data in table 1 (from reference [2]) illustrate this point. This apparent anomaly was indeed disturbing, since both the fluidity and strength of cellulosic materials are regarded as functions of molecular chain length.

As a solution to the difficulty, Davidson [3, 4] made the important suggestion, which he later supported by extensive experimental work [5], that some types of oxidation do not result in direct scission of the chain molecules but reduce the chemical stability of some of the linkages in the cellulose chain towards alkali. Types of oxidation which do not rupture the chains would have little or no effect on strength, but if these types of modification result in a material which is unstable towards alkali, the fluidity in the alkaline cuprammonium solution will be high. This then would explain the lack of an identical correlation between strength and cuprammonium fluidity for all types of oxycelluloses similar to the correlation existing for all types of hydrocelluloses.

TABLE 1.—*Relation between cuprammonium fluidity and tensile strength of various hydrocelluloses and oxycelluloses*

Cuprammonium fluidity	Loss in tensile strength resulting from—		
	Treatment with any acid	Treatment with $K_2Cr_2O_7+(COOH)_2$	Treatment with NaOCl
Rhes	*Percent*	*Percent*	*Percent*
10	10	1	7
20	34	6	25
30	58	16	47

Davidson's hypothesis was lent considerable support by the investigations of Jackson and Hudson [6], who showed that in the oxidation of cellulose by periodic acid, cleavage of the glucose ring between carbon atoms 2 and 3 occurred with the conversion of the secondary alcohol groups to aldehydes, according to the following scheme:

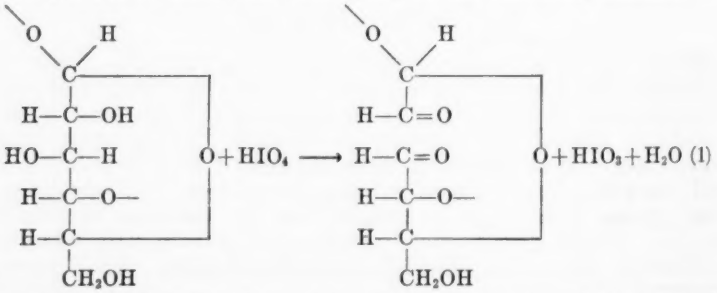

A reaction of this type does not result in a scission of the molecular chains, and hence little, if any, loss in strength occurs.

While it appears that periodic acid (at least during the early stages of oxidation) and a few other oxidizing agents may be quite specific in their attack on cellulose, the action of many oxidizing agents to which cellulose is frequently exposed is more complex and less understood. A major difficulty in attempts to ascertain the exact course of the various types of oxidation has been the lack of analytical methods of sufficient specificity and sensitivity to determine quantitatively the various groups which may be formed and to allocate them to their proper positions in the glucose residues. Recently, however, a number of new methods have been developed and accordingly a series of studies of the course of oxidation of cellulose by various reagents was undertaken. The present paper reports the results obtained with periodic acid.

II. EXPERIMENTAL PROCEDURE

1. PREPARATION OF MATERIALS

Raw cotton was dewaxed by extraction with hot alcohol for 24 hours and then washed thoroughly with cold distilled water. The cotton was further purified by boiling with a 1-percent solution of sodium hydroxide for 8 hours; the procedure was essentially the same as that described by Corey and Gray [7], except that the apparatus of Worner and Mease was used [8].

The oxycelluloses were prepared by steeping samples of the purified cotton in solutions of periodic acid buffered with sodium acetate at pH 4.6. The extent of oxidation was controlled by varying either the concentration of periodic acid or the time of treatment. In most cases, however, a concentration of about 0.025 *N* periodic acid was employed. All treatments were carried out with the ratio of cotton to solution of 1 to 50 and a temperature of 25° C$\pm$0.1°. Immediately following the oxidation, the samples were rapidly washed in cold distilled water until a test of the washing for periodate was negative. The materials were then conditioned in the dark, in a room maintained at a temperature of 21° C and 65-percent relative humidity. Under these conditions, it was found that the properties of the oxycellulose did not change over prolonged periods of time.

2. METHODS

The concentration of periodic acid was determined by titration of an aliquot of the solution with sodium arsenite after the addition of sodium bicarbonate and potassium iodide, according to the method of Müller and Friedberger [9]. The number of milliequivalents of oxidant consumed per gram of dry cellulose was calculated from the difference in the amount of arsenite required by a control solution, and by an identical solution containing the sample.

The aldehyde content of the oxycellulose was determined by a modification (described below) of the iodometric method as used for hydrocellulose by Martin, Smith, Whistler, and Harris [1]. This determination depends on the oxidation of the aldehyde groups to carboxyl groups by iodine. The amount of iodine consumed by the oxycellulose was determined as follows: 10 ml of 0.05 *M* sodium borate solution having a pH of 9.2 at 25° C was pipetted into a 125-ml glass-stoppered Erlenmeyer flask and then placed in a thermostat at 25° C. 20 ml of 0.03 *N* iodine solution containing 20 g of potassium iodide per

liter, previously brought to 25° C, was then added and approximately 100 mg of the sample to be titrated was immediately introduced. (With this amount of sample, it is important that the oxycellulose contain no more than 0.15 millimole of aldehyde groups per gram; the ratio of milliequivalents of iodine to milliequivalents of aldehyde should not be below 25). After 6 hours, 15 ml of 0.1 *N* HCl was added and the iodine remaining in the solution was measured by titration with standard sodium thiosulfate (about 0.013 *N*) with starch as the indicator. Blank determinations on identical solutions which did not contain cotton were made. From the difference in amount of thiosulfate required by the blank solution and by the solution containing the sample, the milliequivalents of iodine consumed per gram of dry sample were calculated. As explained elsewhere [1], a correction for the iodine consumed by purified cotton in the same time interval must be applied in calculating the aldehyde content of the oxycellulose.

An independent check on the iodine method was made by analyzing for carboxyl content after oxidation of the aldehyde groups with chlorous acid. This substance is particularly useful for this purpose in view of the selective action towards aldehyde groups observed by Jeanes and Isbell [18] in their work on the oxidation of certain aldoses. A 0.4 *M* solution of chlorous acid was prepared immediately before use by the acidification of a solution of technical sodium chlorite to pH 2.5 with the appropriate quantity of glacial acetic acid. The oxycellulose was treated with this solution at 25° C.

The carboxyl content was determined by measuring the amount of silver bound by the fiber from a solution of silver *o*-nitrophenolate according to the procedure described by Sookne and Harris [10].

Two types of fluidity measurements were made. The first consisted in measurements on dispersions of cellulose in cuprammonium hydroxide solution by the method of Clibbens and Geake [11] as modified by Mease [12]. The second involves the nitration of the cellulose, as recommended by Berl [13], and the determination of the fluidities of dispersions of the nitrocellulose in acetone. The necessity for making both types of fluidity measurements was made clear in the extensive investigations by Davidson, who showed that a measure of the true chain length of certain oxycelluloses containing alkali-sensitive linkages could not be obtained by dissolution of the material in an alkaline solvent such as cuprammonium hydroxide solution. In order to avoid the degradation that occurs when the oxycellulose is dispersed in such alkaline solutions, recourse was had to the nitrocellulose method.

The nitrocellulose fluidities were calculated from the times of flow of solutions through an Ostwald viscometer at 20° C. To reduce the time required to make measurements, solutions containing 0.1 g (rather than 0.25 g) of nitrocellulose per 100 ml of acetone were used. To render the results comparable to the findings published by others, fluidities were calculated for solutions having a concentration of 0.25 g per 100 ml, by means of Hess and Philipoff's modification [14] of Baker's equation:

$$\eta^{1/8}_{rel}=1+\frac{[\eta]}{8}c,$$

in which η_{rel}=relative viscosity; $[\eta]$=a constant; c=concentration in g/100 ml of solvent.

The fluidities were readily calculated from the η_{rel}. The fluidity of the solution having the concentration of 0.25 g per 100 ml of solvent is referred to as the "nitrocellulose fluidity." The nitrocelluloses derived from samples which had consumed more than 0.05 milliequivalent of oxidant per gram were not completely soluble in acetone [15]. The nitrocellulose fluidity of the soluble portion was determined after removing the insoluble material by centrifuging and making the necessary corrections for concentration. It is recognized that the solution thus obtained is not representative of the entire material. It is noteworthy that when the aldehyde groups are oxidized to carboxyl groups, the derived nitro-celluloses are completely soluble.

The sensitivity of periodic acid-oxycellulose to alkalies is indicated by the increase in nitrocellulose fluidity that occurs when such materials are treated with dilute sodium hydroxide [15]. Preliminary experiments showed that the maximum increase in nitrocellulose fluidity was obtained by a 1-hour boil (under reflux) in 0.25 *N* NaOH, the ratio of sample to solution being 1 to 200. The scission of all alkali-labile linkages is completed under these conditions. The "alkali boil" referred to hereafter represents such a treatment, and the loss in weight that occurs during the treatment, expressed in percentage, is hereafter referred to as "alkali solubility." It should be further pointed out that while the nitrocellulose fluidity does reach a maximum and constant value after a 1-hour boil in the alkali, the alkali-solubility value rises rapidly during the first hour but continues to rise at a very much slower and diminishing rate thereafter. Even after 8 hours the slow dissolution of the cellulose continues to take place.

III. RESULTS AND DISCUSSION

1. ESTIMATION OF OXIDANT CONSUMED BY CELLULOSE

As indicated in figure 1, the consumption of periodic acid during the early stages of oxidation (that is, the oxidation of less than 2 percent of the glucose residues) is directly proportional to time. It was observed, however, that an initial rapid disappearance of a small

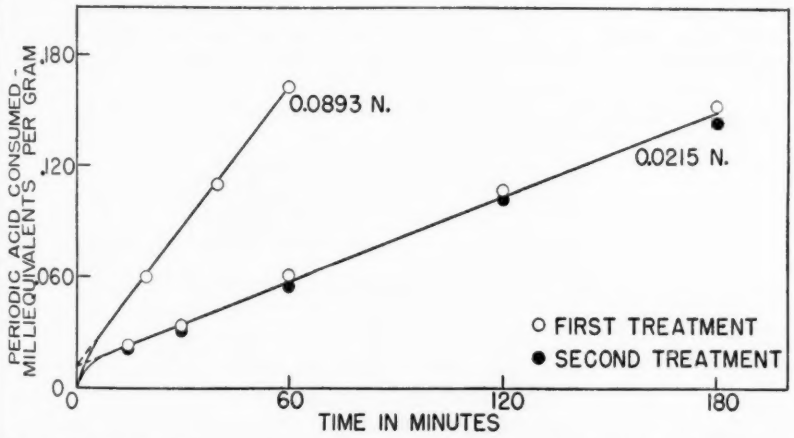

FIGURE 1.—*Rate of consumption of periodic acid by purified cotton from solutions at* pH *4.6 and 25° C.*

portion of the oxidant always occurred. This could conceivably be due either to the oxidation of some rapidly oxidizable material, or to some unexplained adsorption of the oxidant by the fibers. That the latter is the case was indicated by the following experiment. A sample of purified cotton was subjected to two consecutive oxidations with a 0.0215 *N* solution of periodic acid at pH 4.6. The results shown in the lower curve in figure 1, indicate the absence of an easily oxidizable substance, since the same initial rapid disappearance of periodic acid was observed on the second treatment. As also indicated in the figure, a fourfold increase in the concentration of periodic acid did not appreciably alter the amount of oxidant initially taken up. Extrapolation of the straight-line portion of the curves to zero time indicated that 0.012 milliequivalent of periodic acid per gram of cellulose has apparently been adsorbed by the fibers in this manner, and accordingly this amount is deducted from the total apparent amount of oxidant consumed in order to obtain a measure of the periodic acid which has been utilized in the oxidation of the cellulose.

The adsorption noted is not unique with periodic acid, since similar adsorptions by cellulose of other oxidizing agents such as hypochlorite [16], chromic acid [17], and iodine [1] have been reported in the literature.

2. COURSE OF OXIDATION OF CELLULOSE BY PERIODIC ACID

It would be expected that complete oxidation of cellulose by periodic acid, according to eq 1, would require one atom of oxygen per glucose unit. However, as shown by Jackson and Hudson [6], the actual consumption of oxidant considerably exceeds this theoretical amount, a fact which led these investigators to the conclusion that secondary reactions undoubtedly occurred during prolonged contact of the cellulose with the oxidant. This conclusion was supported by the work of Davidson [15], who found that on extensive oxidation appreciable quantities of formaldehyde, formic acid and carbon dioxide were formed.

On the other hand, it appears that during the early stages of oxidative attack, the reaction does proceed principally according to eq 1. The data in table 2 clearly show that in this range of oxidation one aldehyde group is produced for each equivalent of periodic acid consumed; i. e., two aldehyde groups per mole of periodic acid.

TABLE 2.—*Aldehyde content of periodic acid-oxycelluloses*

Net oxidant consumed	Aldehyde content	Total glucose units oxidized, calculated from aldehyde content
Milliequivalents/g	*Millimoles/g*	*Percent*
0.043	0.041	0.33
.064	.069	.56
.081	.081	.66
.095	.097	.79
.115	.113	.92
.153	.156	1.3

The aldehyde groups in oxycellulose were determined by measuring the iodine consumed during the quantitative oxidation of aldehyde groups to carboxyl groups, according to the modified procedure described in section II, 2. The method is similar to that used in the estimation of aldehyde groups in hydrocellulose [1] and it was expected that, similarly, an analysis for carboxyl groups in the fiber after treatment with iodine would also demonstrate that the consumption of iodine was due to reaction with aldehyde groups. Unfortunately, when the oxycellulose was placed in the mildly alkaline buffer used in the iodine titration, reducing groups were dissolved, so that the carboxyl groups left in the fiber could not be equivalent to the reducing groups originally present. However, a check of the oxidation reaction was made by the method described below.

The recent work of Jeanes and Isbell [18], showing that aldoses are readily oxidized to the corresponding aldonic acids by treatment with chlorous acid at pH 2.2 provided a means for oxidation in acid solution. Thus, treatment of the samples for 40 to 60 minutes with chlorous acid resulted in quantitative oxidation of the aldehyde groups to carboxyl groups as shown in table 3. Furthermore, the estimation of the latter affords an independent check on the aldehyde content obtained by the iodine method.

TABLE 3.—*Aldehyde and carboxyl contents of periodic acid-oxycellulose after chlorous acid treatment*

1	2	3	4
Initial aldehyde content	Aldehyde content after $HClO_2$	Carboxyl content after $HClO_2$	Sum of columns 2 and 3
Millimoles/g	*Millimoles/g*	*Millimoles/g*	*Millimoles/g*
0.041	0.000	0.037	0.037
.095	.000	.097	.097
.156	.010	.141	.151
.041	.011	.026	.037
.095	.012	.086	.098
.156	.022	.125	.147

In samples where the oxidation of the aldehyde groups was not completed, it may be seen that the sums of the carboxyl and aldehyde contents after the chlorous acid treatments agree within the experimental error with the aldehyde contents of the periodic acid-oxycelluloses found by the idodine method of analysis. This may be taken to indicate that no new reducing or acidic groups are formed in the oxycellulose as a result of the chlorous acid treatment. Finally, it was found that a similar chlorous acid treatment had no measurable effect on purified cotton cellulose.

3. RELATION BETWEEN ALDEHYDE CONTENT AND ALKALI-SENSITIVITY

As already noted by Davidson, the most characteristic property of the periodic acid-oxycelluloses is the ease with which they are degraded by alkaline solutions. This instability is explained by the fact that rupture of a glucose residue according to eq 1 results in the formation of alkali-sensitive linkages which undergo a scission in

alkaline solutions. Thus, Davidson was able to show that periodic acid-oxycelluloses exhibited low nitrocellulose fluidities (long chains) and high cuprammonium fluidities (short chains). When the samples were subjected to an alkali boil, the nitrocellulose fluidities were considerably increased, but the cuprammonium fluidity remained unchanged. In other words, the treatment with alkali resulted in scission of all of the alkali-labile linkages, a process that is also accomplished in the highly alkaline cuprammonium solution.

Further support for this explanation was obtained in the present investigation. As shown in figure 2, there is only a slight increase in

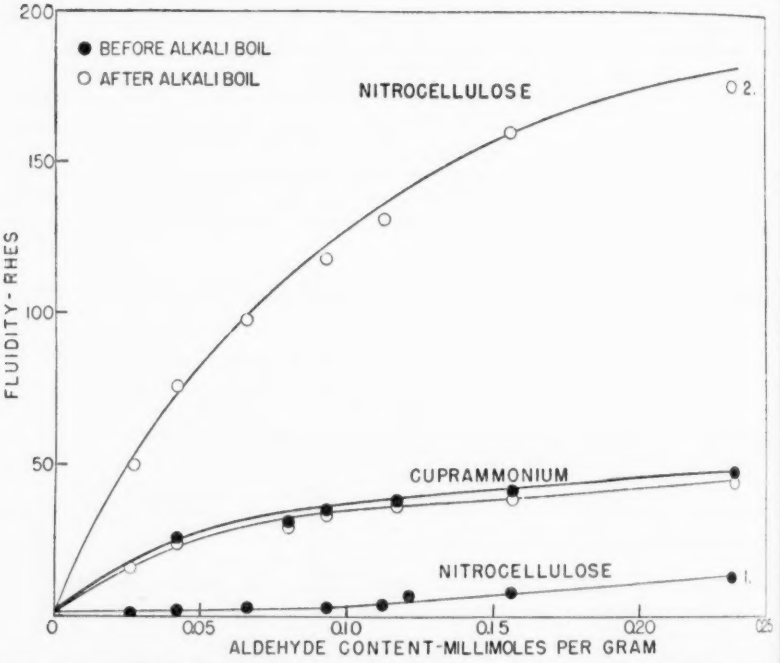

FIGURE 2.—*Fluidities of periodic acid-oxycelluloses, oxidized to various aldehyde contents, before and after boiling in 0.25 N* NaOH *for 1 hour.*

nitrocellulose fluidity with increase in aldehyde content (curve 1) of a series of oxycelluloses, indicating that although an appreciable number of glucose rings had been ruptured, the molecular chain length had not been correspondingly shortened. That the chains contained alkali-labile linkages, however, is suggested by the high nitrocellulose fluidities of a similar set of samples after the alkali boil treatment (curve 2). In contrast, the cuprammonium fluidities (fig. 2) increased rapidly with increasing aldehyde content, regardless of whether the samples were subjected to preliminary alkali treatment, indicating as pointed out earlier, that scission of all alkali-labile linkages in this type of oxycellulose is completed during dissolution of the oxycellulose in cuprammonium solution.

The question arises as to whether the sensitivity to alkalies of this type of oxycellulose depends on the rupture of the glucose ring between carbon atoms 2 and 3 or on a specific instability towards alkali of the dialdehyde formed in the oxidation process. In order to throw some light on this question, samples of oxycelluloses were treated with chlorous acid in order to oxidize the aldehyde groups to carboxyl groups.

As shown in figure 3, the effect of this treatment in every

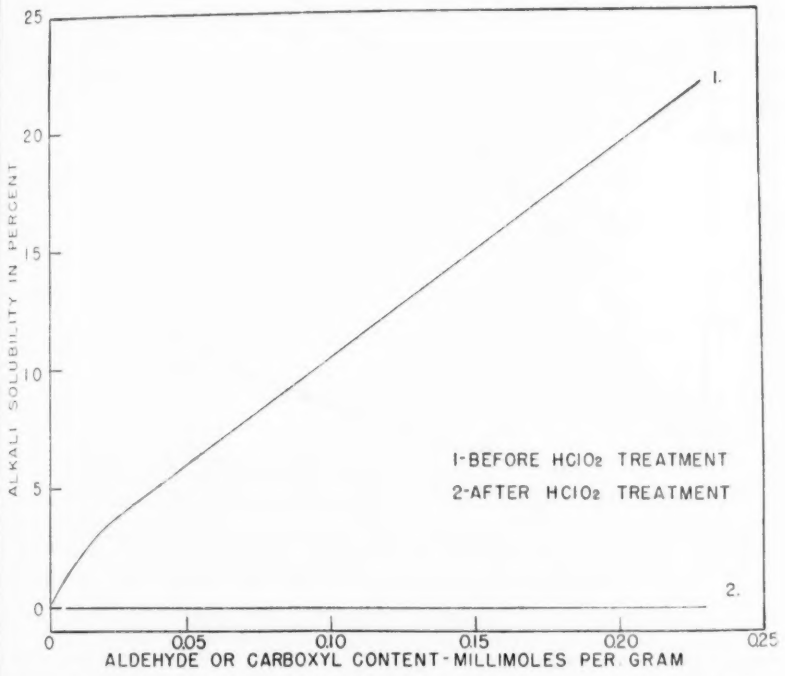

FIGURE 3.—*Percentage weight loss caused by treatment of oxycelluloses with boiling 0.25 N* NaOH *for 1 hour:*

Curve 1. Periodic acid-oxycellulose; percentage weight loss plotted against aldehyde content.
Curve 2. Periodic acid-oxycellulose oxidized further with chlorous acid; percentage weight loss plotted against carboxyl content.

case was to lower the alkali-solubility to nearly zero. If the alkali-solubility values represented a true solubility phenomenon, it might have been expected that conversion of aldehyde to carboxyl groups would have resulted in an increase in solubility. Since this is not the case, it is concluded that the relatively high alkali-solubilities of the original oxycelluloses are related to a specific instability, involving the presence of aldehyde groups, of the products toward alkali. Further support for this conclusion is found in figure 4. Whereas the nitrocellulose fluidities of the oxycelluloses are greatly increased by an alkali boil, treatment of the oxycellulose with chlorous acid yielded products whose nitrocellulose fluidity was much less affected. The results leave little doubt that the sensitivity to

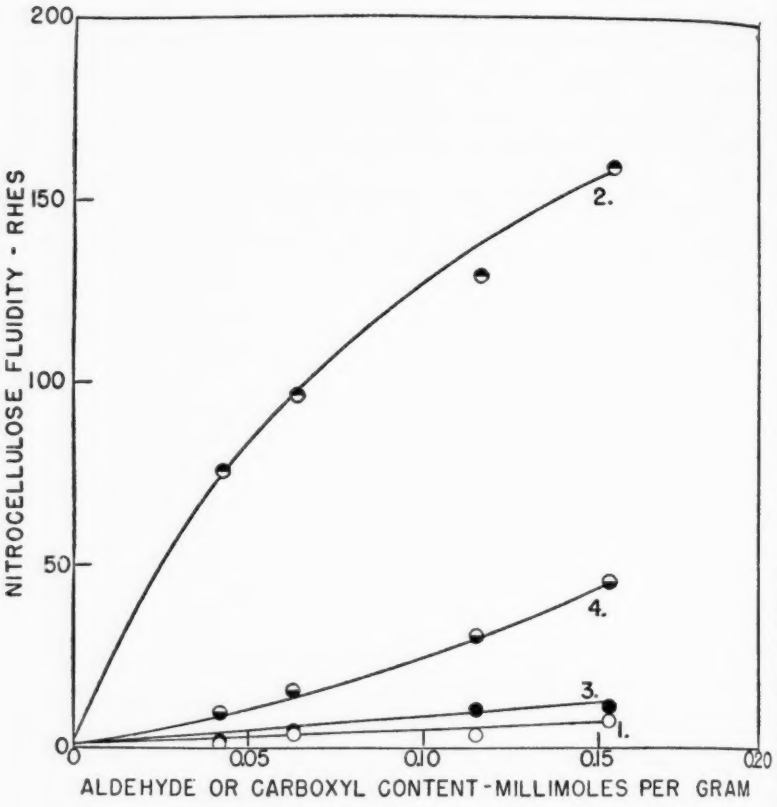

FIGURE 4.—*Nitrocellulose fluidities of periodic acid-oxycelluloses.*

Curve 1. Untreated oxycellulose; fluidity plotted against aldehyde content.
Curve 2. Oxycellulose after alkali boil; fluidity plotted against aldehyde content before boil.
Curve 3. Oxycellulose after chlorous acid treatment; fluidity plotted against carboxyl content.
Curve 4. Chlorous acid-treated oxycellulose after alkali boil; fluidity plotted against carboxyl content before boil.

alkali of these oxycelluloses does not depend solely on the rupture of the glucose ring between carbon atoms 2 and 3, but is related to the specific instability towards alkali of the oxidation product formed according to eq 1.

The authors are indebted to A. Eleanor Davis for assistance in making a number of the determinations reported in this paper.

IV. REFERENCES

[1] A. R. Martin, L. Smith, R. L. Whistler, and M. Harris, J. Research NBS **27,** 449 (1941) RP1432; Am. Dyestuff Rptr. **30,** No. 23, 628 (Nov. 10, 1941).
[2] D. A. Clibbens and B. P. Ridge, J. Textile Inst. **19,** T389 (1928).
[3] G. F. Davidson, J. Textile Inst. **25,** T174 (1934).
[4] G. F. Davidson, J. Textile Inst. **27,** P144 (1936).
[5] G. F. Davidson, J. Textile Inst. **29,** T195 (1938).
[6] E. L. Jackson and C. S. Hudson, J. Am. Chem. Soc. **58,** 378 (1936); **59,** 994 (1937); **59,** 2049 (1937); **60,** 989 (1938).

[7] A. B. Corey and H. L. Gray, Ind. Eng. Chem. **16,** 853 (1924).
[8] R. K. Worner and R. T. Mease, J. Research NBS **21,** 609 (1938) RP1146.
[9] E. Müller and O. Friedberger, Ber. deut. chem. Ges. **35,** 2652 (1902).
[10] A. M. Sookne and M. Harris, J. Research NBS **26,** 205 (1941) RP1370; Am. Dyestuff Rptr. **30,** 107 (1941); Textile Research **11,** 238 (1941).
[11] D. A. Clibbens and A. Geake, J. Textile Inst. **19,** T77 (1928.).
[12] R. T. Mease, J. Research NBS **22,** 271 (1939) RP1179; **27,** 551 (1941) RP1442.
[13] E. Berl, Ind. Eng. Chem., Anal. Ed. **13,** 324 (1941).
[14] K. Hess and W. Philipoff, Ber. deut. chem. Ges. **70B,** 639 (1937).
[15] G. F. Davidson, Shirley Inst. Memoirs **17,** 83 (1939–40); **18,** 69 (1941).
[16] W. Seck, Melliand Textilber. **13,** 314 (1932).
[17] G. F. Davidson, Shirley Inst. Memoirs **18,** 91 (1941).
[18] A. Jeanes and H. S. Isbell, J. Research NBS **27,** 125 (1941) RP1408.

WASHINGTON, June 12, 1942.

U. S. DEPARTMENT OF COMMERCE NATIONAL BUREAU OF STANDARDS

RESEARCH PAPER RP1492

Part of Journal of Research of the National Bureau of Standards, Volume 29, August 1942

A FLOW MANOSTAT FOR VARIOUS PURPOSES, INCLUDING THE CANDY TEST

By Max J. Proffitt

ABSTRACT

The flow manostat described in this paper is virtually a sensitive pressure-reducer in which the valve unit consists of a knife-edged circular orifice which is converted into an annular opening by means of a coaxial tapered core that floats upon a liquid surface which is depressed through contact with the gas at the regulated reduced pressure. Any change in the regulated pressure produces an axial movement of the core, thus expanding or contracting the area of the annular opening by an amount which is just sufficient to compensate approximately the effects of the change in the service pressure that induced the change in the regulated pressure. To minimize friction, the major diameter of the spindle or tapered part of the core is made slightly less than the diameter of the orifice. This allows the spindle to move its full length through the orifice without touching the edges of the orifice. Each valve unit has only a short range of variability in throughput capacity. Any reasonable capacity outside of this range can be obtained by substituting a valve unit of appropriate size in the same manostat. Each valve unit comprises an orifice plate with knife-edged opening (or else a pair of such plates), together with a properly fitting core having one spindle or two as required. The volume of flow always is governed by the discharge characteristics of the nozzle or fixed group of simultaneously operating nozzles served by the manostat. Any change in these characteristics will involve readjustment of the regulated pressure.

An experimental anostat equipped with a double, self-balancing valve unit conforming approximately with this design reduced a gas service pressure varying between the limits of 104 and 164 mm of water to a regulated pressure of 49.6 ± 0.5 mm of water, while serving three burners consuming a total of about 8 cubic feet of gas per hour.

CONTENTS

		Page
I.	Introduction	144
II.	General description and theory of operation	144
III.	Practical application and results obtained	151
IV.	Summary	154
V.	References	155

I. INTRODUCTION

The need of operating a gas burner at approximately a constant rate of heat output frequently is encountered in analytical procedures and in many other types of laboratory work. This requires the maintenance of virtually a steady pressure differential between the gas at the nozzle entrance of the burner and the atmosphere in which the burner is operating. Frequently the gas service pressure is subject to a degree of fluctuation which practically prohibits such procedures. The fluctuations come partly from variations in the pressure of the gas as it is delivered to the laboratory and partly from the intermittent drawing of the gas from the various outlets in the laboratory. Usually the upper and lower limits of the fluctuation are fairly well defined and the most frequent variation occurs over a smaller range of pressure differentials. The simplest means of meeting such circumstances is to provide a pressure regulator for the one particular burner or group of burners which is required to operate at a steady rate of heat output. Some of the commercial devices that are intended to maintain a constant pressure at the burner regardless of the pressure variations in the gas supply have rather consistently failed to perform the service, not only because of mechanical defects in their construction, but also because they were devised apparently without adequate attention to the principles involved. One of the simplest of these devices consists of a stopcock type of throttle linked to the bell of a small gasometer, which many have found aggravates rather than lessens the difficulty. To fill the need of an instrument which will function with the precision requisite for numerous purposes, including candy tests, the flow manostat described below was designed. Its field of usefulness, however, is not confined to the regulation of gas-burner performance. It can be used for the regulation of other gas flows of similar rates that are governed by nozzles, by capillaries, by tubular flow-meters, or by similar means under suitable pressures and pressure differentials.

II. GENERAL DESCRIPTION AND THEORY OF OPERATION

A variable annular orifice, U, constructed as indicated diagrammatically in figures 1 and 2, was chosen as the most feasible form of throttle valve among several that were considered for the purpose of regulating the flow of the gas through the manostat without excessive pressure losses. When carefully designed and constructed, this very simple form of restrictive orifice not only can be made mechanically practical but, as was demonstrated in numerous preliminary experiments, it is capable of yielding a performance that conforms approximately with most of the other requirements (p. 150). As compared, however, with an iris diaphragm, which apparently should present the most favorable form of opening for the purpose except for the mechanical difficulties involved in its construction and operation, the annular orifice has less latitude of practical variability in throughput capacity and presumably less favorable discharge characteristics. The supposed defects in discharge characteristics are attributed to the fact that the annular orifice presents much narrower clearances for the passage of the gas, and much greater areas of passage surfaces, per unit of cross-sectional area of opening, especially at the minimum throughput capacities. Presumably these drawbacks could prove

serious where deposits from the gas may be considerable, but in practice no trouble has been encountered.

The annulus is formed by providing a core in a circular knife-edged hole in a thin plate, *OP*, figure 1, which separates the entrance chamber, *E*, of the manostat from the expansion chamber, *R*, in which the regulated pressure differential, Δh_r, is set up as back-pressure derived principally from the resistance of the burner nozzles at *N*. In operation, the annulus is varied automatically as to width by means of the axial movement of its core. The core comprises a tapered spindle, *V*, arranged to float, coaxially with the hole in the plate, *OP*, upon a "depressed hydrostatic column" which is in contact with the gas in

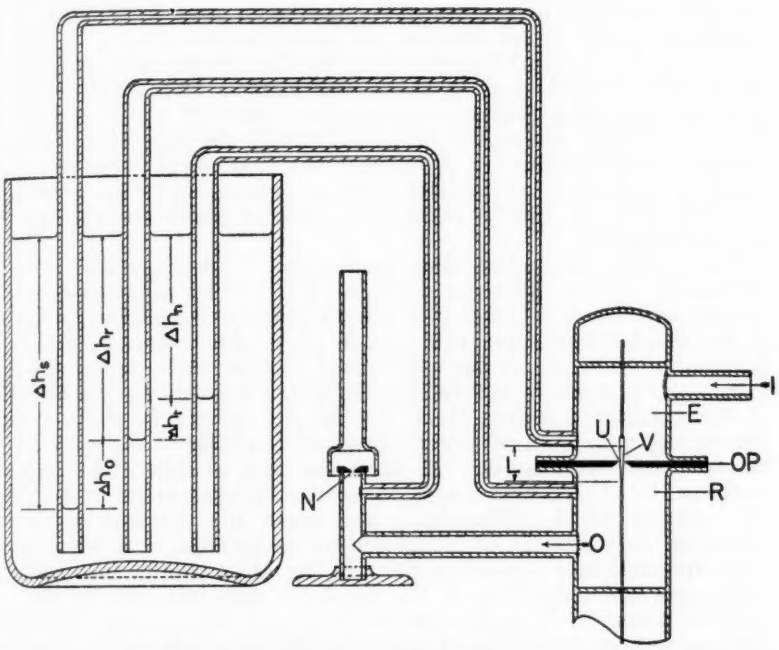

FIGURE 1.—*Relations among pressure differentials, flow-manostat valve, and gas burner nozzle.*

For detailed description, see p. 146.

the expansion chamber and, through a submerged connection, is balanced against another hydrostatic column of the same liquid in contact with the atmosphere. In other words, the spindle in effect floats upon a liquid surface which, because of the pressure of the gas in the expansion chamber above it, is depressed relative to the surface of the main body of the liquid in a connecting reservoir that is open to the atmosphere. The essential features of the arrangement are illustrated at *A* and *B* in figure 2.

Operation of the manostat sets up various static pressure differentials in the current of gas passing through it. Some of these can be used to advantage in explaining the action and performance of the instrument. To illustrate visually the interrelationships of the

differentials of principal interest, and the relationships of each to the apparatus, reference again is made to figure 1, directing special attention to the gages represented in the left-hand part of the diagram. Of the five differentials represented, the service differential, Δh_s, the regulated differential, Δh_r, and the nozzle differential, Δh_n, are all referred to atmospheric pressure as the base, while the two remaining are referred to other bases. Notice that in the last sentence and in most of the remaining text the descriptive terms for these differentials are abridged to avoid repetition of the words not needed to identify the values.

The regulated differential is the most important in the present discussion because the purpose of the manostat is to keep it virtually constant, and because such small changes as do occur in its magnitude supply the power for effectuating the compensations that maintain it. It exceeds the nozzle differential, Δh_n, by the amount of the transport differential, Δh_t, which is the head consumed in transferring the gas from the expansion chamber through the outlet, *O*, to the entrances, *N*, of the burner nozzles. Hence Δh_t is equal to the regulated pressure, referred to the pressure at *N* in place of atmospheric pressure. The nozzle pressure, Δh_n, is the back pressure equivalent to the resistance encountered in forcing the regulated current of gas through the nozzle or nozzles at *N*.

The orifice differential, Δh_o, the second most important in this discussion, is the difference between the service pressure and the regulated pressure. Hence it is equal to the service pressure referred to the regulated pressure as a base in place of atmospheric pressure. Ordinarily, therefore, it has a fluctuating value, for it represents the loss in static pressure suffered by the gas in negotiating the obstacle of the modulated orifice, *U*, of the throttle valve. Its value at any instant depends upon the service pressure available at the moment in the gas entrance chamber, *E;* upon the rate of flow of the gas as governed by the discharge capacity of the burner nozzles at *N* under the existing nozzle differential, Δh_n; upon the existing restrictive effects of the orifice, *U*, as modulated by the spindle, *V*, in accordance with the particular vertical position of the valve core at that instant; and upon the magnitude of the regulated pressure, Δh_r, in the expansion chamber, *R*, against which the flow of the gas into *R* occurs. The percentage deviations of the orifice differential from its mean are bound to exceed the percentage deviations of the service-pressure differential from the mean service differential. This is evident from the fact that the service differential, as the diagram indicates, is represented by

$$\Delta h_s = \Delta h_o + \Delta h_r;$$

for most of the variability in Δh_s has to be absorbed by the orifice differential, so long as Δh_r is virtually constant and the mean value of Δh_o always is smaller than the mean value of the service differential.

Construction diagrams, representing generalized vertical sections of the manostat alone, in two slightly different forms, are presented at *A* and *B* in figure 2. The form illustrated at *B* has a single throttle valve, that illustrated at *A* has a double valve arranged as indicated in the enlarged section at *C*. In sections *B* and *A*, the float wells, *FW*, contain the hydrostatic columns which support the orifice cores

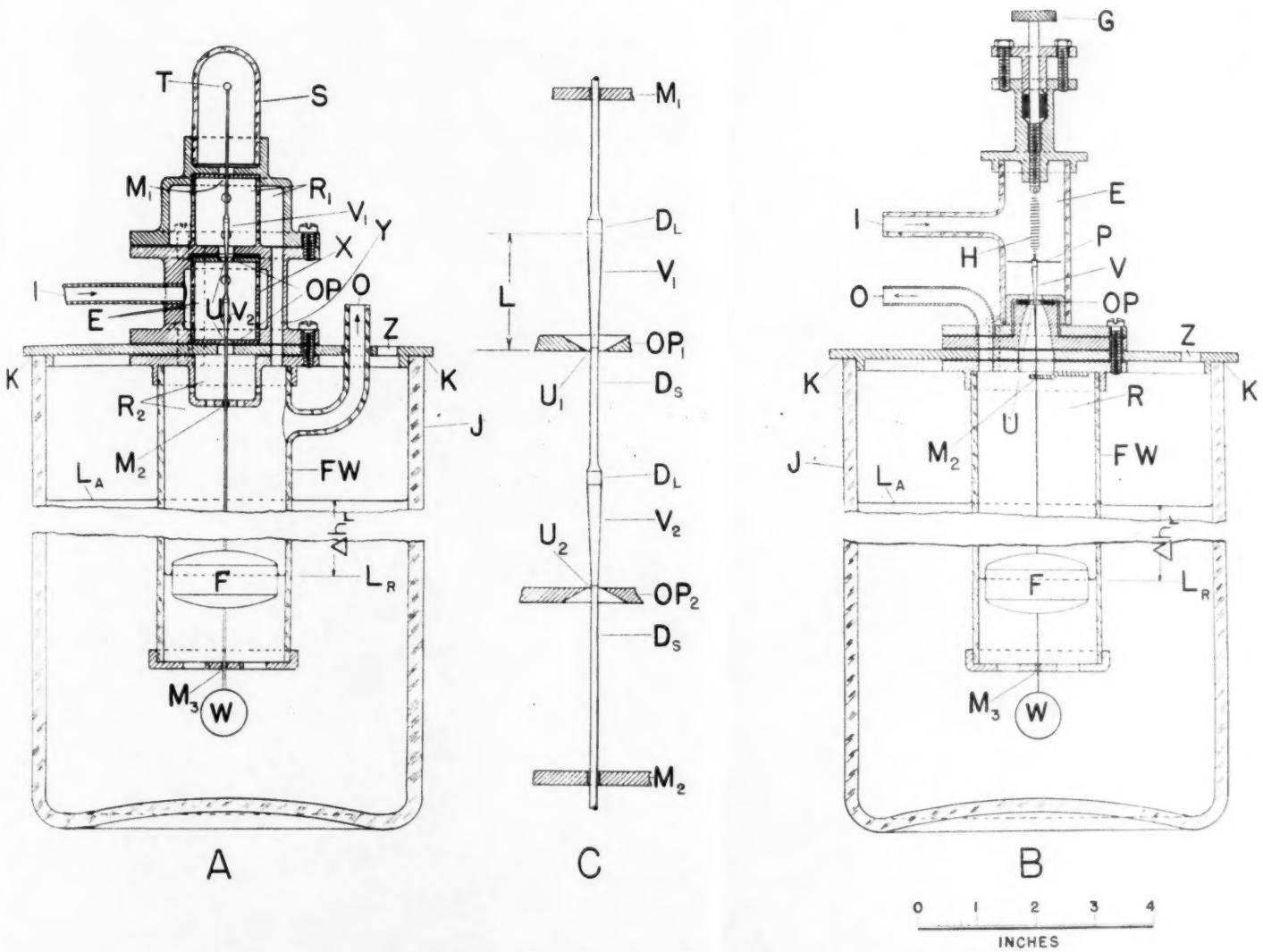

FIGURE 2.—*Construction of flow manostats with double and single modulator valves, respectively.*

A, manostat with balanced double valve; *B*, manostat with spring-balanced single valve; *C*, enlarged view of valve, ×3.
For detailed description of apparatus, see p. 146.

469958 (Face p. 146)

UNIV. OF MICH.

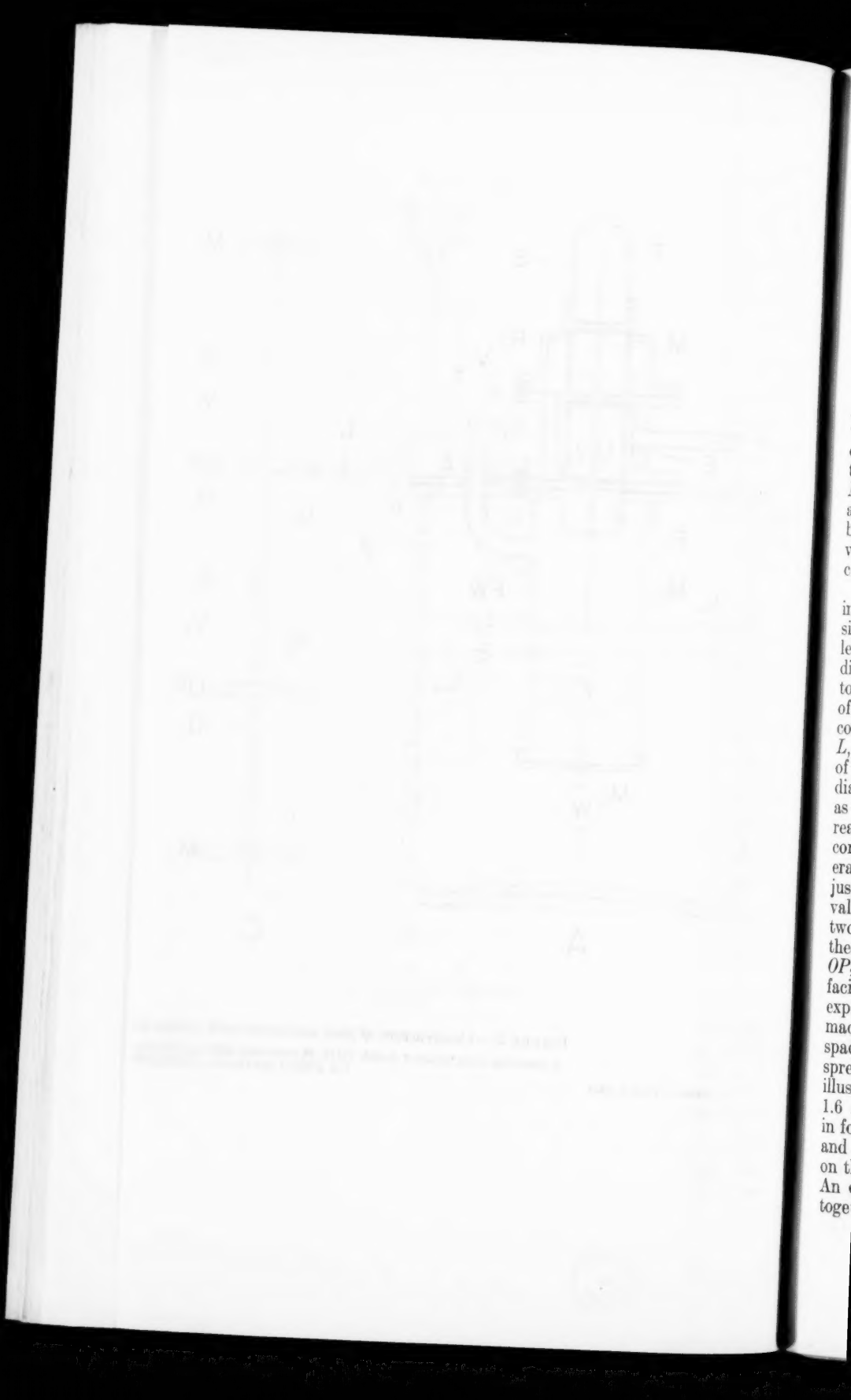

through the floats, F, which are stabilized by the ballast weights, W. Through contact with the gas in the expansion chambers, R and R_2, respectively, in the upper ends of the float wells, the surfaces of these columns (at the levels L_R) are depressed relative to the surfaces (at the levels L_A) of the main bodies of the liquid in the annular reservoir spaces between the float wells and the walls, J, of the vessels in which the float wells are immersed. The vertical distance through which the surfaces of the columns is depressed represents the magnitude of the regulated pressure differential, Δh_r, in terms of the liquid used. The spindle, V, in view B, is retained in a position coaxial with the orifice, U, in the plate, OP, in part by the pull of the suspension spring, H, against the weight of the core, float, and ballast assembly, and in part by the bearings or retaining eyes, M_2, and M_3, through which the tail wire connecting the assembly is threaded. The core comprising the two spindles, V_1 and V_2, in view A, is similarly retained in the proper coaxial position by means of the slip bearings, M_1 and M_3, in which the stems of the assembly slide freely without appreciable radial play. The spindle, V, in view B, preferably should be provided with a stem at the top, to slide in a bearing as at M_1 in view A, because of the difficulty in keeping the spring connections centered properly without it.

With respect to its shape, each spindle has the three parts illustrated in view C of figure 2—regardless of whether the throttle valve is single or double. The upper cylindrical part, D_L, has a minimum length approximating the thickness of the orifice plate, OP, and a diameter which is just enough smaller than the bore of the orifice, U, to let the part enter the opening without ever touching the thin edges of the orifice with any small radial play the bearings may allow. The conically tapered main part (marked V_1, V_2, in this view), of a length, L, between 10 and 20 mm, has a major diameter equal to the diameter of D_L and a minor diameter not greater than one-half of the major diameter. The lower cylindrical part, D_S, having the same diameter as the minor diameter of the tapered part, is relatively long for the reason that, preferably, it should be continuous with the stem of the core below the spindle. The stem of the core above the spindle preferably should be of the same diameter as the other parts of the stem, just as the drawing indicates. In any compound core for a double-valve manostat, the distance between any corresponding parts of the two component spindles is precisely equal to the distance between the knife edges of the orifices, U_1 and U_2, when the plates, OP_1 and OP_2, are properly mounted with the flat side of each orifice plate facing the entrance chamber, E, and with the beveled side facing an expansion chamber, R_1 or R_2. For this reason the compound core is made all in one piece, as illustrated at C, and the orifice plates are spaced precisely the correct distance apart by means of the perforated spreader ring, X, which is pressed into the entrance chamber, E, as illustrated in view A of figure 2. The orifice plates are approximately 1.6 mm thick, and the orifices are required to be precisely circular in form. The knife edges of the orifices are required to be clean-cut and polished and not thicker than 0.1 mm, the edges of the orifices on the exit side being beveled at an angle of 60° with the orifice axis. An orifice plate, or a pair of orifice plates, as the valve may require, together with the simple or compound core, respectively, made for

operating in accordance with the specifications given above, constitute a throttle valve unit. Since both parts are removable, the valve unit is replaceable as a whole. Thus a wide range of throughput capacity can be made readily available by providing a number of valve units in an assortment of sizes that are properly related to each other to provide suitable overlapping of the individual short ranges of throughput capacity.

When the gas connection to the manostat is cut off and the service-pressure differential at the inlet, I, falls to zero, the liquid in the float well, FW, and the liquid in contact with the atmosphere in the reservoir space seek the same level of surface. As the liquid in FW thus rises, it buoys the float upward until the ballast weight, W, coming into contact with the perforated bottom of the float well, stops the uplift of the core at the widest opening of the throttle valve. Then, upon opening the gas connection, the gas flows rapidly through the inlet, I, through the open throttle valve, through the chamber, R, and the connecting ducts, to the entrances of the burner nozzles (at N, in fig. 1). The resistance of the nozzles and the connecting ducts sets up a back-pressure differential in chamber R which at first exceeds the final regulated pressure differential, Δh_r, driving the surface of the liquid in FW (fig. 2) below the level L_R. The resulting descent of the core momentarily closes the valve beyond the correctly modulated opening, allowing less than the correctly regulated current of gas to pass. At once the pressure in R falls below the correct value of Δh_r, and the resulting rise of the liquid in FW to a surface level above L_R starts a train of repetitions of the whole cycle in which the amplitudes of variation become smaller and smaller until within a few seconds, at most, any small pressure variations still occurring in chamber R come solely from the fluctuations of the service-pressure differential at the inlet, I.

Thus, after the manostat has settled down to steady operation, the annular orifice opening of the throttle valve is modulated continually and automatically through the action of the changes occurring in the regulated pressure, small as they are. The cross-sectional area of the orifice opening expands as the regulated pressure differential diminishes through any slackening of the current entering the expansion chamber following a decrease in the service pressure. Contrarywise, the opening contracts as these causal actions reverse. The distance of travel, l, in the spindle's response to a change in Δh_r is bound to be less than the change in Δh_r as measured between the levels L_A and L_R of the hydrostatic liquid. The amount of the difference at equilibrium depends upon the ratio of the inside cross-sectional area of the float well to the cross-sectional area of the hydrostatic reservoir. The amount of the working difference between the distance, l, and the change in Δh_r generally tends to be greater than the equilibrium value, owing to the lag of response. The degree of the lag depends in part upon the viscosity of the hydrostatic liquid and in part upon the dimensions and other characteristics of the ports or ducts provided for the flow of the liquid into and out of the float well. But it depends chiefly, apparently, upon the inertia of the whole system in relation to the magnitude of the forces acting. Hence the influence of the lag can be predetermined (within certain limiting values) in setting up the design of the details of the construction of the apparatus. A suitable construction will prevent hunting in the automatic modulation

of the restrictive orifices. In particular it will serve to damp any probable resonance between the surge effects of the liquid and the fluctuations in the service pressure, Δh_s. This damping can be effectuated by changing the mass of the ballast weight, W, by restricting the openings of the ports at the foot of the float well (as, for example, by bushing the openings, by lengthening the ducts, etc.), and especially by compounding the reservoir. Methods of compounding a reservoir are suggested on pages 151 and 152.

This primary actuation of the modulation of the orifice opening by means of the regulated pressure differential will be called the "column effect." With the "balanced" valves illustrated in figure 2, it is virtually the only effect of consequence that is operative. But with a single unbalanced valve arrangement, like that illustrated in figure 1, where the core is supported solely by the float, as at A in figure 2, it is apparent that the vertical position of the spindle is determined, in part, by an additive secondary phenomenon which will be called the "piston effect." This is the tendency of the spindle to react directly to the pressure change occurring in the orifice differential, Δh_o. The action of this effect upon the modulation is equivalent to the change which would result from altering the ballast weight, W, by the addition or removal of mass.

The operation of the piston effect can be described roughly as follows. The pressure of the orifice differential bears directly upon the spindle itself as though V (fig. 1) were a piston of variable effective area which expands as the spindle descends into the orifice opening. When the orifice differential is increasing, it tends to drive the spindle downward against the buoyancy of the float. As the spindle sinks, the driving force bearing upon the spindle tends to be augmented continuously. The gain in the driving force is due not only to the initial rate of increase in Δh_o, but also to the expansion of the effective piston area on which the pressure bears and to that increment of Δh_o which is due to the contraction of the orifice area. At the same time, any downward movement of the spindle resulting from this force, and not from the column effect, is increasingly opposed by the buoyancy of the float by which the float resists further immersion in the liquid. In addition, any downward movement of the spindle tending to produce greater immersion of the float tends to be curtailed or even overmatched almost at once by the counter-response of the column effect resulting from the contraction of the orifice. When the orifice differential is diminishing, it tends to let the buoyancy of the float lift the spindle, thereby reversing the other tendencies mentioned above. Hence, with favorable construction of the apparatus, the piston effect could be utilized to implement the modulation of the orifice opening and thus further reduce the variation of the regulated pressure.

Utilization of the piston effect for this purpose would depend upon having the cross-sectional area of the float, F, properly related to the taper and the cross-sectional area of the spindle at its major diameter. This relationship is influenced by the density of the hydrostatic liquid and by other conditions. If the ratios are all appropriate, the response to the piston effect will tend to augment or diminish the degree of immersion of the float in the liquid (and thereby depress or elevate the position of the spindle in the orifice) just sufficiently to

perform a major portion of the modulation necessary to counteract any intolerable change in the magnitude of Δh_r. Then a relatively small change in the length of the hydrostatic column by which the float is supported, coming gradually, will complete the modulation. Thus less variation in the value of Δh_r should be involved than in any usual case where the modulation is brought about solely through the column effect. The result would be as though the instrument had foreseen the impending change in Δh_r and had taken appropriate action to forestall most of the change at its source.

It is evident from the statement above that the problems of design and construction would be increased considerably by any rational utilization of the piston effect for the modulation of the orifice. Wider serviceability of the individual manostat, as well as greater freedom of design and construction, would be possible if the piston effect were eliminated. To this end two methods of counterbalancing the piston effect are illustrated in figure 2, on the assumption that one or the other should prove suitable for all usual circumstances.

In the construction illustrated in views *A* and *C* of figure 2, the piston effect is practically eliminated by causing the orifice differential to act in opposite directions upon the two rigidly connected spindles of a compound core. With this method of valve-balancing, the same float and ballast weight should serve for use with a variety of valve units, practically regardless of their differences in throughput capacity. As arranged in the diagram, the expansion chamber is of necessity divided into two sections, R_1 and R_2. The two sections are connected by ducts, one duct being indicated in sectional elevation at *Y*. (If desired, the outlet, *O*, could be taken from R_1 rather than from R_2 as indicated.) The indicator, *T*, attached to the upper end of the valve core, is always visible through the sight-glass, *S*, for observing the vertical position of the core during the adjustment and operation of the manostat.

In the construction indicated at *B* in figure 2, the piston effect is counterbalanced by the variable tension of the spring, *H*, as adjusted by the screw, *G*. The pointer, P, indicating the vertical position of the single spindle, *V*, is always visible through the glass walls of the entrance chamber, *E*. A manostat of this design can be constructed by hand in approximately the form indicated, using ordinary hand tools and materials that generally are available in laboratories. This is an especial advantage where the services of an instrument shop are not at hand. Moreover, single-valve manostats are practicable for smaller throughput capacities. In most other respects they appear to be inferior to the double-valve type.

In a double-valve manostat the regulation of the rate of flow of the gas into the expansion chamber through the operation of the column effect as described above (p. 149) can be made so effective that the back-pressure, Δh_r, is virtually constant with respect to its influence upon the heat output of the burners during any important interval of time. It can be so effective, indeed, that the percentage variation in the magnitude of Δh_r amounts to only a small fraction of the percentage fluctuation usually encountered in the magnitude of the service-pressure differential as measured at the inlet, *I*, or in the entrance chamber, *E*. Far less advantageous results were obtained when, in numerous experiments, the column effect was derived directly from the fluctuation of the service-pressure differential in

place of the regulated pressure differential, notwithstanding that in the service-pressure fluctuation greater power is available for actuating the mechanism.

In the arrangements of the flow manostat illustrated in figure 2, there is no possibility of leakage of oil or other liquids from the apparatus, for there are no openings to the outside below the liquid level. When the liquid level is to be changed, the requisite quantity of oil is removed or introduced through the atmospheric opening (*Z*, fig. 2) in the cover of the vessel, which serves as the support for the mechanism. To facilitate the transfer of the oil, a supply reservoir may be installed above the vessel on supports attached to the cover, with connections to a source of vacuum and to a vacuum-breaker cock. The supply reservoir should have an internal foot valve of the needle or plug type with its stem extending through a stuffing box at the top of the container. The foot valve should open into a transfer tube extending to a point near the bottom of the vessel, *J*. Instead of this, if preferred, the elevation of the mechanism with respect to the vessel, *J*, can be made adjustable. For example, the float, float well, and valve assembly can be supported on the cover of the vessel by means of a jacking device operated by a rack or a screw. Even when arranged as indicated, the effective level of the liquid can be reduced by inserting shims or other spacers at *K-K* between the cover and the rim of the vessel.

In the constructions suggested in figure 2, the float well is made of glass tubing approximately 2 inches in diameter, and the reservoir vessel in which the float well is suspended is a battery jar or similar glass container of not less than 35 square inches cross-sectional area, for the cross-sectional area of the reservoir should be large relative to that of the float well. Thus, in the constructions indicated, the thin-walled brass float, *F*, and the liquid column on which it rides are plainly visible from the outside for convenience in adjusting the manostat. The float is indicated as of approximately 1.75 inches outside diameter, a suitable size for a 2-inch float well. A reservoir of the kind indicated could be compounded very easily by means of a large hollow glass cylinder with open ends and a length somewhat less than the height of the jar inside. The cylinder should be placed inside the jar, with its walls surrounding the float well and with its lower end resting on the bottom of the jar with just enough clearance to allow passage of the liquid at a suitable rate of flow. The most favorable clearance could be found experimentally. The chosen clearance and the central location of the cylinder could be maintained by means of appropriate spreaders which could take the form of a light framework of metal.

III. PRACTICAL APPLICATION AND RESULTS OBTAINED

The principles of design and construction outlined in the foregoing, with particular reference to the double-valve device illustrated at *A* in figure 2, were used as the general basis for constructing the experimental manostat illustrated in figure 3. However, this manostat differs from the form *A* in a number of minor details. For example, both the reservoir and the float well are constructed of brass in place of glass. Hence neither the float nor the depressed hydrostatic column is visible. The glass gage at the right indicates the respective

levels of the liquid in the reservoir and in the float well, and the pointer, T, in the sight-glass, S, indicates the position of the spindle, when the manostat is in operation. The reservoir comprises two vessels, J_1 and J_2, which are connected through the duct, Q. The small entrance chamber, constructed of thin sheet brass, is attached to the gas inlet duct, I, which extends through, and to a point below, the float-well cover, FW. Thus, the entrance chamber is suspended within the upper end of the float well. In this arrangement of the entrance chamber, both orifices of the balanced double valve discharge directly into the single expansion chamber comprising all of that part of the float well which is above the surface level of the depressed hydrostatic column when the manostat is in operation.

As first constructed, the experimental manostat had only the annular reservoir between the walls of J_1 and FW. The resulting variations in Δh_r suggested that the port area at the foot of FW was insufficient. After the port area was increased by the installation of the U-shaped ducts, UD, connecting the foot of the float-well sump with the sloping sides of J_1, surging of the liquid was observed under certain conditions. Installation of the secondary reservoir, J_2, from and to which the liquid flows through the duct, Q, at a rate differing from the rate for the primary reservoir, J_1, not only increased the reservoir area sufficiently to bring about adequate response of the modulator, as indicated by the smallness of the variations in the magnitude of Δh_r resulting under the ordinary frequency of fluctuation in the gas service pressure, Δh_s, but also effectively damped the surging of the liquid under any conditions that have been encountered since. Serving three small burners with a total of probably about 8 ft^3 of gas per hour for many hours, the flow manostat arranged as illustrated in figure 3 has maintained a regulated pressure of $\Delta h_r = 49.6 \pm 0.5$ mm of water column throughout, with very infrequent adjustments. The gas service pressure meanwhile has been subject to variation from 104 to 164 mm and the reverse, within periods of less than 5 minutes. The fluctuations between the limits of 110 and 138 mm of water column have been as many as six times a minute for short intervals.

The effectiveness and the precision of the regulation were evidenced also by the high degree of reproducibility attained in the time intervals consumed in carrying out candy tests in accordance with certain definite procedures that remain to be described in later papers. In properly grouped tests conducted without the use of the flow manostat under fluctuations of the service pressure such as those stated above, the variation in the cooking intervals, expressed as the percentage index of dispersion, $100\sigma/a$, seldom was less than ± 5 and often exceeded ± 10. In other words, the least-squares standard deviation in the time required to cook the candy generally exceeded 5 percent of the average time required for all of the tests in the group, and in many cases it exceeded the tolerance of ± 8.7 percent allowed for the cooking interval in the original specifications of Hooker [2] and in some of the modified Hooker procedures [3], where the limits of the cooking interval are placed at 21 to 25 minutes. By "properly grouped" is meant the statistical assembly of the results of at least four tests carried out with the same apparatus and the same procedure, with no intervening adjustments of the burner or the spatial relations between the burner and the boiling-vessel.

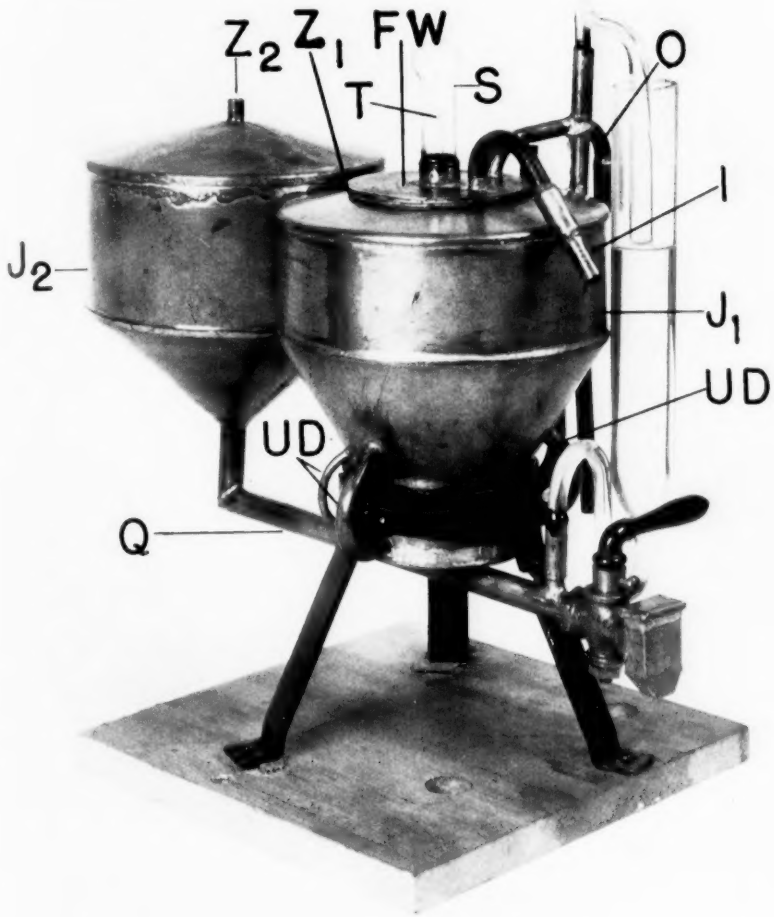

FIGURE 3.—*Experimental flow-manostat.*

For detailed description, see pp. 151 and 152.

UNIV. OF MICH.

TABLE 1.—*Typical variations obtained in the lengths of the cooking intervals of candy tests in which the gas pressure is regulated by means of the flow manostat*

GROUP I[1]			GROUP II			GROUP III		
Sample weight, 100.0 g			Sample weight, 250.0 g			Sample weight, 250.0 g		
Test No.	Date	Cooking interval	Test No.	Date	Cooking interval	Test No.	Date	Cooking interval
		Seconds			*Seconds*			*Seconds*
97	2-2-40	1, 172. 6	105	4-1-40	1, 343	106	4-1-40	1, 326
98	2-8-40	1, 184. 6	107	4-1-40	1, 339	108	4-1-40	1, 307
99	2-8-40	1, 157. 5	110	4-2-40	1, 359	111	4-2-40	1, 324
100	2-8-40	1, 172. 0	112	4-2-40	1, 334	113	4-2-40	1, 314
Average		1, 171. 7	Average		1, 344	Average		1, 318
$100\sigma/a$		±0. 82	$100\sigma/a$		±0. 70	$100\sigma/a$		±0. 58

GROUP IV			GROUP V			GROUP VI		
Sample weight, 250.0 g			Sample weight, 250.0 g			Sample weight, 250.0 g		
Test No.	Date	Cooking interval	Test No.	Date	Cooking interval	Test No.	Date	Cooking interval
		Seconds			*Seconds*			*Seconds*
130	4-17-40	1, 198	133	4-17-40	1, 293	139	4-25-40	1, 263
132	4-17-40	1, 193	135	4-17-40	1, 296	141	4-26-40	1, 247
134	4-17-40	1, 194	137	4-18-40	1, 293	143	4-26-40	1, 231
136	4-18-40	1, 205	138	4-18-40	1, 286	145	4-27-40	1, 245
Average		1, 197. 5	Average		1, 292	Average		1, 246
$100\sigma/a$		±0. 39	$100\sigma/a$		±0. 28	$100\sigma/a$		±0. 88

GROUP VII[2]		
Sample weight, 250.0 g		
Test No.	Date	Cooking interval
		Seconds
140	4-25-40	1, 317
142	4-26-40	1, 316
146	4-27-40	1, 317
150	5- 1-40	1, 330
152	5- 2-40	1, 346
154	5- 2-40	1, 342
Average		1, 328
$100\sigma/a$		±0. 90

[1] 2 vessels used alternately.
[2] 2 vessels used, one in first three, $100\sigma/a = \pm 0.043$; other in last three, $100\sigma/a = \pm 0.51$.

In similar groups of tests using the flow manostat, the index of dispersion was usually less than ± 1.0, although the tests in any one group were seldom carried out consecutively and never all on the same day. This means that tests belonging to other groups and usually carried out in different vessels over different burners were interspersed with the tests in the group considered and that some of the tests were further separated in time by various other interruptions. But at the time of completing the final test in the groups listed in table 1, no manual adjustment of the flow manostat had been made for

more than a year. At the commencement of each run the gas was simply turned into the flow manostat, the burners were lighted, and usually the tests were begun within 1 to 30 minutes. In each of two of the groups, half of the tests were carried out in one boiling vessel and half in another of the same type. Although this renders the grouping improper according to the definition stated above, and according to the rule strictly adhered to in the tests carried out without the manostat, the index of dispersion for these two groups remained under ± 1.0, with several days elapsing between the first and the last of the tests in each case.

Each of the groups included in table 1 represents distinctly unique conditions with respect to at least one of the following particulars—namely, the length of the cooking interval selected (as determined by the bore of the burner nozzle used in conjunction with the other parts of the apparatus), the form of burner employed, the particular boiling vessel used, or the weight of the sample and the dimensions of all of the apparatus employed. Additional experimental data will be given in forthcoming papers.

The principal dimensions of the balanced double valve incorporated in the manostat illustrated in figure 3 are as follows: Thickness of orifice plates, approximately 1 mm; bore of holes, 2.0-mm drill (walls cylindrical, not beveled); major diameter of the spindles, 1.8 mm; minor diameter of the spindles and diameter of the spindle stems, 0.9 mm. The gas outlet is indicated at 0. An annular atmospheric opening to the hydrostatic reservoir, J_1, is located at Z_1, just under the float-well cover, *FW*. The tubular atmospheric opening to the reservoir, J_2, is seen at Z_2. The liquid is an "odorless, tasteless, and colorless" mineral oil of the following specifications: Viscosity, 80/90 sec, or 0.245 poises at 25° C; specific gravity at 25° C, 0.864; flash-point, 171° C; burning point, 207° C; acidity (mg of KOH/g of oil), none; sulfur, none; oxidation number, 0; gum on heating in oxygen, none; discoloration on heating in oxygen, slight orange. The service gas referred to is a carbureted manufactured water gas containing approximately 30 percent of natural gas. It has practically a constant heating value of 600 Btu to the cubic foot.

In the first models of the flow manostat, which are not illustrated, the float-and-spindle assembly was rotated continuously during operation by the action of the incoming gas upon a turbine mounted on the stem of the spindle. The purpose of this arrangement was to prevent any possible sticking of the stem of the spindle in the bearings, sufficient to impede the requisite vertical movement. This precaution was found unnecessary, however, when oil was used as the liquid. Besides keeping the working parts lubricated, the oil seems to delay or prevent the accumulation of deposits from the gas. Moreover, the surface properties of the oil are more favorable than those of water, which served as the liquid in the first models. Finally, evaporation of the oil is entirely negligible.

IV. SUMMARY

A basic design has been presented for the construction of a flow manostat with a floating orifice modulator which, in conjunction with external nozzles (or equivalent devices having constant-discharge characteristics) with which the manostat is to be employed, serves to

regulate the flow of a gas from a source having a moderately variable pressure. The device is designed particularly for use in candy tests for the regulation of the output performance of a gas burner or a fixed group of simultaneously operating burners, but it can be utilized for numerous other purposes as well. It is properly a pressure-reducing valve, for the maximum regulated pressure must be less than the minimum service pressure at the source with which it is connected. Means are provided for varying the regulated pressure as well as the volume of the flow.

V. REFERENCES

[1] A. C. Robertson, Ind. Eng. Chem., Anal. Ed. **3**, 383 (1931).
[2] NBS Circular C440 (1942).
[3] J. A. Ambler and S. Byall, Ind. Eng. Chem., Anal. Ed. **1**, 169 (1935).

Washington, June 12, 1942.

U. S. DEPARTMENT OF COMMERCE NATIONAL BUREAU OF STANDARDS

RESEARCH PAPER RP1493

Part of Journal of Research of the National Bureau of Standards, Volume 29, August 1942

AN EQUATION FOR THE ISOTHERMS OF PURE SUBSTANCES AT THEIR CRITICAL TEMPERATURES

By Cyril H. Meyers

ABSTRACT

An empirical equation is presented for data along the isotherms of pure substances at their critical temperatures and densities up to 1.1 times the critical density. The equation has five constants in addition to the universal gas constant. Of these five, one is limited to a single value, if a simple solution to the equation is to be obtained; three are determined by the critical conditions; and the remaining constant is determined empirically from data other than those for the critical state. Three of the five constants are independent of the substance, one is an explicit function of RT_c/p_cV_c, whereas the reciprocal of the fifth is found to be practically a linear function of RT_c/p_cV_c for values of that ratio up to 3.8 or 3.9. This relation correlates the isotherms for various substances, so that data on two well chosen substances, such as hydrogen and carbon dioxide, suffice to determine the fifth constant and consequently the critical isotherm for other substances, for which RT_c/p_cV_c is not greater than 3.8. For substances such as ammonia (for which RT_c/p_cV_c is 4.08), the fifth constant may not conform to the linear relation.

The equation represents the data for 12 of 13 substances within the experimental error, the exceptional substance being water (for which RT_c/p_cV_c is 4.34).

At low densities the equation reduces to a simpler form which expresses pV/RT as a quadratic function of density.

The fugacity along the critical isotherm can be calculated from the equation. The fugacity at the critical state is approximately two-thirds the critical pressure for all substances. The fungacity of CO_2 is calculated at 1 atmosphere and at the critical pressure.

CONTENTS

		Page
I.	Introduction	158
II.	Failure of the law of corresponding states	158
III.	Equation for the isotherm at the critical temperature	159
IV.	Representation of the experimental data	163
	1. Hydrogen	165
	2. Oxygen and nitrogen	165
	3. Methane	167
	4. Ethane	167
	5. Propane	168
	6. Carbon dioxide	168
	7. Propylene	169
	8. Normal butane	169
	9. Ethyl ether	170
	10. Normal heptane	170
	11. Ammonia	170
	12. Water	171
V.	Virial coefficients for the isotherm at the critical temperature	173
VI.	Fugacity along the isotherms at the critical temperature	175
VII.	Summary	175

I. INTRODUCTION

The isotherm at the critical temperature forms a convenient base from which to proceed in tabulating the properties of vapors. Consequently, a mathematical representation of the critical isotherm is desirable. A mathematical representation of the critical isotherm is especially difficult, since at the critical temperature not only must the equation represent the experimental data, but it must satisfy the conditions that the first and second derivatives of pressure with respect to volume (or density) must equal zero at the critical state.

The notation used in this paper is as follows: R, the universal gas constant; T, absolute temperature; p, absolute pressure; V, molal

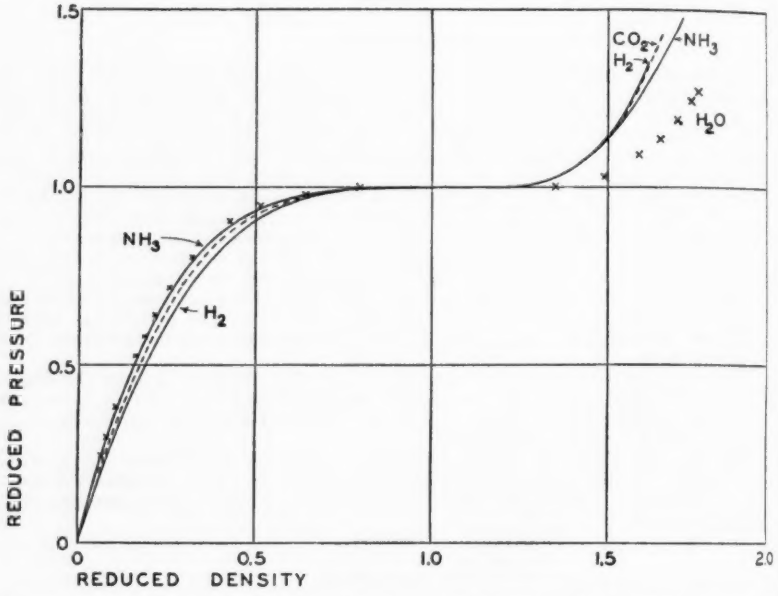

FIGURE 1.—*Comparison of reduced pressures at corresponding densities along the critical isotherms of four substances.*

volume; c, subscript representing critical state; X, V_c/V or reduced density; f, fugacity; m, number of a term in a series; n, empirical constant; and K, empirical constant.

II. FAILURE OF THE LAW OF CORRESPONDING STATES

The law of corresponding states has been used occasionally for predicting the properties of pure substances from the properties of other substances, but this procedure is subject to rather large errors. According to the law of corresponding states, the data for the critical isotherms of all substances would lie on a single curve on a graph with reduced pressure as ordinate and reduced density (or volume) as abscissa. Such a graph, which is illustrated in figure 1 for H_2, CO_2, NH_3, and H_2O, indicates that the assumption of the law of corresponding states may lead to errors as large as 10 percent of the pressure.

For densities less than the critical density, the position of the curves appears to be related to the quantity RT_c/p_cV_c. The greater the value of RT_c/p_cV_c, the greater is the reduced pressure corresponding to any given reduced density, X. This has been found to be true also for other substances studied but is omitted from figure 1 to avoid confusion.

The arrangement for densities greater than the critical is in general reversed from that at smaller densities and appears not to be entirely a function of RT_c/p_cV_c, although this irregularity may be due in part to erroneous critical densities. The data for water are so conspicuously

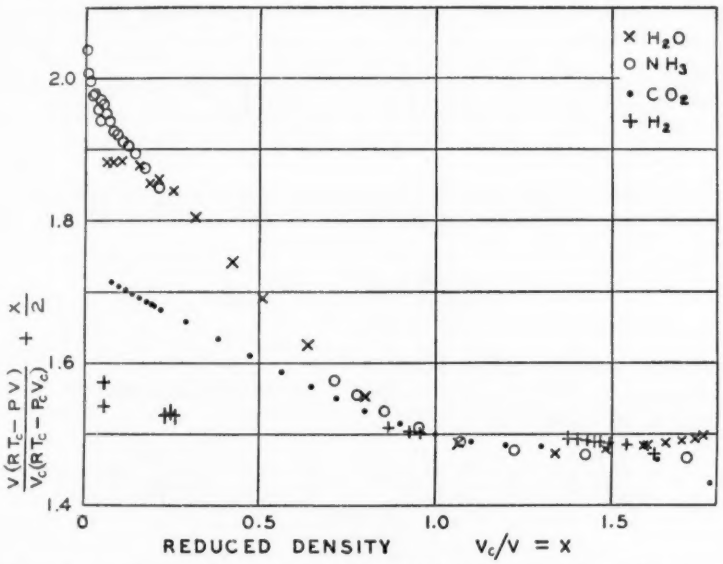

FIGURE 2.—*Comparison of data for the critical isotherms of four substances.*

far below the other curves in figure 1 that the irregularity appears to be greater than any experimental error possible in the critical density.

III. EQUATION FOR THE ISOTHERM AT THE CRITICAL TEMPERATURE

The differences between the critical isotherms of different substances at densities less than the critical are better illustrated by plotting the quantity

$$\frac{V(RT_c-pV)}{V_c(RT_c-p_cV_c)}+\frac{X}{2}$$

as ordinate, and the reduced density, X, as abscissa. Such a graph, in which the same data as in figure 1 are represented, is illustrated in figure 2. The data are on smooth curves which deviate more or less from the straight line,

$$\frac{V(RT_c-pV)}{V_c(RT_c-p_cV_c)}=\frac{3}{2}-\frac{1}{2}X.$$

469958—42——4

Numerous attempts to find directly a function to represent the curves in figure 2 have failed—the functions always yielded graphs with too much curvature at low densities.

When the slopes of the curve for CO_2 in figure 2 were plotted against density, the resulting graph was remarkably similar to that for the function $y=ae^{-bX^n}$. This suggested the general equation

$$\frac{V(RT_c-pV)}{V_c(RT_c-p_cV_c)}=L-MX+a\int_X^1 e^{-bX^n}dX.$$

After determining most of the constants ,[1] one may write the equation in the form

$$\frac{V(RT_c-pV)}{V_c(RT_c-p_cV_c)}=\frac{3}{2}-\frac{1}{2}X+\left(\frac{3}{2}-\frac{1}{1-\frac{p_cV_c}{RT_c}}\right)\int_X^1 e^{(4/n)(1-X^n)}\,dX, \tag{1}$$

which fulfills the requirement that when $X=1$, $p=p_c$, $\partial p/\partial X=0$, and $\partial^2 p_2/\partial X^2=0$, regardless of the value of the constant n; and which reduces to

$$\frac{V(RT_c-pV)}{V_c(RT_c-p_cV_c)}=\frac{3}{2}-\frac{1}{2}X. \tag{2}$$

when the quantity $RT_c/p_cV_c=3$.

When it is desired to calculate pressures corresponding to given densities, eq 1 may be expressed in the form

$$\frac{p}{p_c}=\left(\frac{RT_c}{p_cV_c}\right)X-X^2\left[\frac{3}{2}\left(\frac{RT_c}{p_cV_c}-1\right)+\left(\frac{1}{2}\frac{RT_c}{p_cV_c}-\frac{3}{2}\right)\int_X^1 e^{(4/n)(1-X^n)}dX\right]+\frac{X^3}{2}\left(\frac{RT_c}{p_cV_c}-1\right) \tag{3}$$

For use in calculations with the equation in either form, eq 1 or 3, values of $\int_X^1 e^{(4/n)(1-X^n)}dX$ are given in table 1 for various values of $1/n$ and X. For data of moderate accuracy, for example, pressures accurate to a few parts in a thousand, graphic methods of interpola-

[1] The procedure is as follows: For brevity let F represent temporarily the fraction RT_c/p_cV_c. Then the solution of the general equation for p/p_c gives

$$p/p_c=FX-LX^3(F-1)+MX^3(F-1)-aX^3(F-1)\int_X^1 e^{-bX^n}dX.$$

By differentiation

$$\frac{\delta p/p_c}{\delta X}=F-2LX(F-1)+3MX^2(F-1)-2aX(F-1)\int_X^1 e^{-bX^n}dX+aX^3(F-1)e^{-bX^n},$$

and

$$\frac{\partial^2 p/p_c}{\partial X^2}=-2L(F-1)+6MX(F-1)-2a(F-1)\int_X^1 e^{-bX^n}dX+4aX(F-1)e^{-bX^n}-abnX^{n+1}(F-1)e^{-bX^n}.$$

By substitution of the critical conditions $p/p_c=1$, $X=1$, $\partial(p/p_c)/\partial X=0$, and $\partial^2(p/p_c)/\partial X^2=0$ in these equations, one obtains three simultaneous equations, from which some of the constants can be eliminated. The solution is

$$bn=\frac{6-4F/(F-1)}{2-M-F/(F-1)}.$$

Apparently M can have only one value (one-half) if a simple solution is to be obtained. Assumption of this value leads to values for the other constants as written in eq.1

tion are satisfactory, but for greater accuracy, it may be better to calculate directly the values of the integral [2] for the chosen value of n and the desired values of X. For values of X up to 1.1 or 1.2, the integral is easily calculated by expanding $e^{-(4/n)X^n}$ into series form and integrating each significant term of the series. For greater values of X this method becomes increasingly laborious, and numerical integration of the quantity $e^{-(4/n)X^n}$ becomes the easier method. Where data are to be calculated for a large number of values of X between 0.8 and 1.2, it is easier to calculate only a few values of pressure in this range and to obtain the remainder by interpolation between these pressures.

To maintain the correct relations at the critical point, the quantity RT_c/p_cV_c should be treated consistently as an exact number in calculating the coefficients of the various terms in eq 3, and it is advisable in calculating pressures to carry each term of the equation to more decimal places than the accuracy of the critical data would warrant.

TABLE 1.—*Values of* $\int_X^1 e^{(4/n)(1-X^n)}dX$ *for various values of X and 1/n*

X	Values of $1/n$						
	0	0.05	0.1	0.15	0.2	0.25	1/3
0	1.0	1.2104	1.4428	1.6997	1.9833	2.2965	2.8924
.1	.9	1.0882	1.2936	1.5175	1.7607	2.0247	2.5132
.2	.8	.9661	1.1444	1.3353	1.5382	1.7530	2.1357
.3	.7	.8439	.9952	1.1531	1.3158	1.4824	1.7645
.4	.6	.7218	.8460	.9709	1.0943	1.2147	1.4065
.5	.5	.5997	.6969	.7893	.8751	.9541	1.0710
.6	.4	.4775	.5479	.6092	.6616	.7063	.7675
.7	.3	.3554	.3996	.4333	.4591	.4793	.5046
.8	.2	.2333	.2539	.2668	.2754	.2815	.2878
.9	.1	.1124	.1166	.1186	.1197	.1204	.1212
1.0	0	0	0	0	0	0	0
1.1	0	−.0696	−.0773	−.0794	−.0803	−.0809	−.0814
1.2	0	−.0781	−.1080	−.1193	−.1253	−.1286	−.1317
1.3	0	−.0781	−.1124	−.1328	−.1452	−.1526	−.1601
1.4	0	−.0781	−.1127	−.1353	−.1517	−.1627	−.1747
1.5	0	−.0781	−.1128	−.1358	−.1532	−.1662	−.1813
∞	0	−.0781	−.1128	−.1359	−.1534	−.1673	−.1855

The constant n is the only quantity in eq 1 which is not explicitly determined by the critical data. The most convenient method for

[2] It may be of academic interest to note that for $n=\infty$, when $X<1$,

$$\int_X^1 e^{(4/n)(1-X^n)}dX = 1-X$$

and when $X>1$,

$$\int_X^1 e^{(4/n)(1-X^n)}dX = 0.$$

When $n=0$

$$\int_X^1 e^{(4/n)(1-X^n)}dX = \int_X^1 e^{-4\ln X}\,dX = \int_X^1 \frac{dX}{X^4} = -\frac{1}{3X^3}-\frac{1}{3}.$$

As an aid in checking calculations, it may be of interest to note that

$$\int_0^\infty e^{-y^n}dy = (1/n)\Gamma(1/n).$$

See Bierens de Haan, Nouvelles Tables d'Intégrales Définies, 1867, table 81, formula 8. (Printed by J. C. Drabbe.) Formulas for calculating $(1/n)\Gamma(1/n)$ are given in Jahnke-Emde Funkionentafeln 3d (revised) edition, p. 10, published by G. B. Teubner, Leipzig and Berlin (1938). Then

$$\int_0^\infty e^{(4/n)(1-X^n)}dX = (n/4)^{1/n}e^{4/n}\int_0^\infty e^{-y^n}dy = (n/4)^{1/n}e^{4/n}(1/n)\Gamma(1/n).$$

determining n is to substitute the critical data in the equation and to calculate the quantity

$$\left(\frac{V(RT_c-pV)}{V_c(RT_c-p_cV_c)}-\frac{3}{2}+\frac{1}{2}X\right)\Big/\left(\frac{3}{2}-\frac{1}{1-(p_cV_c)/RT_c}\right),$$

which is equal to

$$\int_X^1 e^{(4/n)(1-X^n)}dX.$$

The corresponding value of n is obtained by interpolation in table 1. For this purpose, experimental data at slightly less than one-half the critical density are most desirable, since calculations from eq 1 at various densities with the same critical data, but with two slightly different values of n, yield two sets of calculated pressures which differ by a maximum amount at a little less than one-half the critical density and which become equal as X approaches 0 or 1.

Of the three critical data, the critical volume is usually known with the least accuracy. Fortunately, however, there is a compensating action between the various terms of eq 1, such that a change in the critical volume alone produces very little change in the pressures calculated at given densities.

A limit which the constant n can neither equal nor exceed, if eq 1 is to represent properly the critical state, is afforded by consideration of the third and higher derivatives of pressure with respect to density.

The value at the critical state of the third and higher derivatives is probably beyond experimental determination. It is reasonable to suppose, however, that for densities less than the critical density, the pressure does not exceed the critical, and that for densities greater than the critical density no pressure less than the critical exists. This supposition leads to the conclusion that if all derivatives of pressure with respect to density up to and including any derivative of odd order are zero, then the derivative of next higher (even) order must also be zero.

One finds by differentiation of eq 1 for the condition X=1, that $\partial^3 p/\partial X^3$ is zero when

$$n=\left(2\frac{RT_c}{p_cV_c}-3\right)\Big/\left(\frac{RT_c}{p_cV_c}-3\right)$$

and that within the useful range of n, $\partial^4 p/\partial X^4$ is zero only when n is approximately 6.7. Hence one may say that in general n can neither equal nor exceed the ratio

$$\left(2\frac{RT_c}{p_cV_c}-3\right)\Big/\left(\frac{RT_c}{p_cV_c}-3\right).$$

The fact that the values of the constant n determined for various substances usually are less than

$$\left(2\frac{RT_c}{p_cV_c}-3\right)\Big/\left(\frac{RT_c}{p_cV_c}-3\right)$$

by considerable amounts does not preclude the possibility of $\partial^3 p/\partial X^3$ (and $\partial^4 p/\partial X^4$) actually being zero at the critical point. The equation

is only empirical and therefore not exact. In the neighborhood of the critical point only very minute differences exist between the pressures calculated from the values of n which were used and from those which equal

$$\left(2\frac{RT_c}{p_cV_c}-3\right)\Big/\left(\frac{RT_c}{p_cV_c}-3\right).$$

For example, the reduced pressure of normal heptane calculated for $X=0.9$ and $n=3.66$ is 0.9997, whereas the use of $n=5$ or approximately

$$\left(2\frac{RT_c}{p_cV_c}-3\right)\Big/\left(\frac{RT_c}{p_cV_c}-3\right)$$

gives 0.99997 for the reduced pressure—a difference of about 3 parts in 10,000. The experimental data in this case indicate an intermediate value.

The method described for determining n from experimental data was used for H_2O, ($RT_c/p_cV_c=4.335$, $n=3.12$); NH_3 ($RT_c/p_cV_c=4.075$, $n=3.20$) and for CO_2($RT_c/p_cV_c=3.649$, $n=5.48$). A value of n for H_2($RT_c/p_cV_c=3.203$, $n=16.6$) was chosen more or less arbitrarily as being equal to

$$\left(2\frac{RT_c}{p_cV_c}-3\right)\Big/\left(\frac{RT_c}{p_cV_c}-3\right),$$

since the experimental data were best represented by the use of as large a value of n as possible. Although this procedure is mathematically incorrect, the errors introduced are practically negligible. As indicated in table 3, the calculated reduced pressure at $X=1.1$ is 0.9999, that is low by 1 or more parts in 10,000.

In figure 3 the value of RT_c/p_cV_c is plotted as ordinate and that of $1/n$ as abscissa. The dotted curve indicates the values of $1/n$ for which $\partial^3p/\partial X^3=0$ at the critical state, whereas the values for the substances mentioned are indicated by the labeled crosses. The continuous, straight line in figure 3 through the point for H_2 and that for CO_2 passes between the points representing water and ammonia. The values of n given in table 2 for other substances were obtained from this line and were found to represent the data within the experimental accuracy.

IV. REPRESENTATION OF THE EXPERIMENTAL DATA

Although table 2 contains the critical temperatures, pressures, and volumes for the substances discussed in this paper, the main purpose of this table is to present the empirical constants actually used in representing the critical isotherms. For this reason some of the data are given to more places than is warranted by the experimental accuracy. As noted at the bottom of the table, data differing slightly from those chosen by the authors have been used in some instances.

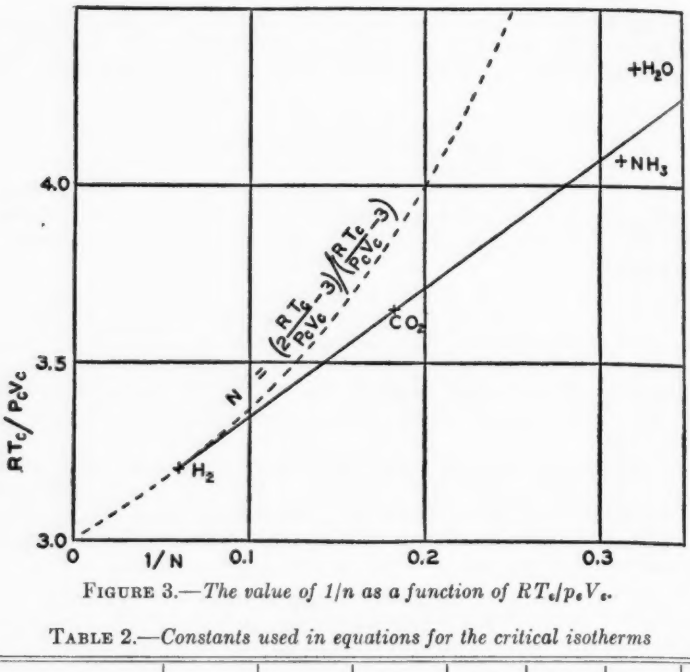

FIGURE 3.—*The value of 1/n as a function of RT_c/p_cV_c.*

TABLE 2.—*Constants used in equations for the critical isotherms*

Substance	T_c[a]	P_c	V_c[b]	$\frac{RT_c}{P_cV_c}$	$\frac{P_cV_c}{RT_c}$	1/n	Reference
	°K	atm					
Hydrogen	33.18	(13.03)	0.002909A	3.203	0.3122	0.060)	1
		12.75		3.273	.3055	.080)	
Oxygen	154.27	49.713	.003324A	3.422	.2922	.120	1
Nitrogen	125.96	33.490	.004027A	3.422	.2922	.120	1
Methane	191.1	45.8	.0993	3.448	.2901	.128	2
Ethane	305.43	48.20	.148	3.513	.2847	.145	3
Propane	369.96	42.004	(.201)	3.592	.2784	.167	4
CO_2	304.197		.004216A	3.649	.2740	.1823	5
		72.885					6
Propylene	364.56	45.4	.180	3.660	.2732	.184	7
n-Butane	425.16	37.468	(.2544)	3.660	.2732	.184	8
Ethyl ether	466.6	36.30	.279	3.774	.2650	.218	9
n-Heptane	540.17	27.00	.416	3.946	.2534	.264	10
Ammonia	406.1						11
		112.1					12
			.0730	4.075	.2454	.312	13
Water	647.27	219.4					14
			.0558	4.335	.2368	.32	15

[a] The temperatures for H_2, O_2, and N_2 are as reported in the reference cited. In other instances, °K= 273.16+°C.

[b] Liters per mole, unless marked "A", in which cases Amagat units were used. The numbers in parentheses are different from those given in the references cited. The reasons for these changes are explained in the text.

REFERENCES

1. F. P. G. A. J. van Agt, Comm. Phys. Lab. Univ. Leiden No. 176c, **16** (1925).
2. C. S. Cragoe, Int. Critical Tables **3**, 230 (1928).
3. J. A. Beattie, C. Hadlock, and N. Poffenberger, J. Chem. Phys. **3**, 93 (1935).
4. J. A. Beattie, N. Poffenberger, and C. Hadlock, J. Chem. Phys. **3**, 96 (1935).
5. A. Michels, C. Michels, and H. Wouters, Proc. Roy. Soc. (London) [A] **153**, 201 (1935).
6. C. H. Meyers and M. S. Van Dusen, BS J. Research **10**, 381 (1933) RP538.
7. W. E. Vaughan and N. R. Graves, Ind. Eng. Chem. **32**, 1252 (1940).
8. J. A. Beattie, G. L. Simard, and Gouq-Jen Su, J. Am. Chem. Soc. **61**, 24 (1939).
9. Erich Schroer, Z. physik. Chem. [A] **140**, 241 (1929).
10. J. A. Beattie and W. C. Kay, J. Am. Chem. Soc. **59**, 1586 (1937).
11. C. S. Cragoe, C. H. Meyers, and C. S. Taylor, BS Sci. Pap. **16**, 1 (1920) S369.
12. F. G. Keyes, J. Am. Chem. Soc. **53**, 965 (1931).
13. C. S. Cragoe and D. R. Harper, 3d, BS Sci. Pap. **17**, 287 (1922) S420.
14. F. G. Keyes, L. B. Smith, and H. T. Gerry, Proc. Am. Acad. **70**, 319 (1935).
15. N. S. Osborne, H. F. Stimson, and D. C. Ginnings, J. Research NBS **23**, 261 (1939) RP1229.

A knowledge of the weight of the normal liter is involved in the use of Amagat units, but this quantity is so much more accurately known than the other data involved that it is considered unnecessary to quote the source of the data used for the normal liter.

1. HYDROGEN

Since a discrepancy of about 2 percent exists between the experimental data for the superheated vapor of hydrogen and those for the saturated vapor,[3] two sets of constants were used in eq 3 for calculating values of p/p_c. One set with $p_c=13.03$ atm (see table 2) was used in calculating values used for comparing with the superheat data in figure 4, and a second set was used with $p_c=12.75$ atm for comparison with tables which may be based upon this value of the critical pressure. The values calculated from these two sets of constants are given later in columns 2 and 3, respectively, of table 3. Although there is a considerable difference at low densities between the reduced pressures calculated from these two sets of constants, the absolute

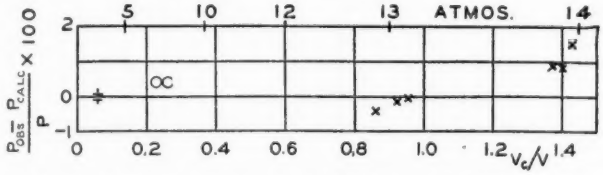

FIGURE 4.—*Comparison of pressures calculated from equation 3 with pressures observed for hydrogen.*

+ Interpolated from data by G. P. Nijhoff and W. H. Keesom in Comm. Phys. Lab. Univ. Leiden No. 188e, 17 (1924-28).
○ Averages of data by H. K. Onnes and P. M. Penning in Comm. Phys. Lab. Univ. Leiden No. 165b, 15 (1920-26).
× C. A. Crommelin and J. C. Swallow, Comm. Phys. Lab. Univ. Leiden No. 172a 16 (1924-26).

values of pressure calculated for $X=0.1$ or less differ by only 1 or 2 parts in 1,000.

Figure 4 presents a comparison of experimental and calculated pressures for hydrogen. The agreement is as good as can be expected in view of the discrepancy already mentioned. The two plus marks at $X=0.058$ represent the largest and the smallest pressures which were obtained by different assumptions in interpolating between the experimental data at other temperatures. The trend of the crosses indicates that this isotherm is above the critical temperature. This fact, combined with the 2-percent discrepancy already mentioned, suggests a possible error in temperature measurement.

2. OXYGEN AND NITROGEN

The experimental data for both oxygen and nitrogen are at irregular intervals and therefore not subject to easy interpolation to the critical temperature. For the purpose of comparing these data, use is made of an equation developed by Leib,[4] which, for diatomic gases, may be written in the form

$$\frac{pV}{RT}=\frac{K(T_c/T)^{5/2}V_c/V}{e^{K(T_c/T)^{3/2}V_c/V}-1}$$

[3] H. K. Onnes, C. A. Crommelin, and P. G. Cath, Comm. Phys. Lab. Univ. Leiden No. 151c, 14 (1914-22).
[4] E. F. Leib, Trans. Am. Soc. Mech. Engrs. 63, 157 (1941).

and may be expanded into the form

$$pV/RT=1-(K/2)(T_c/T)^{5/2}V_c/V+(K(T_c/T)^{5/2}V_c/V)^2/12-\ \ldots\ .$$

At low densities this leads to

$$(T/T_c)^{5/2}(V/V_c)(1-pV/RT)+(K/2)^2(T_c/T)^{5/2}(V_c/V)/3=K/2,$$

where $K/2$ is a single arbitrary constant which may be determined from the experimental data. Equation 1 may be expanded to a somewhat similar series, in which 1.157 corresponds to $K/2$ and 0.454 to the third virial coefficient (see table 4). According to Leib, the third virial coefficient would then be one-third of $(K/2)^2$, or 0.446. With the choice of coordinates in figures 5 and 6, the left-hand portion of the continuous curve representing eq 1 must be horizontal. The

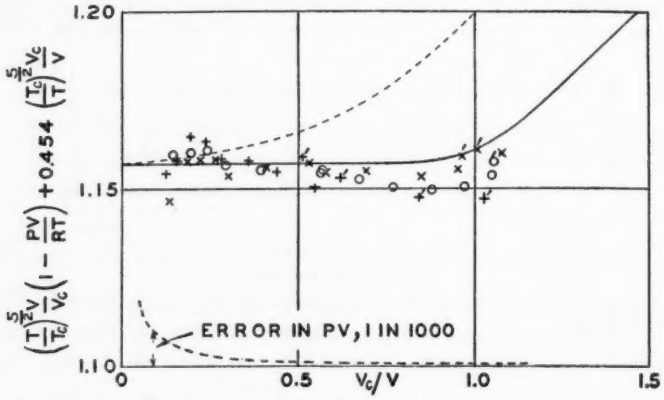

FIGURE 5.—*Comparison of data calculated from equation 1 with data observed for oxygen.*

———154.27° K. Calculated from equation 1.
– – – –154.27° K. From E. F. Leib's equation, Trans. Am. Soc. Mech. Engrs., **63**, 157 (1941).
× 156.10° K. } H. K. Onnes and H. A. Kuypers, Comm. Phys. Lab. Univ. Leiden No. 169a, 16
○ 157.08° K. } (1924–26).
\+ 159.11° K. }

dotted curve just above the continuous curve represents Leib's equation. Leib's theory indicates that with the introduction of $(T_c/T)^{5/2}$, the data for the different isotherms should lie on a single curve, which is approximately the case at the lower densities. Figure 5 indicates that eq 1 represents the data for oxygen within the precision of the experimental data. The data for nitrogen are more precise, and it would appear in figure 6 that at the higher densities, the critical isotherm calculated from eq 1 is slightly too low to correspond to the uniform spacing per degree of the different isotherms. This must be interpreted as a discrepancy between the reported critical data and the other isothermal data, rather than a failure of eq 1, since the form of the calculated isotherm appears to be correct and, at the critical state, the equation is determined exactly by the critical data substituted in it.

The dotted curve at the bottom of figures 5 and 6 provides means for estimating the errors in pressure equivalent to deviations in the ordinate.

All observations made on the oxygen, using a piezometer with a reported normal volume of 1820.6,[5] are designated in figure 5 with a prime mark. These points deviate systematically from smooth curves through the other data. The deviation corresponds in size to an

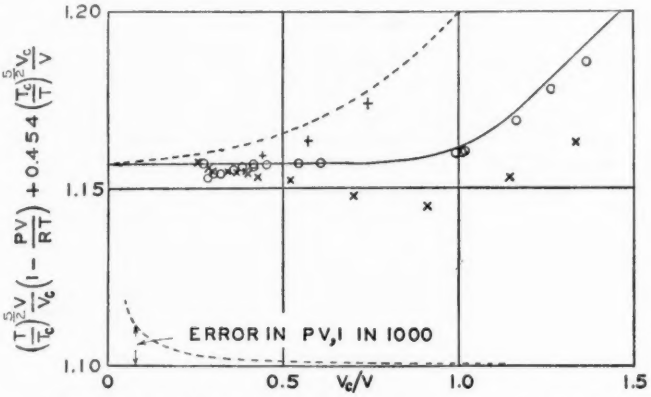

FIGURE 6.—*Comparison of data calculated from equation 1 with data observed for nitrogen.*

———125.96°K. Calculated from equation 1.
– – – –125.96°K. From E. F. Leib's equation, Trans. Am. Soc. Mech. Engrs., **63**, 157 (1941).
\+ 124.51°K.
○ 126.77°K. } H. K. Onnes and A. Th. van Urk, Comm. Phys. Lab. Univ. Leiden No. 169d, **16** (1924–26).
× 128.63°K.

error of 1 gram in the weight of mercury in calibrating the small end of that particular piezometer.

3. METHANE

There are no data for methane at temperatures near the critical, but the calculated pressures are in agreement with those extrapolated from the observed data.[6]

4. ETHANE

A comparison of the pressures calculated from eq 3 with the observed data for ethane is given in figure 7. The critical constants were those

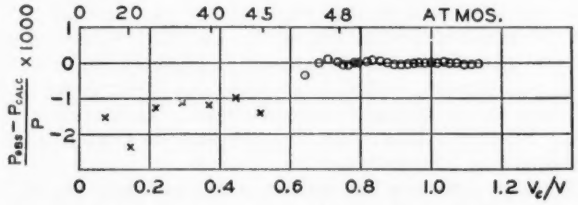

FIGURE 7.—*Comparison of pressures calculated from equation 3 with pressures observed for ethane.*

× J. A. Beattie, C. Hadlock, and N. Poffenberger, J. Chem. Phys. **3**, 93; 1935.
○ J. A. Beattie, Gouq-Jen Su, and G. L. Simard, J. Am. Chem. Soc. **61**, 924 (1939).

obtained from the data near the critical density, represented by circles in the figure. The observed pressures at lower densities repre-

[5] H. K. Onnes and H. A. Kuypers, Comm. Phys. Lab. Univ. Leiden No. 169a, **16**, 5 (1924–26).
[6] H. M. Kvalnes and V. L. Gaddy, J. Am. Chem. Soc., **53**, 394 (1931).

sented by crosses are lower than the calculated values. This difference appears to be due to a difference between the two sets of experimental data rather than a failure of the equation. Possibly there is a difference in the purity of the two samples.

5. PROPANE

The critical volume of propane 0.201 liter per mole was used in place of the value 0.195 chosen by Beattie, Poffenberger, and Hadlock. The value used here corresponds to the mean of the densities of the vapor and of the liquid at 96.70° C (about 0.1° below the critical temperature). The pressures calculated from eq 3 are compared with the values observed for propane in figure 8. Values calculated from the equation agree with the data represented by circles, and agree as well as can be expected with the data for the other sample (represented by crosses), since there is a consistent difference of about 1 part in 1,000 between corresponding pressures for the two samples.

6. CARBON DIOXIDE

Two previous papers in which the critical temperature was chosen first [7] near 31.1°C and later [8] at 30.96°C have appeared to be rather contradictory. This apparent contradiction seems to be cleared up

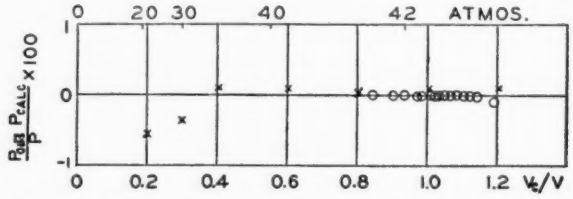

FIGURE 8.—*Comparison of pressures calculated from equation 3 with pressures observed for propane.*

× J. A. Beattie, W. C. Kay, and J. Kaminsky, J. Am. Chem. Soc. 59, 1589 (1937).
○ J. A. Beattie, N. Poffenberger, and C. Hadlock, J. Chem. Phys. 3, 96 (1935).

by the theoretical work of Mayer and Harrison [9], in which they conclude that a temperature exists for which, at the critical density, $p=p_c$, and the first and second derivatives of pressure with respect to volume are zero; but that the sharp dividing surface between the liquid and the gas phases disappears at a slightly lower temperature. For the present purpose, 31.037°C was used as the critical temperature, that being the value reported by Michels. The critical density is chosen from Michels' data, but the pressure is that observed at the National Bureau of Standards.

The agreement between the two sets of data (see fig. 9) is remarkable in view of the fact that volumes were only roughly measured in the latter investigation. The calculated pressures agree very well with the observed data, as is shown in figure 9, the maximum deviation only slightly exceeding 3 parts in 10,000. There is a possibility that these small deviations might be further reduced if the data had been at a temperature about 0.05°C higher.

[7] C. H. Meyers and M. S. Van Dusen, BS J. Research **10**, 381 (1933) RP 538.
[8] H. T. Kennedy and C. H. Meyers, Refrig. Eng. **15**, 125 (1928).
[9] J. E. Mayer and S. F. Harrison, J. Chem. Phys. **6**, 87 (1938).

The pressures calculated from eq 3 in the range $X=1.1$ to 1.3 are apparently too large. As the density is increased beyond $X=1.3$, the calculated pressures soon become too small and rapidly diverge from the observed values. For example, when $X=1.2$ the pressure observed at this Bureau is 72.97 atm, the calculated 73.13, or 22 parts in 10,000 higher. For $X=1.3$, the observed pressure is 73.61 atm, whereas the calculated value is 74.04, or 50 parts in 10,000 higher. Michels reports 81.261 atm at a density corresponding to

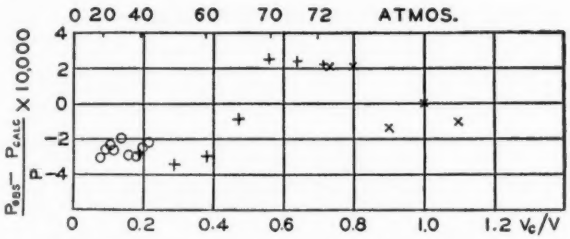

FIGURE 9.—*Comparison of pressures calculated from equation 3 with pressures observed for carbon dioxide.*

× C. H. Meyers and M. S. Van Dusen, BS J. Research **10**, 381 (1933) RP 538.
○+ A. Michels and C. Michels, Proc. Roy. Soc. (London) [A] **153**, 201 (1935).

$X=1.485$. Here, however, the calculated value, 80.08 atm, is 161 parts in 10,000 lower. In the region where X is greater than 1.1, the equation deviates in a similar manner in the case of other substances.

7. PROPYLENE

The data reported for propylene consist of values of pV/RT tabulated for even reduced pressures. In figure 10 these values are compared with those calculated from eq 3.

Since the comparison is on the basis of pV/RT, a decrease of about 1 percent in the assumed critical volume would be sufficient to cause

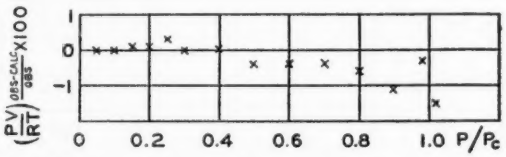

FIGURE 10.—*Comparison of data calculated from equation 3 with data observed for propylene.*

W. E. Vaughan and N. R. Graves, Ind. Eng. Chem. **32**, 1252 (1940).

practical agreement between calculated and observed values. An accuracy of only 1 percent is estimated by the authors for the data.

8. NORMAL BUTANE

The use in this paper of the critical volume 0.2544 liter per mole, together with the other constants in table 2, leads to a value 0.2732 for p_cV_c/RT_c. The pressures calculated with this value of the critical volume, together with n from figure 3, are in slightly better agreement with the observed pressures than those calculated with the aid of the

reported value, 0.258 liter per mole. The excessive number of decimal places in the value 0.2544 was used for convenience to make the constants in eq 3 the same as for propylene.

As shown in figure 11, the pressures observed near the critical state and the values calculated from eq 3 are in excellent agreement. The difference between the calculated and observed pressures at lower

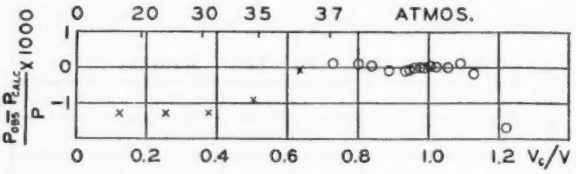

FIGURE 11.—*Comparison of pressures calculated from equation 3 with pressures observed for normal butane.*

× J. A. Beattie, G. L. Simard, and Gouq-Jen Su, J. Am. Chem. Soc. **61**, 24 (1939).
○ J. A. Beattie, G. L. Simard, and Gouq-Jen Su, J. Am. Chem. Soc. **61**, 26 (1939).

densities amounts to about 1 part in 1,000, but this difference is only about one-fifth the difference between the observed pressures and values calculated from the equation given by the authors cited in figure 11.

9. ETHYL ETHER

As illustrated in figure 12, the difference between the pressures observed for ether and those calculated from eq 3 is less than 2 parts in 1,000.

10. NORMAL HEPTANE

The comparison of data on heptane in figure 13 suggests a systematic difference between the two sets of observed data. However, this ap-

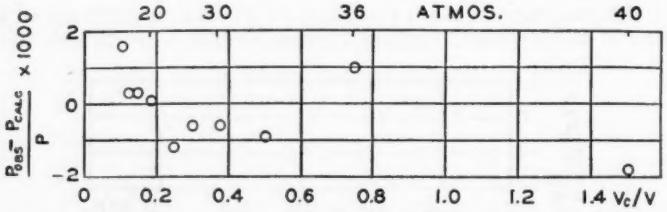

FIGURE 12.—*Comparison of pressures calculated from equation 3 with pressures observed for ethyl ether.*

J. A. Beattie, J. Am. Chem. Soc. **46**, 342 (1924).

parent difference may be in part caused by errors in extrapolation from 275° to 267° C, for the data represented by crosses.

11. AMMONIA

The comparison of data for ammonia in figure 14 shows the agreement for low densities (see upper portion of figure) to be excellent not only between the calculated and the observed pressures but also between the two sets of observed data. The deviations from eq 3 rarely exceed 5 parts in 10,000. A study of a graph similar to figure 2, in which other isotherms than the critical are plotted for ammonia,

gives the impression that this good agreement between the calculated and observed values is somewhat fortuitous. The isotherms at higher temperatures bend upward at low densities too sharply to be represented by eq 3, whereas the isotherms at lower temperatures are similar to those for water in being convex upward. The calculated

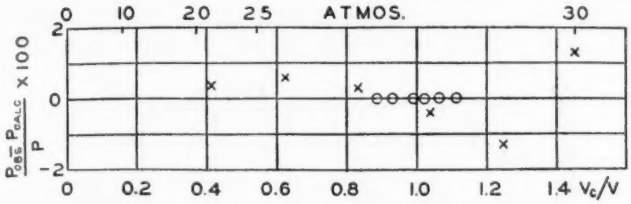

FIGURE 13.—*Comparison of pressures calculated from equation 3 with pressures observed for normal heptane.*

× L. B. Smith, J. A. Beattie, and W. C. Kay, J. Am. Chem. Soc. **59**, 1587 (1937).
○ J. A. Beattie and W. C. Kay, J. Am. Chem. Soc. **59**, 1586 (1937).

pressures at higher densities (see lower portion of fig. 14) show larger differences from the observed values; but below the critical density, the differences are probably due to experimental error and uncertainty of extrapolation—in this region there are no corresponding deviations of this size for other substances. The differences at densities greater

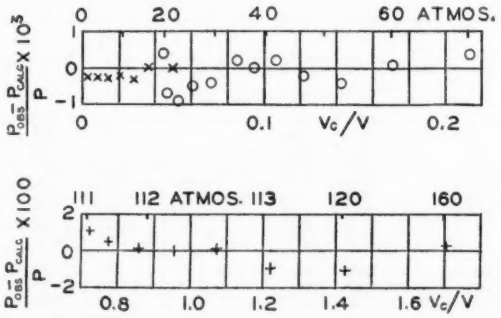

FIGURE 14.—*Comparison of pressures calculated from equation 3 with pressures observed for ammonia.*

× C. H. Meyers and R. S. Jessup, Refrig. Eng. **11**, 345 (1925).
○ J. A. Beattie and C. K. Lawrence, J. Am. Chem. Soc. **52**, 6 (1930).
+ F. G. Keyes, J. Am. Chem. Soc. **53**, 965 (1931).

than the critical are mainly due to inadequacy of eq 3, as mentioned in the discussion of carbon dioxide.

12. WATER

Figure 2 shows that eq 3 does not represent the data for water as satisfactorily as it does the data for other substances. The differences of over ½ percent between the observed and calculated pressures, illustrated in figure 15, appear to be greater than can be attributed to experimental error. Water differs from ammonia in that its isotherms when plotted on a graph similar to figure 2 are all convex upward at low densities.

Table 3 contains values of reduced pressure calculated from eq 3 for 13 substances at various reduced densities, using the constants given in table 2. In some instances the value of the integral in the equation may not have been calculated with sufficient accuracy to determine the corresponding value of the reduced pressure to better than two or three units in the last decimal place. The values of reduced pressure for densities up to and including $X=1.1$ are believed to agree with the observed data within reasonable limits of experimental accuracy

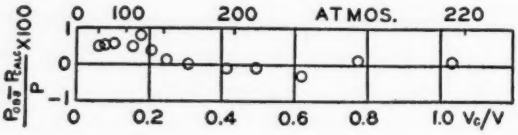

FIGURE 15.—*Comparison of pressures calculated from equation 3 with pressures observed for water.*

F. G. Keyes, L. B. Smith, and H. T. Gerry, Proc. Am. Acad. 70, 319 (1935).

except in the case of water, where some of the calculated values appear to be in error by about ½ percent.

TABLE 3.—*Reduced densities and corresponding reduced pressures calculated from equation (3) for various substances at the critical temperature*

X	Reduced pressures											
	[a]H_2	[b]H_2	O_2 and N_2	CH_4	C_2H_6	C_3H_8	CO_2	C_3H_8 and C_4H_{10}	Ether	C_7H_{16}	NH_3	H_2O
0.1	0.2872	0.2927	0.3041	0.3061	0.3110	0.3169	0.3211	0.3219	0.3300	0.3419	0.3500	0.3689
.2	.5132	.5215	.5384	.5413	.5484	.5566	.5624	.5636	.5745	.5898	.5991	.6249
.3	.6854	.6943	.7122	.7151	.7223	.7305	.7361	.7373	.7472	.7606	.7670	.7920
.4	.8109	.8190	.8347	.8372	.8432	.8497	.8540	.8550	.8620	.8711	.8735	.8935
.5	.8992	.9038	.9154	.9170	.9212	.9255	.9281	.9288	.9325	.9368	.9364	.9496
.6	.9522	.9563	.9634	.9643	.9664	.9685	.9699	.9702	.9716	.9737	.9708	.9779
.7	.9826	.9846	.9878	.9881	.9890	.9896	.9900	.9901	.9901	.9900	.9884	.9914
.8	.9960	.9967	.9975	.9975	.9977	.9977	.9977	.9977	.9975	.9972	.9966	.9977
.9	.9997	.9998	.9998	.9998	.9998	.9998	.9998	.9998	.9997	.9996	.9995	.9997
1.0	1	1	1	1	1	1	1	1	1	1	1	1
1.1	[c].9999	1.0000	1.0000	1.0002	1.0002	1.0003	1.0003	1.0003	1.0005	1.0004	1.0005	1.0005
1.2	1.0012	1.0016	1.0015	1.0022	1.0025	1.0030	1.0033	1.0035	1.0041	1.0051	1.0062	1.0060
1.3	1.0141	1.0130	1.0127	1.0132	1.0138	1.0150	1.0158	1.0161	1.0181	1.0210	1.0241	1.0241
$\frac{RT_c}{p_cV_c}$	3.203	3.273	3.422	3.448	3.513	3.592	3.649	3.660	3.774	3.946	4.075	4.333

[a] Calculated with $p_c=13.03$ atm, $1/n=0.060$ (see table 2).
[b] Calculated with $p_c=12.75$ atm, $1/n=0.080$ (see table 2).
[c] Actually calculated as less than unity because of choice of constants (see text).

As already mentioned, two sets of values are given for hydrogen, since the choice of a value for the critical pressure of that substance is to some extent a matter of personal judgment.

The value of RT_c/p_cV_c is also given at the base of the table as an aid in comparing with data for other substances not included in the table. For example, the ratio RT_c/p_cV_c for argon is very nearly the same as that for oxygen and nitrogen, consequently the reduced pressures given for those two substances should apply also to argon. It may be convenient also to represent the reduced pressures for other substances by interpolation between the values given in table 3.

V. VIRIAL COEFFICIENTS FOR THE ISOTHERM AT THE CRITICAL TEMPERATURE

Equation 1 may be transformed to

$$1-\frac{pV}{RT}=X\left[\frac{3}{2}\left(1-\frac{p_cV_c}{RT_c}\right)+\left\{\frac{3}{2}\left(1-\frac{p_cV_c}{RT_c}\right)-1\right\}\int_X^1 e^{(4/n)(1-X^n)}dX\right]$$
$$-\frac{X^2}{2}\left(1-\frac{p_cV_c}{RT_c}\right). \tag{4}$$

Or approximately for small values of X

$$1-\frac{pV}{RT}=X\left[\frac{3}{2}\left(1-\frac{p_cV_c}{RT_c}\right)+\left\{\frac{3}{2}\left(1-\frac{p_cV_c}{RT_c}\right)-1\right\}\int_0^1 e^{(4/n)(1-X^n)}dX\right]$$
$$-X^2\left[\frac{1}{2}\left(1-\frac{p_cV_c}{RT_c}\right)+\left\{\frac{3}{2}\left(1-\frac{p_cV_c}{RT_c}\right)-1\right\}e^{4/n}\right] \tag{5}$$

The range over which this approximation fulfills a given requirement depends upon the value of n. For example, pV/RT calculated from eq 5 does not differ more than 1 in 10,000 from the same quantity calculated from eq 4 for values of X up to 0.5 or 0.6 for H_2; up to 0.3 or 0.4 for CO_2; and up to 0.1 for NH_3.

One may rewrite eq 5 briefly as

$$pV/RT=1+BX+CX^2. \tag{6}$$

Table 4 gives values of B and C for various substances as calculated from eq 5. The virial coefficients, as sometimes defined from the equation

$$(pV)_A=(RT)_A+\frac{B_A}{V_A}+\frac{B_A}{V_A{}^2},$$

can be derived easily from these coefficients.

TABLE 4.—*Virial coefficients for critical isotherms*

Substance	Coefficients from			Comparison values	
	Equation 5		Berthelot		
	$-B$	C	$-B$	$-B$	C
Hydrogen	1.072	0.384	1.126	[a] 1.05	
Oxygen	1.157	.454	1.203	[b] 1.23	[b] 0.595
Nitrogen	1.157	.454	1.203	[c] 1.23	[c] .586
Methane	1.164	.460	1.212		
Ethane	1.195	.488	1.235		
Propane	1.230	.521	1.263		
Carbon dioxide	1.256	.548	1.283	[d] 1.261	[d] .580
Propylene	1.261	.552	1.287		
n-Butane	1.261	.552	1.287		
Ethyl ether	1.318	.613	1.333		
n-Heptane	1.413	.729	1.387		
Ammonia	1.492	.837	1.433		
Water*	1.548	.902	1.524		

[a] G. P. Nijhoff and W. H. Keesom, Comm. Phys. Lab. Univ. Leiden No. 188e **17** (1924-28).
[b] H. A. Kuypers, Comm. Phys. Lab. Univ. Leiden No. 169b, **16** (1924-26).
[c] A. Th. van Urk, Comm. Phys. Lab. Univ. Leiden No. 169e, **16** (1924-26).
[d] Proc. Roy. Soc. (London) [A] **153**, 201 (1935).
* Allowing for the effect of C, the value of B estimated from the 2 lowest observed pressures is about 1.46.

The fourth column of table 4 contains values of $-B$ calculated from Berthelot's equation

$$pV=RT\left[1+\frac{9pT_c}{128p_cT}\left(1-6\frac{T_c^2}{T^2}\right)\right],$$

which leads to a value $-45RT_c/128p_cV_c$ for B at the critical temperature. Comparison values presented by other authors are given in some cases.

In general, the agreement of pressures calculated from eq 3 has been shown to be very good, hence the values of B in table 4 obtained from eq 5, with the exception of that for water, are considered to be within 2 percent or less of the correct values.

The accuracy of the data on hydrogen is not a sufficient basis for a choice between the coefficient calculated from eq 5 and that given by the Leiden Laboratory.

The data on oxygen and nitrogen confirm the coefficients presented in table 4 from eq 5. The value 1.23 given by the Leiden Laboratory for B for oxygen and nitrogen, in other words, the intercept for the critical isotherm at zero density in figures 5 and 6 is out of line with the experimental data for both substances.

The discrepancy of about ½ percent between the value of B for CO_2 calculated from eq 5 and that given by Michels, is insignificant for the purpose of calculating pressures at low densities. For example, for 1 atm eq 5 gives $pV/RT=0.99526$, whereas Michel's equation gives 0.99524; even at 19 atm the difference in pV/RT amounts to only 3 parts in 10,000.

It will be seen from table 4 that the values of B from Berthelot's equation are about 5 percent too high at the top of the table, but for larger values of RT_c/p_cV_c (see table 2), the difference between the two sets of values decreases and changes sign between ethyl ether and *n*-heptane.

The deviations shown in figure 15 indicate that pressures calculated from eq 3 are either in agreement with or slightly greater than the observed data for ammonia at the lowest densities. Consequently, the value of B from eq 5 in table 4 is not too large, and the value of B from Berthelot's equation is about 4 percent too small.

The fact that eq 5 and Berthelot's equation lead to values of B for water respectively 6 and 4 percent too large, indicates that water is an exceptional substance, in fact, the only one encountered which eq 5 obviously does not represent within the limits of experimental accuracy.

From Leib's equation already mentioned in the discussion of oxygen and nitrogen, the third virial coefficient C is equal to $B^2/3$, a ratio which is in agreement with eq 5 only when the value of RT_c/p_cV_c is 3 for the substance considered. For substances having larger values of RT_c/p_cV_c, smaller values of C are calculated from Leib's equation than from eq 5. The larger is the value of RT_c/p_cV_c, the greater is the difference between the two values of C. For ammonia the difference between the two values of C is about 11 percent.

VI. FUGACITY ALONG THE ISOTHERM AT THE CRITICAL TEMPERATURE

For the purpose of calculating fugacity along the critical isotherm, an expansion of the integral appearing in eq 3 into series form is convenient. Then solving for $\partial(p/p_c)/\partial X$ by differentiating that equation, substituting this derivative in the equation

$$\ln\frac{f}{p}=-\frac{1}{RT_c}\int_0^p \alpha dp=\frac{1}{RT_c}\int_0^p Vdp-\int_0^p\frac{dp}{p}=\frac{p_cV_c}{RT_c}\int_0^X\frac{1}{X}\left(\frac{\partial p/p_c}{\partial X}\right)dX-\int_0^p\frac{dp}{p}$$

and integrating, one obtains

$$\ln\frac{f}{p}=\ln\frac{RT_c}{pV}-3\left(1-\frac{p_cV_c}{RT_c}\right)\left(X-\frac{X^2}{4}\right)$$
$$-\left(1-\frac{3p_cV_c}{RT_c}\right)e^{(4/n)}\left\{1-\frac{4/n}{n+1}+\ldots+\frac{(-1)^m(4/n)^n}{(mn+1)(m!)}+\ldots\right\}X$$
$$+\frac{1}{2}\left(1-\frac{3p_cV_c}{RT_c}\right)e^{(4/n)}\left\{\frac{3}{2}X^2-\frac{(4/n)(n+3)X^{n+2}}{(n+1)(n+2)}+\ldots\right.$$
$$\left.+\frac{(1-)^m(4/n)^m(mn+3)X^{mn+2}}{(mn+1)(mn+2)(m!)}+\ldots.\right\}. \qquad (7)$$

For a hypothetical substance with a value of 3 for RT_c/p_cV_c, eq 7 becomes

$$\ln\frac{f}{p}=\ln\frac{RT_c}{pV}-3\left(1-\frac{p_cV_c}{RT_c}\right)\left(X-\frac{X^2}{4}\right),$$

and for the critical state of such a substance, $\ln(f_c/p_c)=(\ln 3)-1.5$, or $f_c/p_c=0.6694$. For carbon dioxide with the constants in table 2, $_c/p_c=0.6593$. This is in perfect agreement with the value interpolated between the data given by Deming and Deming.[10]

For carbon dioxide under a pressure of 1 atm, the equation presented in this paper leads to $pV/RT=0.99526$ and to $f/p=0.99528$, whereas the corresponding value given by Deming and Deming for f/p is 0.99504. The fact that Michels obtains $pV/RT=0.99524$ and that f/p should approximate pV/RT very closely, confirms the value 0.99528 or f/p for carbon dioxide at 1 atm and the critical temperature.

It is to be noted that the value of f/p at the critical state is very slightly over 2/3 when $RT_c/p_cV_c=3$ and decreases only slightly with increase in RT_c/p_cV_c, so that for any substance at the critical state, f/p deviates from 2/3 by only a few percent.

VII. SUMMARY

The equation

$$\frac{V(RT_c-pV)}{V_c(RT_c-p_cV_c)}=\frac{3}{2}-\frac{1}{2}X+\left(\frac{3}{2}-\frac{1}{1-p_cV_c/RT_c}\right)\int_X^1 e^{(4/n)(1-X^n)}dX,$$

where n is an empirical constant and $X=V_c/V$, the reduced density, has been shown to fulfill the requirements at the critical state and to

[10] W. E. Deming and L. S. Deming, Phys. Rev. **56**, 108 (1939).

represent the critical isotherms for 12 out of 13 substances in the range of densities up to 1.1 times the critical density, within the reasonable limits of experimental error. The deviations for the one exception, water, amount to ½ percent, which exceeds the tolerance set by the experimental accuracy. For the very accurately measured critical isotherm of carbon dioxide, the differences between calculated and observed pressures do not exceed 3 parts in 10,000.

Of the five constants in the equation, one is limited to a single value for a simple solution, three are directly determined by the critical data, which when substituted in the equation make it automatically fulfill the requirement of the critical state, that the first and second derivatives of pressure with respect to density shall be zero. The reciprocal of the fifth constant, n, has been shown to be very nearly a linear function of RT_c/p_cV_c. In fact, when RT_c/p_cV_c does not exceed 3.8 or 3.9, this linear relation established by the values determined for hydrogen and for carbon dioxide furnishes a correlation from which n may be determined for other substances, and consequently, the critical isotherm may be predicted with great accuracy for densities up to 1.1 times the critical density. The value of n for substances with larger values of RT_c/p_cV_c will probably need to be determined individually, although even then pressures may be predicted within a few percent, from the critical data and the linear relation mentioned for the fifth constant.

For low pressures the equation may be reduced to one expressing pV/RT as a quadratic function of the density, from which pressures may be calculated with an accuracy exceeding that of most measurements.

Although the equation is applied only to the critical temperature, the wide range of densities covered with such accuracy makes it valuable for establishing the critical isotherm as a base line in the tabulation of smoothed values of the properties of substances.

Values of fugacity along the critical isotherm can be calculated from the equation. The fugacity at the critical state is very nearly two-thirds the critical pressure for all substances, but varies slightly with the value of RT_c/p_cV_c.

The author acknowledges with thanks several suggestions from Carl S. Cragoe for the improvement of this paper.

WASHINGTON, February 11, 1942.

U. S. DEPARTMENT OF COMMERCE NATIONAL BUREAU OF STANDARDS

RESEARCH PAPER RP1494

Part of Journal of Research of the National Bureau of Standards, Volume 29, August 1942

X-RAY MEASUREMENT OF THE THICKNESS OF THE COLD-WORKED SURFACE LAYER RESULTING FROM METALLOGRAPHIC POLISHING

By Herbert C. Vacher

ABSTRACT

Different thicknesses of cold-worked layers, each representative of a specific abrasive treatment used in metallographic polishing, were produced on annealed specimens of steel (0.34% C), copper, and aluminum. The back-reflection patterns of the specimens showed a progressive increase in the degree of diffuseness with thickness in the range from 2 to 25 microns on the steel specimens, 2 to 42 microns on the copper specimens, and 5 to 95 microns on the aluminum specimens. A comparison of these patterns with others obtained from copper and steel specimens indicated that the cold-worked layers produced by certain fine-abrasive treatments were thicker than those produced by certain coarse-abrasive treatments.

CONTENTS

	Page
I. Introduction	177
II. Preparation of representative abraded surfaces	178
III. Thickness of the altered surface layer	178
IV. Back-reflection patterns of representative abraded surfaces	179
V. Reduction of thickness of a cold-worked layer by specific abrasive treatments	180
VI. Summary	181

I. INTRODUCTION

The purpose of metallographic polishing, consisting in a series of abrasive treatments, is to produce a smooth flat surface with minimum alteration of structure of the metal at the surface. The film of altered metal, invariably present at the surface, should be removable by a a light etch. Frequently, however, microscopic examination of the etched surface fails to reveal a structure truly characteristic of the metal, the structure being modified by the various abrasive treatments used. Obviously there is need for a method for estimating the extent to which the normal structure is affected by each abrasive treatment used. In this way an individual abrasive treatment could be evaluated with respect to its effect on the thickness of a structurally altered layer as well as the surface characteristics, such as fineness of scratches and pitting.

Consideration of X-ray patterns produced by the back-reflection method led to the conclusion that this method could be used to detect structural changes in the surface layer of a metal, such as low-carbon steel, copper, and aluminum, when in the annealed condition. A back-reflection pattern, obtained by conventional methods, records reflections from planes of crystals located as much as 0.001 to 0.002 inch (25 to 50 microns) below the surface. Alteration in the structure

of an annealed metal in a layer of this thickness would result in a change in the appearance of the X-ray pattern. In the following experiments, back-reflection patterns were made, and the thickness of the cold-worked surface layer was determined for steel (0.34% C), oxygen-free copper, and aluminum specimens that were representative of specific abrasive treatments commonly used in metallographic polishing.

II. PREPARATION OF REPRESENTATIVE ABRADED SURFACES

The steel specimens (1-inch squares ¼ inch thick) were cut from an annealed plate, the copper specimens (⅞-inch disks ¼ inch thick) from an annealed rod of oxygen-free copper, and the aluminum specimens (1-inch disks ¼ inch thick) from a rod of annealed commercially pure aluminum. Surfaces representative of different abrasive treatments were prepared on these specimens as follows: Smooth surfaces, free from cold-work, were prepared by conventional metallographic polishing and etching procedures. The completeness of the removal of the cold-worked layer was established for a number of specimens by the presence of well-defined spots in the back-reflection patterns of the etched surfaces. Each surface then was abraded by one of the treatments listed in table 1. This covered the surface completely with nearly parallel scratches, after which the specimen was turned 90 degrees and the abrasion continued until the first scratches were removed. The back-reflection patterns of the aluminum specimens obtained prior to abrasion indicated that they were not in the fully annealed condition. These specimens were annealed separately in a gas flame and then abraded.

TABLE 1.—*Thickness of the altered surface layer on metals after different abrasive treatments*

Abrasive	Thickness of altered layer			Corresponding diffraction patterns
	Steel	Copper	Aluminum	
	Microns	*Microns*	*Microns*	
(1) Levigated alumina [1]	2.1	2		2
(2) Aluminum oxide (Alundum) powder, grit No. 600 [1]			5	2
(3) Emery polishing paper, grit No. 3/0 [2]	13	21	50	5
(4) Emery polishing paper, grit No. 0 [2]			26	3
(5) Aluminum oxide (Aloxite) polishing paper grit No. 400–A [3]	5	12		3
(6) Emery polishing paper, grit No. 1–G [2]	12.5	17	33	4
(7) Aluminum oxide cloth-backed belt, grit No. 100 [4]	25	42	95	6

[1] A specimen was pressed lightly by hand against a power-driven disk rotating in a vertical plane, covered with broadcloth which had been sprayed with a water suspension of the abrasive.
[2] The abrasive paper was kept covered with a kerosine-paraffin solution, and the specimen was abraded by moving it manually back and forth under light pressure.
[3] A specimen was abraded in the same way as described in footnote 2 but without a lubricant.
[4] A specimen was abraded by holding it under light pressure against a power-driven horizontal belt.

III. THICKNESS OF THE ALTERED SURFACE LAYER

The method used in determining the thickness of the surface layer, throughout which the structure of the metal had been altered, to some extent at least, by the abrasive treatments was a repetition of the following sequence of operations: A back-reflection pattern was obtained from the surface, a small amount of metal was removed by treatment with a suitable solvent, and the loss in weight was determined. Radiation from a chromium target was used in obtaining the back-reflection patterns. At the stage when no further change in

the definition of the spots in the X-ray patterns could be detected, the thickness of the layer removed by the successive treatments with the solvent was computed from the loss in weight, initial area, and density of the specimen. In order to facilitate the detection of small changes in the definition of the spots, special care was taken after each treatment to replace the specimen in the same position with respect to the collimated beam.

The treatment used to remove a small amount of metal from the iron and copper specimens consisted in an electrolytic (anodic) etch. The electrolyte was a 0.5-percent solution of hydrochloric acid for iron and a 2-percent solution of ammonium persulfate for copper. Flick's etch [1] was used for the aluminum specimens.

The values obtained for the thickness of the structurally altered layer representative of different abrasive treatments are listed in table 1. It is noteworthy that with the exception of the No. 100-grit belt, abrasion with No. 3/0 emery polishing paper affected the metal to a greater depth than the coarser-abrasive treatments. This has been taken to indicate that the rolling action of loose abrasive particles, torn from the paper during an abrasive treatment, is a serious factor when minimum alteration of the structure is desired. It may also indicate that even when care is taken fine scratches do not necessarily signify a thinner altered surface layer than do coarse scratches. The results (table 1) also show that for the same abrasive treatment the thickness of such a layer increases on steel, copper, and aluminum in the order given. This is in agreement with the relative difficulty encountered in preparing a satisfactory surface on these metals for metallographic examination.

IV. BACK-REFLECTION PATTERNS OF REPRESENTATIVE ABRADED SURFACES

The back-reflection X-ray patterns of the representative abraded surfaces were obtained with a cold-cathode tube [2] operating on a half-wave rectified current of 5 to 7 ma at about 30 kvp. The exposures were 1 to 1½ hours, and a collimator consisting of two 1-mm drill holes 6 cm apart was used. Prints showing 60-degree sections of the circular patterns, arranged in order of increasing thickness of the structurally altered layer of the three materials used, are shown in figures 1, 2, and 3, respectively. The *A* sections show patterns obtained by using a cobalt target for the steel specimens and a copper target for the copper and aluminum specimens; the *B* sections show patterns obtained by using a chromium target.

An inspection [3] of the patterns in figures 1, 2, 3 and of the results in table 1 shows that in nearly every case there was a detectable increase in the degree of diffuseness for each increase in the thickness of the layer affected by the abrasive treatment and that, in general, small changes can be detected more easily in patterns obtained by using a chromium target than by using a cobalt or copper target. The degree of diffuseness of back-reflection patterns obtained by a conventional procedure, therefore, can be used to estimate relative differences in the thicknesses of cold-worked layers.

[1] Flick's etch consists in immersing the specimen in a solution containing 10 ml of HF, 15 ml of HCl, and 90 ml of H_2O, then washing in warm water, following with a dip in concentrated HNO_3.

[2] C. J. Ksanda, *A metal X-ray tube for characteristic radiation*, Rev. Sci. Instr. **3**, 531–534 (1932); American Instrument Co., Silver Spring, Md. Bul. 1045 (1938).

[3] The comparisons described in the following discussion were made from an inspection of the pattern on the original negative. It is not always possible to detect small differences in the diffuseness of patterns by comparing the prints.

Inspection of the *6A* and *6B* sections (figs. 1, 2, and 3) shows that a few diffuse spots were obtained from surfaces abraded with No. 100-grit abrasive when cobalt and copper targets were used and a diffuse ring when a chromium target was used. This indicated that the maximum thickness of cold-worked layers that can be estimated by increases in the degree of diffuseness are about 25 microns on annealed steel, 42 on annealed copper, and 95 on annealed aluminum. The minimum thickness of cold-worked layers that could be detected on these metals was determined in the following way. Back-reflection patterns made of representative surfaces finished with rouge and magnesia, respectively, showed no detectable change in diffuseness when compared with patterns obtained from the same surfaces prior to the finishing treatments. A comparison of the *1A* and *1B* sections with the *2A* and *2B* sections (figs. 1, 2, and 3) shows that abrasion with levigated alumina on the steel and copper specimens and with grit No. 600 aluminum odide powder on the aluminum specimens caused a barely detectable blurring of the spots. This was more noticeable in patterns obtained with a chromium target than with a cobalt or copper target. Hence (table 1) the minimum thickness of a structurally altered layer that can be detected is about 2 microns on annealed steel and annealed copper and 5 microns on annealed aluminum.

In some metallographic polishing procedures the use of No. 3/0 emery polishing paper is followed by treatment on a wet canvas lap loaded with grit No. 320 aluminum oxide powder (Alundum). Sometimes several of the successive treatments on abrasive papers are replaced by treatments on lead-tin laps loaded respectively with a coarse and a fine emery. To estimate the thickness of the layer affected by various treatments of this kind on annealed copper, back-reflection patterns were made of surfaces representative of each. A comparison of the patterns with those in figure 2, *B*, indicated that the layer showing structural changes resulting from treatments on lead-tin laps loaded with grade Nos. 302 and 303½ emery (American Optical Co.) was thicker than that resulting from No. 3/0 emery polishing paper, and in the case of treatment on the canvas lap, loaded with No. 320 aluminum oxide powder, was less than that resulting from No. 400-grit paper. It was concluded that, in polishing annealed copper specimens for metallographic examination, treatment on a canvas lap should follow, whenever possible, a treatment on No. 400-grit paper, and treatments on No. 3/0 emery polishing paper and lead-tin laps should be omitted.

V. REDUCTION OF THICKNESS OF A COLD-WORKED LAYER BY SPECIFIC ABRASIVE TREATMENTS

A few experiments were made with annealed-copper specimens to determine if the thickness of the altered surface layer representative of a coarse abrasive could be reduced to that representative of a fine-abrasive treatment by a single treatment. For the remainder of this discussion an abrasive treatment is defined as abrasion in a direction 90 degrees to the direction of a previous abrasion sufficient to remove the scratches caused by the latter. Back-reflection patterns were obtained after each of the following abrasive treatments: (1) No. 100-grit belt; (2) No. 1–G grit emery paper; (3) treatment (2) repeated; (4) No. 400-grit paper; (5) treatment (4) repeated; (6) No. 320 aluminum oxide powder on a canvas lap. Sections of the circular patterns corresponding to these treatments are shown in figure 4, *B*.

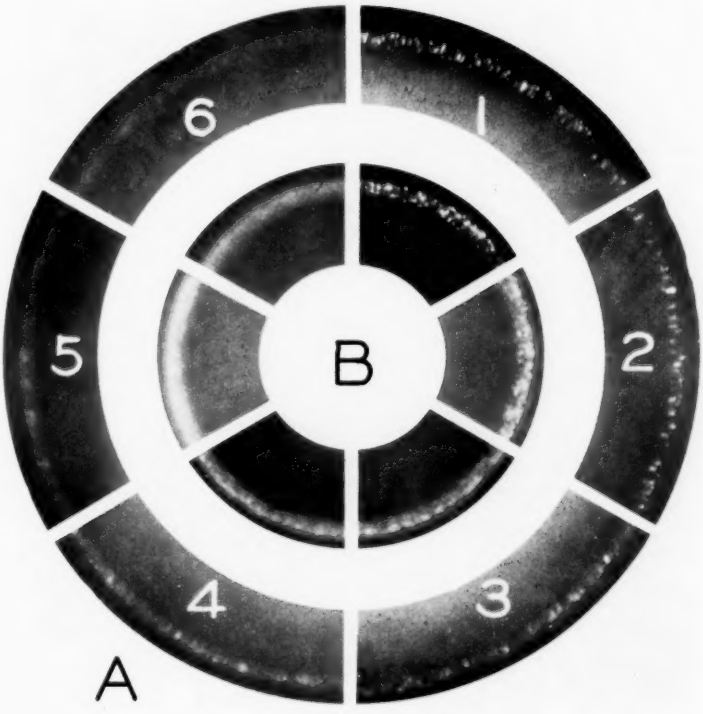

FIGURE 1.—*Back-reflection X-ray patterns of surfaces on annealed steel (0.34 C).*

Patterns 1 indicate the condition of the surface layer prior to specific abrasive treatments; patterns 2 indicate the alteration of this condition by levigated alumina; patterns 3 by No. 400-grit paper; patterns 4 by No. 1-G grit emery paper; patterns 5 by No. 3/0 emery polishing paper; patterns 6 by No. 100-grit belt. The *A* and *B* patterns were obtained by using cobalt and chromium targets, respectively. The film-to-specimen distances were 3.2 and 5.5 cm, respectively.

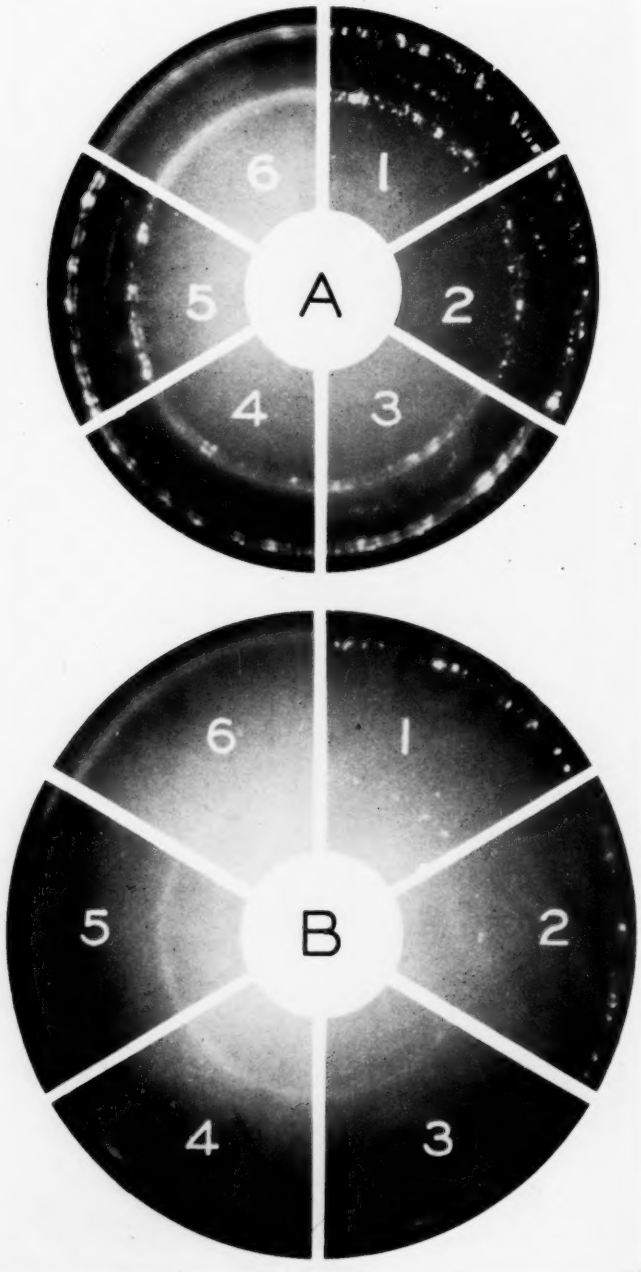

FIGURE 2.—*Back-reflection X-ray patterns of surfaces on annealed copper.*

Patterns 1 indicate the condition of the surface layer prior to specific abrasive treatments. Patterns 2 indicate the alteration of this condition by levigated alumina; patterns 3 by No. 400-grit paper; patterns 4 by No. 1–G grit emery paper; patterns 5 by No. 3/0 emery polishing paper; patterns 6 by No. 100-grit belt. The *A* and *B* patterns were obtained by using copper and chromium targets, respectively. The film-to-specimen distances were 4.35 and 3.65 cm, respectively.

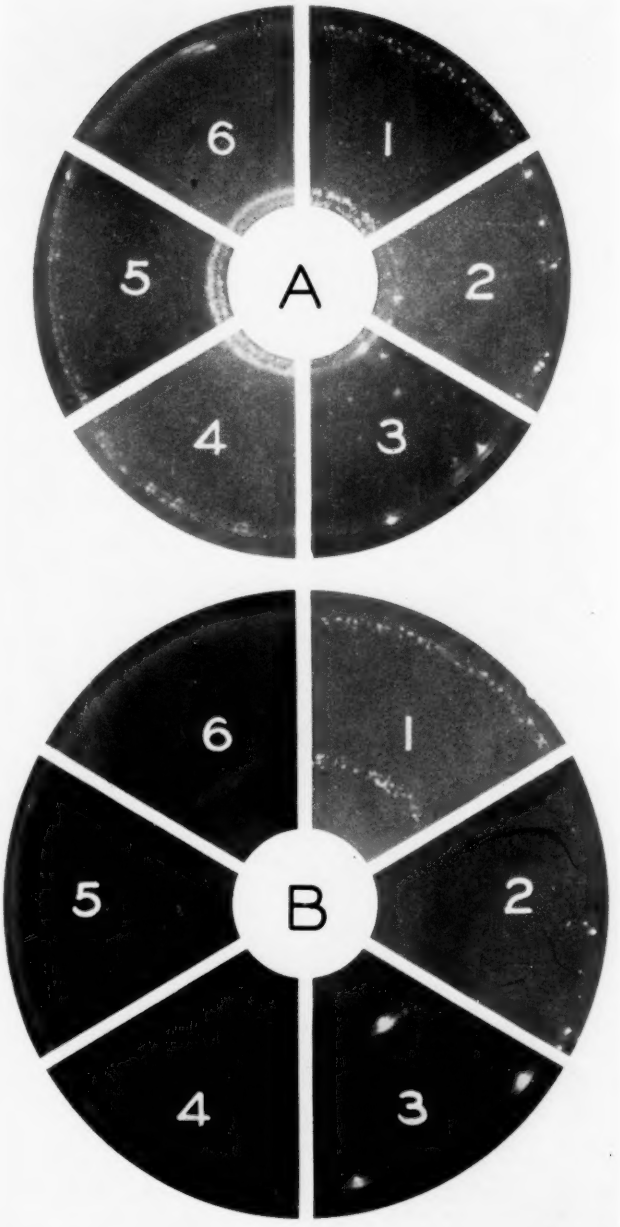

FIGURE 3.—*Back-reflection X-ray patterns of surfaces on annealed aluminum.*

Patterns 1 indicate the condition of the surface layer prior to specific abrasive treatments; patterns 2 indicate the alteration of this condition by No. 600 aluminum oxide powder, patterns 3 by No. 0 emery polishing paper; patterns 4 by No. 1–G grit emery paper; patterns 5 by No. 3/0 emery polishing paper; patterns 6 by No. 100-grit belt. The *A* and *B* patterns were obtained by using copper and chromium targets, respectively. The film-to-specimen distances were 4.45 and 5.5 cm, respectively.

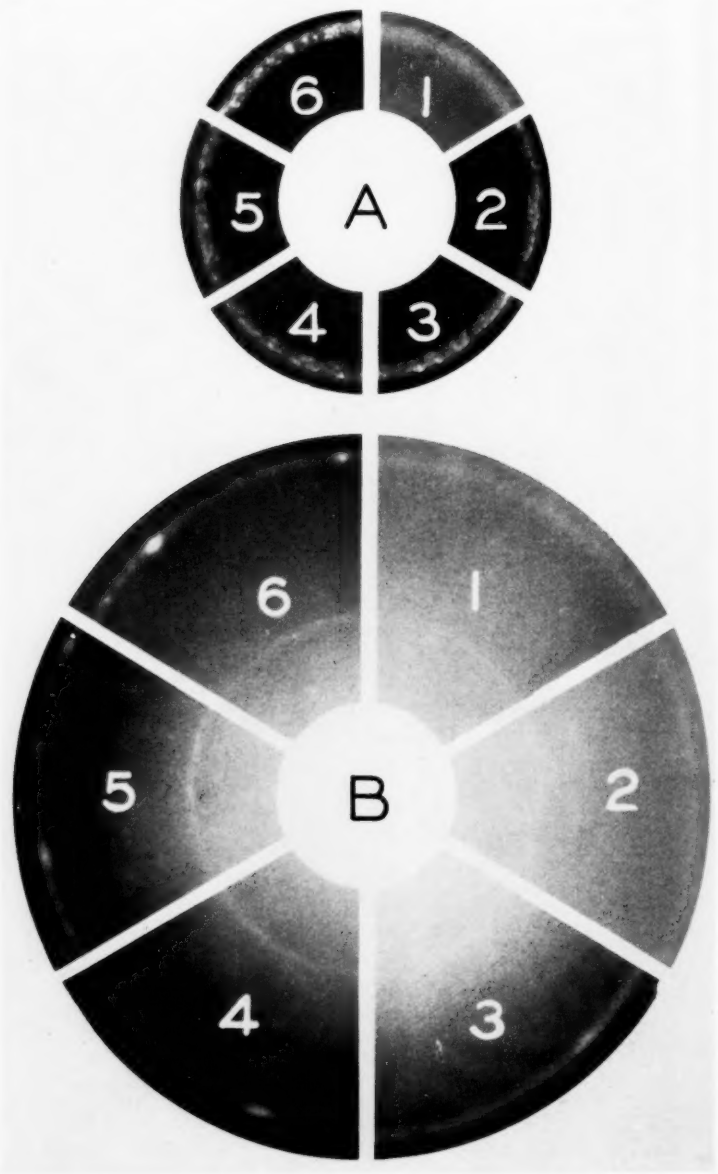

FIGURE 4.—*Back-reflection patterns of surfaces after successive abrasive treatments.*

A patterns—steel specimen: pattern 1 by No. 100-grit belt; pattern 2 by No. 1-G grit paper; pattern 3 by No. 400-grit paper; patterns 4 and 5 by fine and coarse lead-tin laps, respectively; pattern 6 by rouge on a wet velvet lap.

B patterns—copper specimen: pattern 1 by No. 100-grit belt; patterns 2 and 3 by No. 1-G grit paper first and second treatments, respectively; patterns 4 and 5 by No. 400-grit paper first and second treatments, respectively; pattern 6 by No. 320 aluminum oxide powder on a wet canvas lap.

A comparison of patterns 2 and 3 with pattern *5B* of figure 2 shows that two abrasive treatments with No. 1–G grit emery paper were necessary to reduce the thickness of the altered surface layer resulting from abrasion on a No. 100-grit belt to that representative of No. 1–G grit emery paper. A comparison of patterns 4 and 5 with pattern *3B* of figure 2 shows that this also was true for No. 1–G grit paper when followed by No. 400-grit paper. Pattern 6 shows that the thickness of the cold-worked surface layer after treatment (5) was reduced further by one treatment with No. 320 aluminum oxide powder on a canvas lap but not sufficient to be representative of the latter. In general, these results indicate that the cold-worked layer produced by a series of abrasive treatments with abrasives of increasing fineness is thicker than the cold-worked layer produced by many treatments of the last member of the series when used alone.

The reduction in the thickness of the altered surface layer on a steel specimen by a series of abrasive treatments, frequently employed to attain a metallographic polish, was determined by means of back-reflection patterns. The abrasive treatments were (1) No. 100-grit belt; (2) No. 1–G grit emery paper; (3) No. 400-grit aluminum oxide paper; (4) lead-tin lap loaded with grade No. 302 emery; (5) lead-tin lap loaded with grade No. 303½ emery; (6) ½ hour on a rotating velvet lap loaded with rouge. A comparison of the back-reflection patterns obtained (fig. 4, A) indicates that the altered surface layer was increasingly thinner for the No. 1–G grit (pattern 2) and No. 400-grit papers (pattern 3). However, for the coarse lead-tin (pattern 4) little or no difference was noted, and for the fine lead-tin (pattern 5) and rouge (pattern 6) laps, only slight improvement was obtained. A comparison of pattern 6 with pattern *3B* of figure 1 indicates that the thickness of the altered surface layer was about equal to that representative of No. 400-grit paper. If the thickness had been reduced to the value representative of rouge, pattern 6 of figure 4 should appear as pattern *1B* of figure 1. These results indicate that the thickness of the altered layer would have been less if additional abrasive treatments with the No. 1–G grit and No. 400-grit papers had been made and the lap treatment had been omitted.

VI. SUMMARY

A series of annealed specimens, each having a surface free from cold-work, was prepared from each of the following metals: steel (0.34% C), copper, and aluminum. The surface was finished with one of several abrasives commonly used in preparing a surface for metallographic examination, and X-ray back-reflection patterns were obtained by using copper, cobalt, and chromium targets. The thicknesses of the layers altered by the abrasive treatments then were determined. The results showed that back-reflection patterns can be used to estimate the thicknesses of cold-worked layers between 2 and 25 microns on annealed steel, 2 and 42 microns on annealed copper, and 5 and 95 microns on annealed aluminum.

The experiments are described to illustrate the use of back-reflection X-ray patterns as a means of evaluating individual abrasive treatments employed in obtaining a metallographic polish.

WASHINGTON, June 12, 1942.